



HAL
open science

Modeling and Service Life Monitoring of Mooring Lines of Floating Wind Turbines

Hong-Duc Pham

► **To cite this version:**

Hong-Duc Pham. Modeling and Service Life Monitoring of Mooring Lines of Floating Wind Turbines. Solid mechanics [physics.class-ph]. École centrale de Nantes, 2019. English. NNT : 2019ECDN0030 . tel-02466337

HAL Id: tel-02466337

<https://theses.hal.science/tel-02466337>

Submitted on 4 Feb 2020

HAL is a multi-disciplinary open access archive for the deposit and dissemination of scientific research documents, whether they are published or not. The documents may come from teaching and research institutions in France or abroad, or from public or private research centers.

L'archive ouverte pluridisciplinaire **HAL**, est destinée au dépôt et à la diffusion de documents scientifiques de niveau recherche, publiés ou non, émanant des établissements d'enseignement et de recherche français ou étrangers, des laboratoires publics ou privés.

THESE DE DOCTORAT DE

L'ÉCOLE CENTRALE DE NANTES
COMUE UNIVERSITE BRETAGNE LOIRE

ECOLE DOCTORALE N° 602
Sciences pour l'Ingénieur
Spécialité : «Mécanique des Solides, des Matériaux, des Structures et des Surfaces »

Par

« Hong-Duc PHAM »

**« MODELISATION ET SUIVI EN SERVICE DES LIGNES D'ANCRAGE
DES EOLIENNES FLOTTANTES »**

« Modeling and Service Life Monitoring of Mooring Lines of Floating Wind Turbines »

Thèse présentée et soutenue à Nantes, le 26 septembre 2019

Unité de recherche : Institut de Recherche en Génie Civil et Mécanique (GeM), UMR CNRS 6183

Rapporteurs avant soutenance :

Lars JOHANNING Professeur, University of Exeter (Royaume-Uni)
Guillaume PUEL Professeur, Ecole Centrale Supélec (France)

Composition du Jury :

Président : Emmanuelle VIDAL-SALLE Professeur, INSA de Lyon (France)
Examineurs : Peter DAVIES Chargé de recherche HDR, IFREMER (France)

Dir. de thèse : Patrice CARTRAUD Professeur, Ecole Centrale de Nantes (France)
Co-dir. de thèse : Franck SCHOEFS Professeur, Université de Nantes (France)
Co-encadrant : Christian BERHAULT Docteur, Ecole Centrale de Nantes (France)

Invité

Thomas SOULARD Ingénieur, Ecole Centrale de Nantes (France)

ABSTRACT

In this work a methodology for service life monitoring of mooring lines of floating wind turbines is proposed.

First, an empirical expression of dynamic stiffness of a nylon rope is obtained from the testing data in the literature. A practical modeling procedure is proposed which allows accounting for the non-linear dynamic axial stiffness of nylon mooring ropes.

The second part is devoted to the prediction of fatigue life of mooring lines. Cutting-edge methods for fatigue analysis in frequency domain and for simulation of nonlinear mooring response (e.g. Artificial Neural Network) are investigated in order to perform a quick fatigue estimate and strength check in a reliability framework. The present methodology aims to support making decisions regarding maintenance or replacement of lines based on the level of reliability estimated during the expected service life.

Keywords: Floating Wind Turbine, Mooring line, Nylon, Fatigue, Reliability, Nonlinear simulation

RÉSUMÉ

On propose dans ce travail une méthodologie pour le suivi en service des lignes d'ancrage des éoliennes flottantes.

Tout d'abord, une expression empirique de la raideur dynamique d'un câble en nylon est obtenue à partir des données d'essais dans la littérature. Une procédure pratique de modélisation est proposée en tenant compte de la raideur axiale dynamique non-linéaire des câbles en nylon.

La deuxième partie est consacrée à la prédiction de la durée de vie des lignes d'ancrages. Des méthodes avancées pour l'analyse de fatigue dans le domaine fréquentiel et la simulation des réponses non-linéaires (par exemple le réseau de neurones artificiels) sont donc également étudiées afin de réaliser une estimation rapide de la fatigue et de la résistance dans un cadre fiabiliste. La présente méthodologie vise à faciliter la prise de décisions concernant la maintenance ou le remplacement des lignes en fonction du niveau de fiabilité estimé à différents instants pendant la durée de vie prévue.

Mots clés : Eolienne flottantes, Ligne d'ancrage, Nylon, Fatigue, Fiabilité, Simulation non-linéaire

To my Father

To my Wife Nhu-Trang, my Son, my Daughter
To my Mother

Acknowledgement

First of all, I want to thank Prof. Patrice CARTRAUD for giving me the opportunity to undertake this PhD work under his supervision, for his critical but open work attitude that always “forced” me to end up with the best “revision” of my ideas, for his patience and for his life advice that I will never forget. My thoughts also turn to my second supervisor Prof. Franck SCHOEFS who was a great support especially for the reliability part of the present work. And I want to thank Dr. Christian BERHAULT who launched the project, who stepped in, for his energy and scientific rigour.

I want to thank the SEMREV team of the LHEEA laboratory at the Ecole Centrale de Nantes, for their co-operation. My special thanks to Thomas SOULARD, who is research engineer and project manager at SEMREV, for sharing his experience and invaluable advice in hydrodynamics, mooring systems and marine renewable energy throughout many of our discussions.

Further, I would like to acknowledge the members of my thesis committee including Prof. Emmanuelle VIDAL-SALLE as president and Mr. Peter DAVIES as internal examiners, Prof. Guillaume PUEL and Prof. Lars JOHANNING as external examiners for their comments and advice on my work.

I would like to acknowledge the funding from the Vietnamese scholarship program 911 and the financial support from France Energies Marines and the State, managed by the National Research Agency under the “Investissements d'avenir” program with the reference ANR-10-IEED-0006-19 and the FP7-EU FLOATGEN project with the support of the European Union, without which this work would not have been possible.

I'm also grateful to Prof. Pierre FERRANT and Dr. Xiao-bo CHEN who recommended me to my thesis supervisors so that I can have this opportunity to work in a wonderful working environment between two laboratories GEM and LHEEA at the Ecole Centrale de Nantes.

And I want to thank my teachers and colleagues at the National University of Civil Engineering, Hanoi, Vietnam (especially Prof. PHAM Khac Hung, Assoc. Prof. PHAM Hien Hau and Dr. MAI Hong Quan) who gave me a solid and wide scientific knowledge base and developed my interest in fatigue and reliability of offshore structures.

Finally, on a personal note, I want to thank my colleagues at GEM and LHEEA (especially Anh-Tuan, Fabien, Charles, Léna, Vincent, Baptise, Erwan, Dasha) for their support, and for being important parts of my lovely memory of these three hectic and eventful years at Centrale Nantes and in Nantes.

TABLE OF CONTENTS

ABSTRACT	2
RÉSUMÉ	4
ACKNOWLEDGEMENT	9
TABLE OF CONTENTS	11
LIST OF FIGURES	15
LIST OF TABLES	19
NOMENCLATURE	22
CHAPTER 1- INTRODUCTION	24
1. INTRODUCTION	25
2. BACKGROUND.....	27
2.1 <i>Mooring design and standards</i>	28
2.2 <i>Mooring components and configurations</i>	29
2.3 <i>Mooring analysis and software applications</i>	36
2.4 <i>Survivability and fatigue analysis</i>	42
2.5 <i>Methodology for reliability assessment</i>	45
2.6 <i>Methodology for service life monitoring of mooring lines</i>	46
3. OBJECTIVES	46
4. THE RESEARCH METHODOLOGY	47
5. SCOPE	48
6. REFERENCES	50
CHAPTER 2- MECHANICAL BEHAVIORS OF MOORING COMPONENTS FOR THE MODELING AND SERVICE LIFE MONITORING OF OFFSHORE MOORING LINES	55
1. INTRODUCTION	56
2. CHAIN	57
3. NYLON	59
3.1 <i>Load-elongation characteristics</i>	60
3.2 <i>Fatigue characteristics</i>	68
3.3 <i>Application for numerical modeling of nylon mooring ropes</i>	79
4. MARINE ENVIRONMENTAL IMPACTS.....	88
5. CONCLUSIONS.....	91
6. REFERENCES	93
CHAPTER 3 – METHODOLOGY FOR MODELING AND SERVICE LIFE MONITORING OF MOORING LINES OF FLOATING WIND TURBINES. 100	
1. INTRODUCTION	101
2. STATE-OF-THE-ART IN MOORING LINE FATIGUE ANALYSIS	103
2.1 <i>Time domain fatigue analysis</i>	104
2.2 <i>Frequency domain (spectral) fatigue analysis</i>	105

2.3 Comparison of fatigue damage calculated by spectral fatigue approaches and time domain analysis.....	109
3. METHODOLOGY FOR MODELING AND SERVICE LIFE MONITORING OF MOORING LINES	110
4. METHODOLOGY FOR RELIABILITY ASSESSMENT	112
4.1 Reliability in strength condition (ULS).....	113
4.2 Reliability in fatigue condition (FLS)	114
4.3 Reliability assessment for the case study.....	114
5. SIMULATION OF NON-GAUSSIAN PROCESSES BASED ON ARTIFICIAL NEURAL NETWORK.....	123
5.1 Artificial Neural Network (ANN) for simulation of nonlinear mooring response.....	127
5.2 Comparison and application for reliability assessment	134
6. CONCLUSIONS.....	142
7. REFERENCES	145
CHAPTER 4 – CONCLUSIONS AND FUTURE WORK	153
1. CONCLUSIONS.....	154
2. FUTURE WORK	156
APPENDIX.....	159
LIST OF PUBLICATIONS & COMMUNICATIONS.....	160

LIST OF FIGURES

<i>Figure 1-1: A met-ocean buoy installed at the SEM-REV site.</i>	25
<i>Figure 1-2: The FLOATGEN FWT installed at the SEM-REV site.</i>	25
<i>Figure 1-3: A MRE Mooring System (Flory et al., 2016).</i>	26
<i>Figure 1-4: Different floating wind foundation technologies (LesEchos, 2019).</i>	28
<i>Figure 1-5: Common studlink and studless chains (Ramass, 2014).</i>	30
<i>Figure 1-6: Common wire ropes constructions (Engineeringcontent, 2018).</i>	31
<i>Figure 1-7: Single filament tensile properties for different fibers (Weller et al., 2015).</i>	32
<i>Figure 1-8: Some rope constructions: 1, parallel yarns; 2, parallel strands, 3, stranded (wire-lay), 4, plaited and 5, braided (Tension Technology International -TTI, 2019).</i>	32
<i>Figure 1-9: Comparison of the load-elongation characteristics of nylon and polyester ropes (Ridge et al., 2010).</i>	33
<i>Figure 1-10: Comparison of the fatigue tests results on the Bridon's "Superline" nylon sub-rope, with other material mooring components (Ridge et al., 2010). (LR stands- Load Range, BL- Breaking Load).</i>	34
<i>Figure 1-11: A Single Point Mooring (SPM) system (Culofsea, 2019).</i>	35
<i>Figure 1-12: A spread mooring system (2b1Consulting, 2019).</i>	35
<i>Figure 1-13: Mooring configurations for Marine Energy Converters (MEC): 1- Single taught line (rope); 2- Multiple taught lines (rope); 3- Catenary shape (rope and chain); 4- Catenary shape with surface buoy (fiber rope and chain); 5- Lazy wave (rope and chain) (Karimirad et al., 2014).</i>	36
<i>Figure 1-14: The catenary shape of mooring lines.</i>	37
<i>Figure 1-15: A regular wave (up) and an irregular wave (down).</i>	39
<i>Figure 1-16: A random wave characterized by the Jonswap spectrum.</i>	40
<i>Figure 1-17: The finite element model of a line (Orcina, 2012).</i>	41
<i>Figure 1-18: The HydroStar mesh of a floating structure.</i>	42
<i>Figure 1-19: Mooring S-N fatigue curves (DNV, 2010).</i>	44
<i>Figure 1-20: Mooring T-N fatigue curves (API, 2005).</i>	44
<i>Figure 2-1: The layout of the floating structure and its hybrid mooring lines (chains plus nylon ropes).</i>	57
<i>Figure 2-2: A mooring system and the influencing factors (Brown et al., 2012). Right: An underwater fairlead (Royal IHC, 2018).</i>	59
<i>Figure 2-3: In-plane bending and out-of-plane bending modes (Kim et al., 2017).</i>	59
<i>Figure 2-4: The spring-dashpot model (Flory et al., 2007).</i>	60
<i>Figure 2-5: Fast + slow springs tension-stretch curve (Flory et al., 2007).</i>	61
<i>Figure 2-6: The Syrope model (Falkenberg et al., 2017, 2018).</i>	62
<i>Figure 2-7: Dynamic stiffness of the wire-lay nylon rope depending on the mean tension, L_m (data obtained from Huntley, 2016).</i>	64
<i>Figure 2-8: Dynamic stiffness of the wire-lay nylon rope depending on the tension amplitude, L_a (data obtained from Huntley, 2016).</i>	64

<i>Figure 2-9: Mooring analysis procedure taking into account the impact of tension amplitudes on the dynamic stiffness of nylon ropes.</i>	<i>65</i>
<i>Figure 2-10: Failure time vs. maximum stress for polyester yarns under creep rupture (Ra=1) and cyclic fatigue (Ra=0.1, f=1Hz) – Ra = Minimum Load/Maximum Load (Mandell et al., 1987).</i>	<i>69</i>
<i>Figure 2-11: Some rope construction (Ridge et al., 2010; Banfield et al., 2017; Huntley, 2016).</i>	<i>70</i>
<i>Figure 2-12: Inter-strand damage in a polyester rope (left) after a 48-million-cycle fatigue test (Banfield et al., 2018) and a nylon subrope (right) after a ten-million-cycles fatigue tests (Banfield et al., 2017).</i>	<i>70</i>
<i>Figure 2-13: A nylon fatigue curve based on the testing data of the TTI (Ridge et al.2010, Banfield et al., 2017).</i>	<i>71</i>
<i>Figure 2-14: Comparison of nylon fatigue characteristics (Huntley, 2016) (the red line is the fatigue curve obtained from the nylon subrope tests performed by the Ridge et al., 2010) (LR- Load Range, BL: Breaking Load).</i>	<i>72</i>
<i>Figure 2-15: A creep model fatigue curve, Tmax- maximum tension in the rope.</i>	<i>72</i>
<i>Figure 2-16: A yarn-on-yarn abrasion machine (Chevillotte et al., 2018).</i>	<i>73</i>
<i>Figure 2-17: 6t sub-rope load/extension curves up to break for new rope (after 10 conditioning cycles) and after fatigue testing (Bandfield et al., 2018).</i>	<i>74</i>
<i>Figure 2-18: The influence of material loss on the residual dynamic stiffness of polyester ropes (Liu et al., 2015) (D- the damage level in % of MBS)</i>	<i>75</i>
<i>Figure 2-19: Non-destructive fatigue tests on nylon subropes (MBS: Minimum Breaking Strength).</i>	<i>77</i>
<i>Figure 2-20: Extrapolating the non-failure fatigue test results.</i>	<i>78</i>
<i>Figure 2-21: An internal abrasion fatigue curve.</i>	<i>78</i>
<i>Figure 2-22: Left- The FLOATGEN FWT (ECN, 2018); Right- The floating structure modeled by HydroStar (BV, 2016).</i>	<i>79</i>
<i>Figure 2-23: Power spectral density of the incoming wave and the tension response.</i>	<i>80</i>
<i>Figure 2-24: Dynamic tension of a mooring line in ULS condition applied the present fiber rope mooring analysis procedure presented in Figure 2-9.</i>	<i>83</i>
<i>Figure 2-25: Dynamic tension of a mooring line in FLS condition applied the present fiber rope mooring analysis procedure presented in Figure 2-9.</i>	<i>83</i>
<i>Figure 2-26: Comparison of maximum tensions for different cases of stiffness with the design breaking tension (i.e. which considers the safety factor of 1.67 according to API-RP-2SK (API, 2005)).</i>	<i>84</i>
<i>Figure 2-27: Expected fatigue lives for different stiffness cases (a safety factor of 3 according to API-RP-2SK (API, 2005) is already consider for the fatigue life in each case).</i>	<i>85</i>
<i>Figure 2-28: Tension responses, ULS.</i>	<i>88</i>
<i>Figure 2-29: Tension responses, FLS.</i>	<i>88</i>
<i>Figure 2-30: Biofouling colonization survey using under-water camera at the SEM-REV test site (Spraul et al., 2017).</i>	<i>89</i>

<i>Figure 2-31: Corroded chain mooring lines of a met-ocean buoy at the SEM-REV sea test site (Berhault, 2017).</i>	90
<i>Figure 3-1: Comparison of time-domain and frequency-domain fatigue analyses....</i>	104
<i>Figure 3-2: A bi-modal spectrum (Gao et al., 2010).</i>	104
<i>Figure 3-3: The rainflow counting method (Pham, 2010).</i>	105
<i>Figure 3-4: Comparison of different improved frequency-domain fatigue analysis methods with time domain simulations (Pham et al., 2019-b).</i>	110
<i>Figure 3-5: Methodology for modeling and service life monitoring of mooring lines</i>	112
<i>Figure 3-6: Time history and PSD of the tension response, $T_s(t)$, in the design extreme sea state.</i>	118
<i>Figure 3-7: Time-dependent reliability index in strength condition of the chain link.</i>	119
<i>Figure 3-8: The tension response PSD obtained from the tension time history calculated by Orcaflex using Fast Fourier Transformation (FFT).</i>	120
<i>Figure 3-9: Different approaches to calculate the fatigue damage of the chain links highlighting the effect of corrosion. The added damage due to extreme sea states (e.g. those with a return period of 10, 20, 50 or 100 years that might probably happen during operation) are illustrated in green, yellow, violet and red color of the case S4.</i>	120
<i>Figure 3-10: Time-dependent reliability index calculated based on different approaches, $rc = 0.4$ mm/year.</i>	122
<i>Figure 3-11: Time-dependent reliability index calculated based on different approaches, $rc = 0.8$ mm/year.</i>	122
<i>Figure 3-12: Example of a mild (top) and a strong (bottom) non-Gaussian processes and its underlying Gaussian ones.</i>	123
<i>Figure 3-13: A neural network with only one intermediate (hidden) layer.</i>	126
<i>Figure 3-14: Regression results.</i>	128
<i>Figure 3-15: Comparison of a tension sample with the simulated tension based on the neural network.</i>	129
<i>Figure 3-16: Comparison of the PDF of a tension sample with the simulated tension based on the neural network.</i>	130
<i>Figure 3-17: Sea states used for training the neural network and sea state to be simulated.</i>	131
<i>Figure 3-18: Regression results.</i>	132
<i>Figure 3-19: Comparison of a tension sample with the simulated tension based on the neural network (fatigue sea state $H_s = 2.75$ m, $T_p = 12.5$ s).</i>	133
<i>Figure 3-20: Comparison of the PDF of a tension sample with the simulated tension based on the neural network (fatigue sea state $H_s = 2.75$ m, $T_p = 12.5$ s).</i>	134
<i>Figure 3-21: Probability of failure (P_f) for different run (th) considering the number of simulations (N_s).</i>	139
<i>Figure 3-22: Probability of failure (P_f) for different number of simulations (N_s).</i>	140

*Figure 3-23: A time history of the tension response at fairlead point of the front line 1
in the ULS condition. 141*

LIST OF TABLES

<i>Table 2-1: Empirical coefficients for determining the dynamic stiffness of the nylon rope.</i>	64
<i>Table 2-2: Classification of fatigue characteristics of fiber ropes (Weller et al., 2015)</i>	68
<i>Table 2-3: Mooring line properties.</i>	80
<i>Table 2-4: Extreme and moderate sea states at the SEMREV sea test site.</i>	81
<i>Table 2-5: Different dynamic stiffness cases of the nylon rope and the resulting standard deviation of the tension response.</i>	81
<i>Table 2-6: Different dynamic stiffness cases of the nylon rope and the resulting platform motions.</i>	82
<i>Table 2-7: Mooring line properties.</i>	86
<i>Table 2-8: Motion statistics.</i>	87
<i>Table 3-1: Comparison of fatigue damage calculated by time domain analysis and different frequency domain fatigue analysis approaches for different sea states (Pham et al., 2019-b).</i>	109
<i>Table 3-2: The time-dependent Breaking Tension of chain link at the fairlead connection point considering an annual reduction in diameter, $r_c = 0.4$ mm/year.</i>	117
<i>Table 3-3: The time-dependent Breaking Tension of chain links at the fairlead connection point considering an annual reduction in diameter, $r_c = 0.8$mm/year</i>	117
<i>Table 3-4: The uncertainties of the Palmgren-Miner rule and the DNV's S-N curve (Lardier et al., 2008; Mathisen et al., 2005).</i>	121
<i>Table 3-5: Different sea states taken as input to train the neural network.</i>	130
<i>Table 3-6: Statistical properties considering the number of simulations.</i>	136
<i>Table 3-7: Reliability assessment by using the ANN-based Monte Carlo simulation</i>	138
<i>Table 3-8: Mean Probability of failure for each number of simulations</i>	138

Nomenclature

Symbols

A	cross section	R	Structural resistance
B	Damping matrix	S	Load effect
D	Diameter	T_{\max}	Maximum tension
D	Fatigue damage	T_{\min}	Manimum tension
F_{Mooring}	Pre-tension force	T_p	Peak period
F_{LF}	Low frequency force	T_0	Period of loading
F_{Static}	Static forces	x	Displacement vector
F_{WF}	Wave frequency force	α_i	Bandwidth parameter
G	Failure function	β	Reliability index
H_S	Significant wave height	δ	Spectral parameter
K	Stiffness matrix	ω	Wave angular frequency
K_{rs}	Quasi-static stiffness	ω_p	Peak wave angular frequency
K_{rd}	Dynamic stiffness	σ	Standard deviation
L	Initial Length of the rope	γ	Peak-enhancement factor
L_a	Tension amplitude	γ_m, γ_T	Partial safety factor
L_m	Mean load	Δl	Stretch
M	Mass matrix	ϵ_a	Amplitude of strain
M_a	Added mass matrix	Δ	Critical damage
N	Number of loading cycles	λ_n	Spectral moments
P_f	Probability of failure	v_0	Mean-zero up-crossing rate
R_a	Tension ratio	v_p	Frequency of peak

Acronyms

ABS American Bureau of Shipping	MBS Minimum Breaking Strength
ALS Accidental Limit State	MBL Minimum Breaking Load
API American Petroleum Institute	MRE Marine Renewable Energy
BV Bureau Veritas	OPB Out-of-Plane Bending
CTF Cycles to Failure	ORQ Oil Rig Quality
DNV Det Norske Veritas	PSD Power Spectral Density
FLS Fatigue Limit State	RBS Residual Breaking Strength
FM Fracture Mechanics	RFC Rainflow counting
FPSO Floating Production Storage and Offloading	SPM Single Point Mooring
FWT Floating Wind Turbine	TCLL Thousand Cycle Load Levels
IPB In-Plane Bending	TTI Tension Technology International
LF Low Frequency	ULS Ultimate Limit State
LRFD Load and Resistance Factor Design	WF Wave Frequency

CHAPTER 1- INTRODUCTION

CHAPTER 1- INTRODUCTION..... 24

- 1. INTRODUCTION 25
- 2. BACKGROUND..... 27
 - 2.1 *Mooring design and standards* 28
 - 2.2 *Mooring components and configurations* 29
 - 2.3 *Mooring analysis and software applications* 36
 - 2.4 *Survivability and fatigue analysis*..... 42
 - 2.5 *Methodology for reliability assessment* 45
 - 2.6 *Methodology for service life monitoring of mooring lines* 46
- 3. OBJECTIVES 46
- 4. THE RESEARCH METHODOLOGY 47
- 5. SCOPE 48
- 6. REFERENCES 50

1. Introduction

Nowadays, the service life monitoring of mooring lines attracts more and more attention from the Marine Renewable Energy (MRE) industry where developers desire to have a closer look on the safety margin in order to reduce the Levelized Cost of Energy (LCOE). There is also motivation for the MRE industry to adopt existing lessons from the offshore industry and to improve current offshore mooring standards in order to assure safe and cost-effective design of MRE devices. A better estimate of fatigue damage and reliability is believed to be the key, which can be achieved by better modeling combined with monitoring.



Figure 1-1: A met-ocean buoy installed at the SEM-REV site.

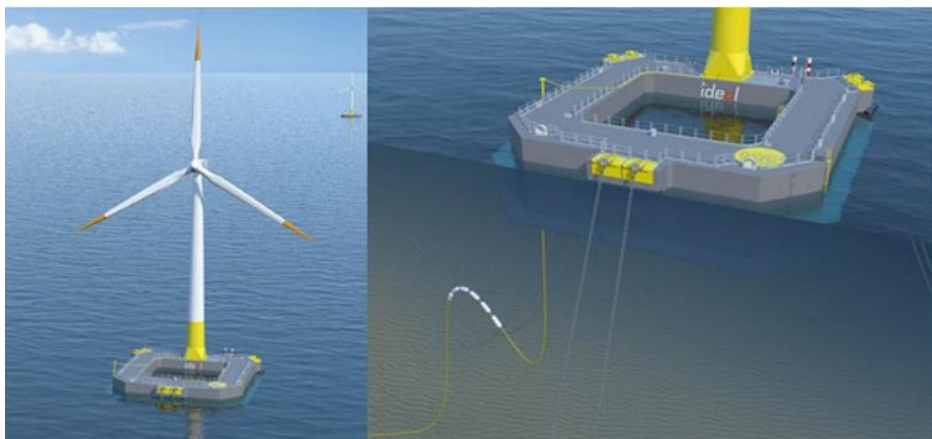


Figure 1-2: The FLOATGEN FWT installed at the SEM-REV site.

Figures 1-1 and 1-2 illustrate the met-ocean buoy and the FLOATGEN FWT currently installed for monitoring and testing at the SEM-REV site located 20km off the coast

Le Croisic, France. SEM-REV is a sea test site for multi-technology offshore testing which plays a decisive role in meeting the challenge of MRE development in France. It is operated by the Research Laboratory in Hydrodynamics, Energetics and Atmospheric Environment (LHEEA), Ecole Centrale de Nantes/CNRS, with the aim of helping industrialists to develop new energy production capacities.

The first main objective of this thesis is to propose a comprehensive methodology for modeling and service life monitoring of mooring lines of Floating Wind Turbines (FWTs) where it is believed that monitoring and modeling should be implemented in parallel, in a so-called digital twin, in order to better estimate the actual state of the mooring system during deployment. Indeed, it seems crucial to clarify the mechanics of the mooring line responses, to understand why and how they are modified during deployment, and how those modifications can be accounted for in order to update the actual fatigue damage and predict the remaining allowable service life. The present methodology is based on the reliability approach where the reliability regarding strength resistance (Ultimate Limit State – ULS) and fatigue endurance (Fatigue Limit State – FLS) are checked. Then, decisions regarding maintenance or replacement of lines can be made based on their levels of reliability estimated during the expected service life. The methodology may also be considered for a more detailed mooring design once the information from similar structures, projects, sites, etc. are known. Although the chosen case study is focused on FWT mooring lines, it is believed that the methodology could be equally applicable to other types of MRE devices and Oil & Gas platforms.

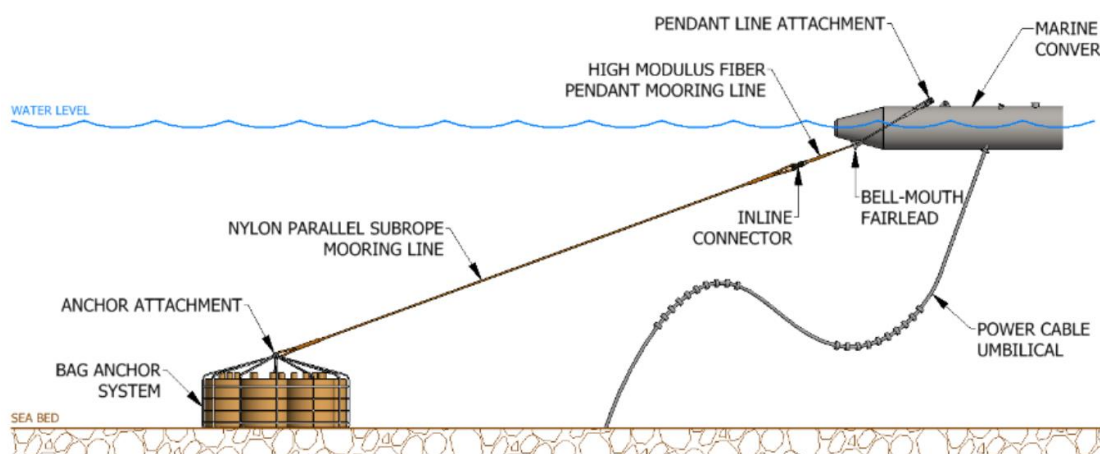


Figure 1-3: A MRE Mooring System (Flory et al., 2016).

Besides, recent interest in floating wind and wave energy draws the attention of industrialists (e.g. by IDEOL, SAIPEM, WindFloat, etc.) on synthetic moorings where the application of nylon as a mooring component might provide a more cost-effective design thanks to its low-stiffness, low-cost and corrosion-free. However, the nonlinear

behaviors of nylon ropes (e.g. load-elongation properties, fatigue characteristics) complicate the design and modeling of such mooring systems. Those nonlinear behaviors should, therefore, be carefully investigated, which are the second main objective of the present work.

Figures 1-3 illustrates the mooring system of a Marine Energy Converter (Flory et al., 2016) which employs nylon mooring rope as a principal mooring component.

For convenience, section 2 of this chapter presents a literature review on the state-of-the-art in mooring design, fatigue and reliability analysis where a large amount of information is based on the recent research work of Harris (2014) and Parish (2015). Section 3 presents the research questions that the author addresses in the present work based on the research methodology proposed in section 4. The scope of work is discussed in section 5.

2. Background

The emergency of fighting against global warming effect of the planet leads to an ever increasing need of substituting conventional coal and fossil fuels by green energy sources where wind energy is one of the promising alternatives. Wind can be captured on the mainland (onshore wind turbines) or on the ocean (offshore wind turbines). Offshore wind turbines can be either: fixed to the sea bottom (bottom-fixed offshore wind turbines) or self-floated and moored to the sea bed by a mooring system (Floating Offshore Wind Turbines). Floating Wind Turbines (FWTs) have several advantages as they are less dependent on the constraint of water depth, thus can be installed further offshore. Therefore, not only a low or even inexistent visual impact from the mainland is achievable but also more stable and strong wind may be captured. The latter is very important since it can increase directly the efficiency of power generation. FWTs are, therefore, often referred as the future of offshore wind.

More than 3200 offshore wind turbines have been installed worldwide (corresponding to the capacity of nearly 12 GW), only 6 floating units installed by the end of 2015 such as in Norway (1 unit), Portugal (1 unit) and Japan (4 units). In 2015, Statoil launched the first floating wind farm project in the world, Hywind, off Peterhead in Scotland. In October 2017, Hywind has started powering the Scottish grid. In April 2018, the Floating Offshore Wind Turbine FLOATGEN was tugged to its permanent offshore installation site – the SEM-REV sea-test site (Le Croisic, France) and became fully operational since September 2018. In France, 6 commercial projects of fixed offshore wind turbines of 500MW each (at the sites of Tréport, Fécamp, Courseulles-sur-Mer, Saint-Brieuc, Noirmoutier-en-l'Île / Isle of Yeu and Saint-Nazaire) and 4 pre-

commercial floating wind turbine projects of 25 MW each (at the sites of Groix, Leucate, Gruissan and Fos-sur-Mer) have already been awarded by the French government with the installation objectives between 2020 and 2021.

Four technologies which are currently competing for the prospects of the floating wind market are presented in Figure 1-4. Each of them leads to a different mooring design. Moorings are therefore innovation driven, which reinforce the need for better understanding, modeling, and monitoring. The floating structure and tensioned legs mooring system (4) developed by SBM Offshore and IFP Energies nouvelles is inspired by technologies that has been already used for the O&G industry. The “WindFloat” technology (2) developed by Principle Power using concrete or steel “semi-submersible” floaters is also a variation of technologies from the O&G industry. The “Spar” technology (3) developed by Statoil is based on the use of a steel cylinder anchored foundation which allows the installation of FWTs at water-depths up to 800 meters. This technology has already been producing electricity for 20,000 households off the Scottish coast at the water-depth of 95 to 130 meters. The “Free Floating” technology (1) driven by the start-up Ideol was classified by the Carbon Trust and IHS Markit as a damping pool semi-submersible platform but was claimed as a “unique barge design” by the developer. The technology is being experimented by two demonstrators, off Le Croisic coast in Britany (France) and in Kitakyushu (northern Japan) where it suffered 3 typhoons without flinching (LesEchos, 2019).

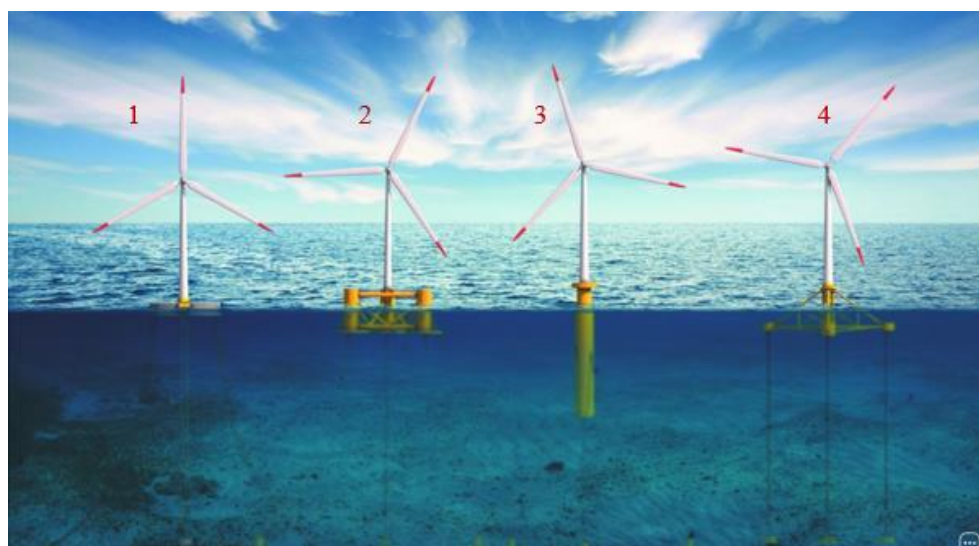


Figure 1-4: Different floating wind foundation technologies (LesEchos, 2019).

2.1 Mooring design and standards

The aim of a mooring design is to ensure safe and cost-effective deployment of floating devices for a certain period of time against environmental actions (i.e. wave, wind, current, marine growth, corrosion, etc.).

Mooring design for Oil & Gas platforms has been extensively addressed by standards such as DNV-OS-E301 (DNV, 2010), API-RP-2SK (API, 2005), BV-NR-493-DT-R03-E (Bureau Veritas, 2015), etc. The main design issues such as strength and fatigue analysis, manufacturing, handling, installation, operation, maintenance and reliability are investigated. More specific guides and recommended practices such as BV-NI-604-DT-R00-E (Bureau Veritas, 2014), DNV-OS-E302 (DNV, 2008), DNVGL-RP-E305 (DNVGL, 2015), API-RP-2SM (API, 2014), BV-NI-432-DTO-R01E (Bureau Veritas, 2007), DNVGL-OS-E304 (DNVGL, 2015), DNV-RP-E303 (DNV, 2005), etc. are also available for different mooring components such as chains, fiber ropes, wire ropes, anchors, etc.. However, it has been witnessed by the O&G industry that mooring failures still happened although the design guides recommended by standards had been respected (Ma et al., 2013). Mostly, it is due to the fact that there is no clear industry consensus on failure mechanisms or even defect initiation that may incur (Angulo et al., 2017). Indeed, due to the lack of experience and validation from deployment and testing facilities, there is a great need to improve current offshore standards in order to ensure a safe and cost-effective design of newly developed devices such as FWTs. Some recent standards includes DNVGL-RP-0286 (DNVGL, 2019) for Coupled analysis of floating wind turbines and floating offshore wind turbine installations (ABS, 2014), etc.

2.2 Mooring components and configurations

A mooring system is a station keeping structure used to tether and keep in position a floating structure under varied effect of the environment (e.g. wind, wave, current, tide, etc.). It should also limit horizontal excursions of the floating body and in some cases, restrict the range of heading. Mooring systems have been used for thousands of years to moor boats (Bradney, 1987) and fish farms (Seaweb, 2013). Permanent mooring systems have been developed for O&G platforms in the late 40's (ABS, 2012) in order to keep them in position for a long period of time (e.g. 20 to 30 years) even in extreme (i.e. storm) conditions. Currently, there is a great interest to develop mooring systems for marine renewable energy devices such as floating wind turbines (Pham et al., 2019; Zhao et al., 2012), wave energy converters (Hanois, 2014; Parish, 2015; Johanning et al. 2005; Harris et al., 2004), etc.

Harris et al. (2004) highlighted that it is crucial to consider the mooring system as an integral part of the Wave Energy Converter (WEC) which contribute not only to the capital costs but also other costs from installation, deployment, maintenance and decommissioning.

Mooring components

A mooring system comprises lines, connectors, clump weights, sub-surface buoys and sea-bottom anchors. Three different materials are usually used for a mooring lines such as: chains, wire ropes and fiber ropes. The mechanical characteristics of these materials are briefly discussed in the following.

1, Chain

Chains have been widely used for offshore mooring applications for a long time. Chain can be studless or studlink as shown in Figure 1-5.

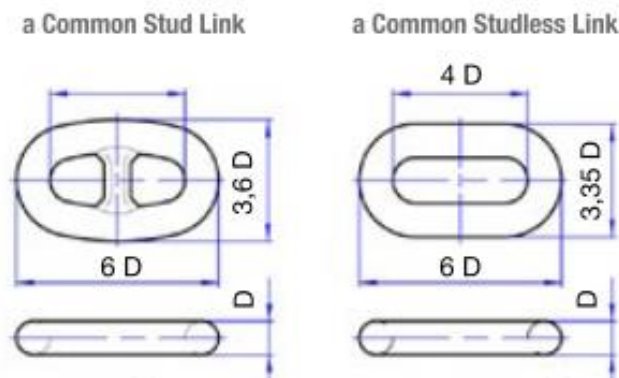


Figure 1-5: Common studlink and studless chains (Ramass, 2014).

Different grade of chains depending on the quality of steel employed can be obtained as R3, RS3, K3, R4, R4S, R5, etc. Material loss due to seabed friction and vertical loads on anchors can be reduced or avoided thanks to the excellent abrasion-resistance and heavy weight of chains. However, the considerable weight and the sensitivity to corrosion may limit simple chain catenary mooring applications to some extent such as MRE devices.

2, Wire ropes

Wire ropes might be a better option for deepwater moorings than chains since they offer greater elasticity, lighter weight and lower cost for a corresponding strength (Barltrop, 1998). There are several types of constructions for wire ropes which result in different load-elongation and fatigue characteristics. Common wire rope constructions are presented in Figure 1-6.

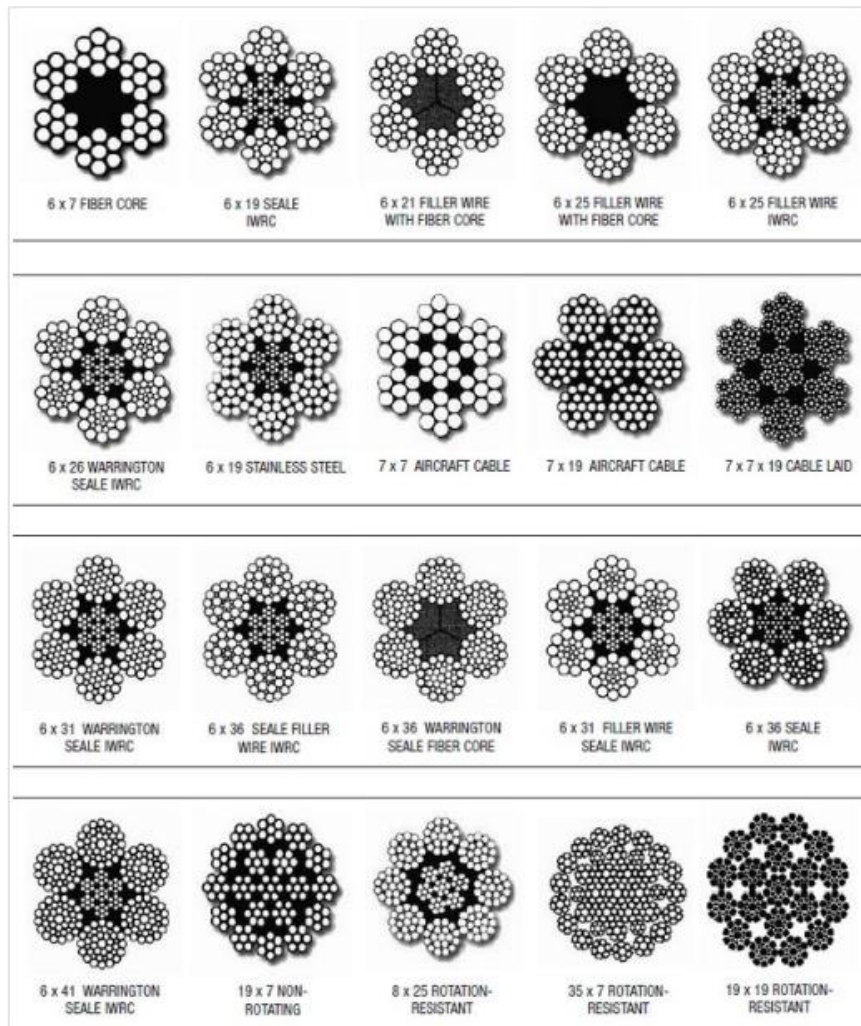


Figure 1-6: Common wire ropes constructions (Engineeringcontent, 2018).

3, Fiber ropes

Compared with steel wire ropes, synthetic fiber ropes are lighter in weights and have lower stiffness for a given breaking strength. Moreover, their elastic and hysteresis characteristics are of great interest for reducing extreme and snap loads in mooring systems. Fiber ropes are typically made of polyester (polyethylene terephthalate), aramid (para-aramid), HMPE (High Modulus Polyethylene), liquid Crystal Aromatic Polyester (LACP) or nylon (polyamide). They are hierarchical structures made of filaments that are twisted together to form yarns, which are in turn twisted together to form assemblies of yarns and then strands, which finally form the ropes either in twisted or braided construction (Davies, 2014). In order to obtain ropes at large scale, the common practice is to group together smaller ropes (so-called sub-ropes) in a protective jacket. Synthetic ropes have nonlinear load-elongation behaviors and fatigue characteristics which are strongly different in static and dynamic conditions. One of the most important properties of fiber ropes is the axial stiffness that can be determined either by the slope of the tension/strain curve in the unit of Newtons (N)

(McKenna et al., 2004) or by a relative tensile property in term of the applied stress in the unit of N/tex (Davies et al., 2014), where tex is the linear density of fibers which equals to 1 gram per kilometer. The tenacity of different synthetic fibers are compared in Figure 1-7 showing clearly low modulus for nylon fibers comparing with other materials. In addition to the fiber category, the rope construction also influences its stiffness, strength and fatigue behaviors (Weller et al., 2017). Some rope constructions are illustrated in Figure 1-8.

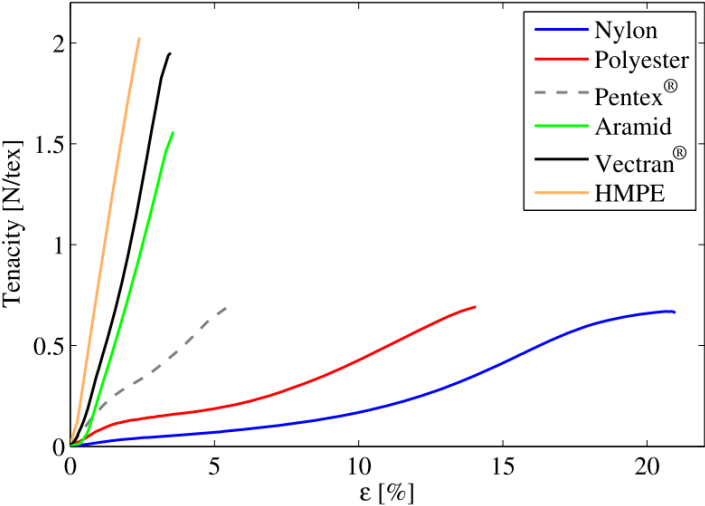


Figure 1-7: Single filament tensile properties for different fibers (Weller et al., 2015).

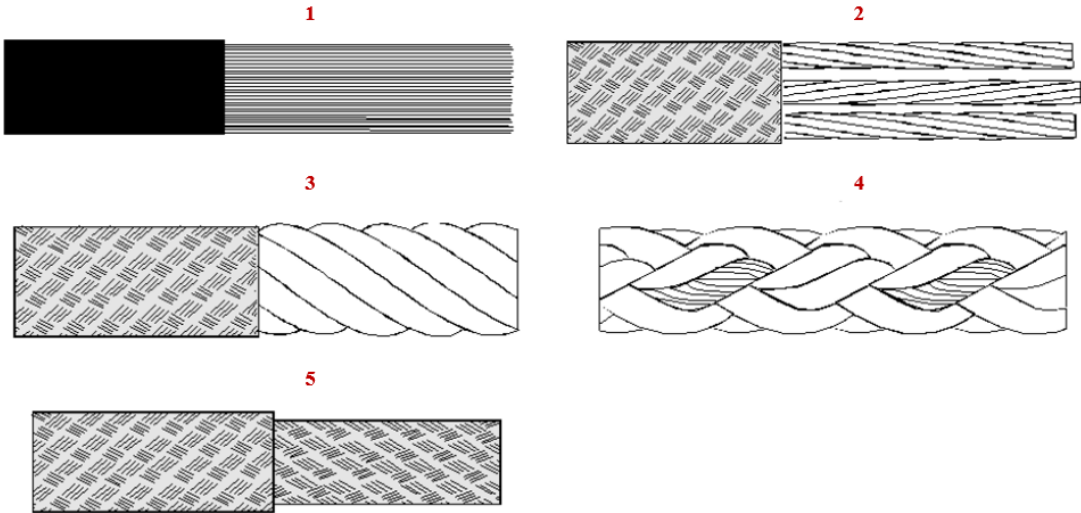


Figure 1-8: Some rope constructions: 1, parallel yarns; 2, parallel strands, 3, stranded (wire-lay), 4, plaited and 5, braided (Tension Technology International -TTI, 2019).

Offshore standards such as DNVGL-RP-E305 (DNVGL, 2015), API-RP-2SM (API, 2014), ABS BV-NI432DTO-R01E (BV, 2007) have given guides and specifications for design and tests of synthetic mooring ropes. However, specific standards for floating MRE applications are still awaited, particularly, for nylon mooring. Basically,

unlike polyester which is commonly used for deep-water mooring, nylon shows nearly a double in compliance but far more nonlinear behaviors in load-elongation characteristics (François et al., 2010). This is illustrated in Figure 1-9 by Ridge et al., (2010). Moreover, it is found that conventional nylon has very low fatigue endurance when wetted. This is mainly due to its poor inter-strand behavior under dynamic loads. Based on the fatigue tests on a superline nylon sub-rope performed by the TTI (Figure 1-10), Ridge et al. (2010) argue that nylon mooring endurance could be improved by replacing the commonly-used double braid or 8 strand constructions by the parallel lay construction. The application of recent coating technologies (i.e. marine finish) plays also a significant role for improving the endurance of such nylon mooring. However, the load levels tested were at the mean tension of 40% of Minimum Breaking Load (MBL) with the tension ranges vary from 40% to 70% of MBL, which raise the concern about whether or not this fatigue testing data can be extrapolated to lower tension levels in order to capture internal abrasion fatigue.

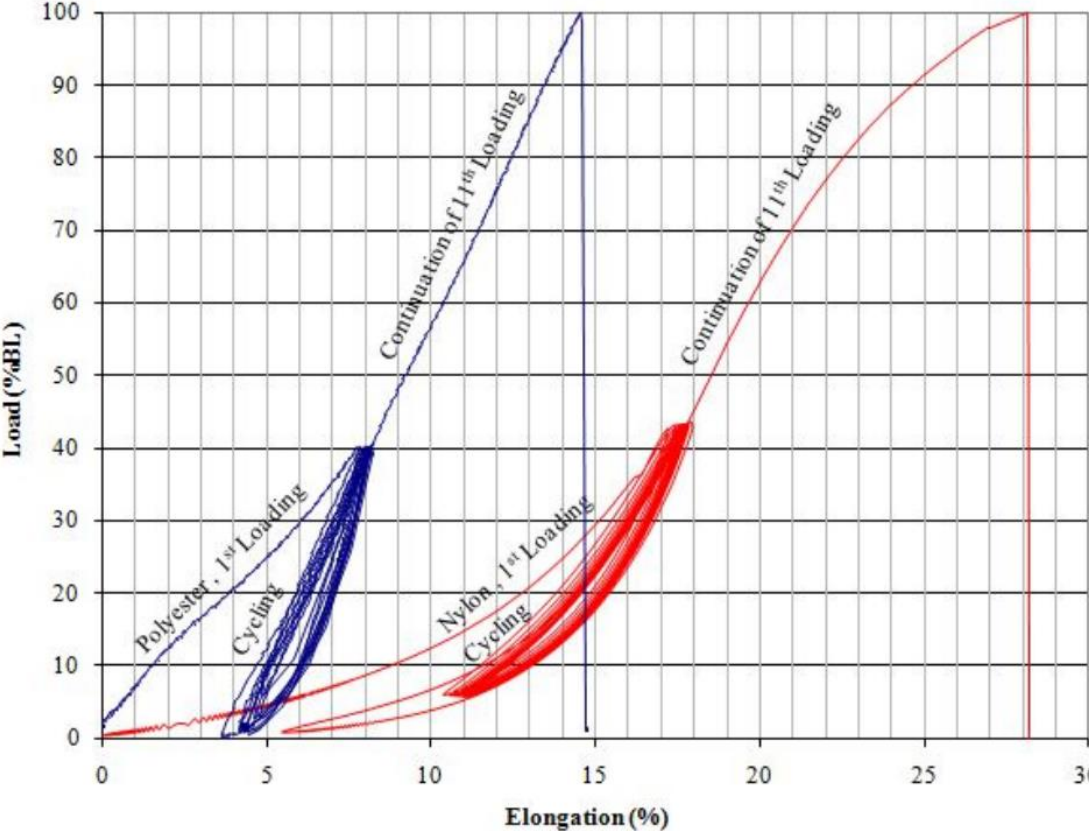


Figure 1-9: Comparison of the load-elongation characteristics of nylon and polyester ropes (Ridge et al., 2010).

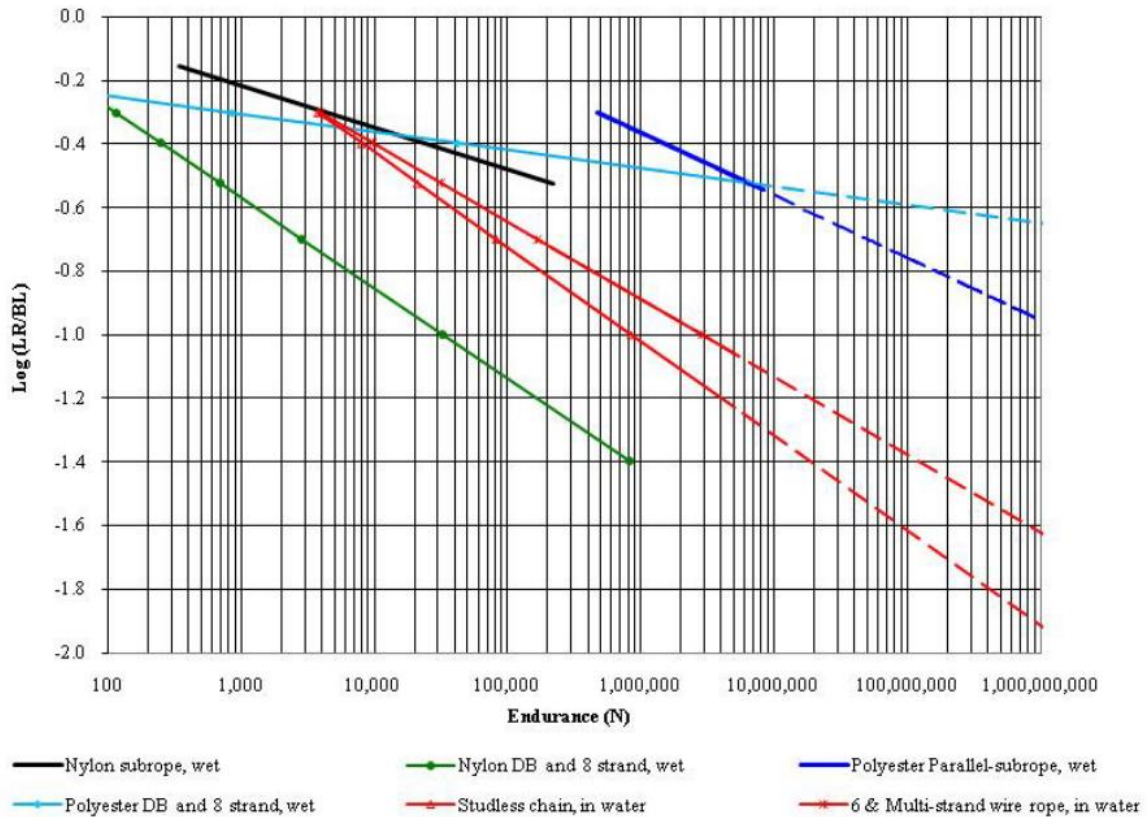


Figure 1-10: Comparison of the fatigue tests results on the Bridon's "Superline" nylon sub-ropes, with other material mooring components (Ridge et al., 2010). (LR stands- Load Range, BL- Breaking Load).

Mooring configurations

A mooring system can be either in Single Point Mooring (SPM) and spread mooring configuration. The former refers to a concept where one or several mooring lines are attached at one end to the seabed and at the other end to an intermediate buoy which is connected to the floating structure. The buoy contains a bearing system that allows a part of it to rotate around the moored geostatic part. When moored to this rotating part of the buoy with a mooring connection, the vessel is able to freely weathervane around the geostatic part of the buoy (Culofsea, 2019). The later refers to a concept where multiple mooring lines are attached at one end to the seabed and at the other end at different locations on the floating structure. While the vessel is in a fixed heading relative to the seabed, its bow typically heads into the dominant environment which is usually the direction where the largest waves are coming from (2b1Consulting, 2019). Figures 1-11 and 1-12 illustrate a SPM system and a spread mooring system respectively.

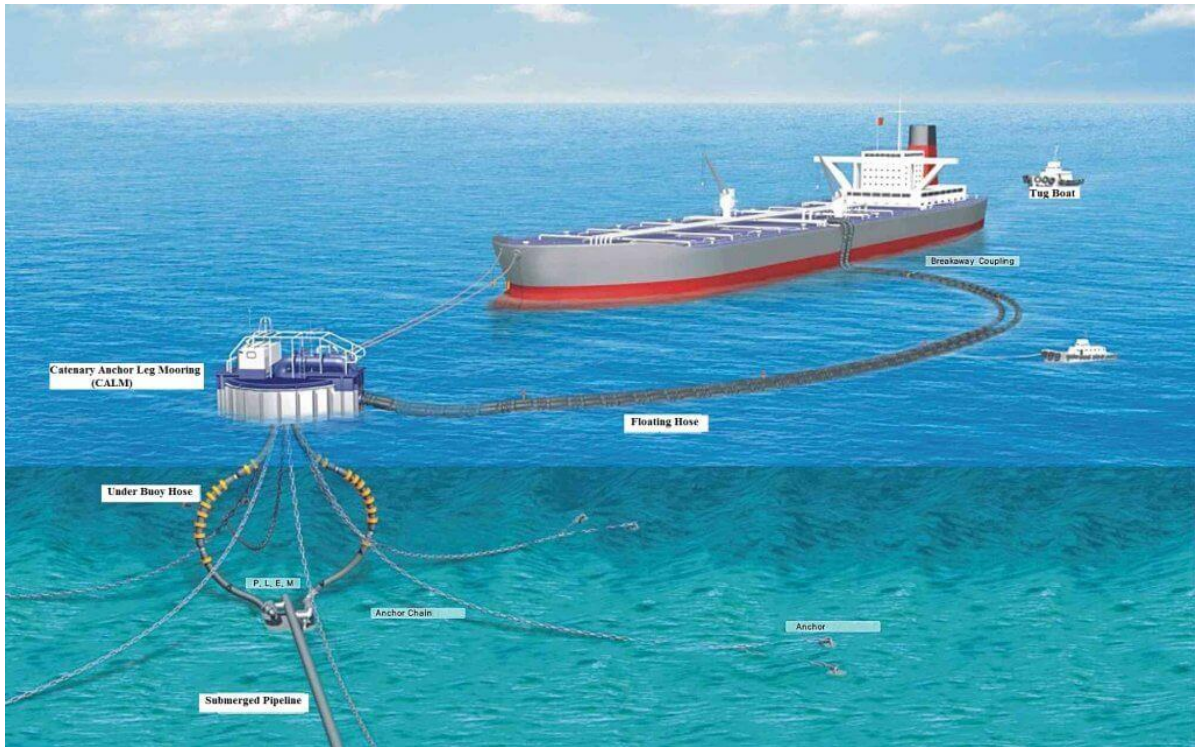


Figure 1-11: A Single Point Mooring (SPM) system (Culofsea, 2019).

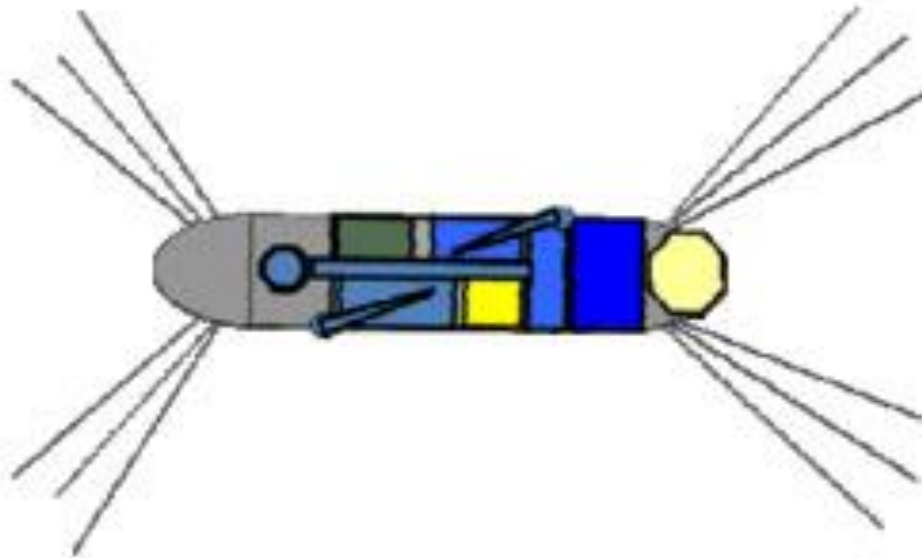


Figure 1-12: A spread mooring system (2b1Consulting, 2019).

Mooring lines can be either in catenary (slack) or taut configuration which offer compliance through changes in the catenary geometry or in the compliance of the mooring lines themselves. Specifically, in catenary mooring systems the restoring force is provided by the weight of the catenary chain while in taut mooring systems it depends strongly on the axial stiffness of the mooring line components. Some possible mooring configurations for MRE devices are presented in Figure 1-13.

Harris et al. (2004) argue that free hanging chain catenary configurations may induce excessive loads on the mooring systems. Fitzgerald et al., 2007 also confirmed the disadvantages of simple catenary mooring systems for WECs. They argue that a mooring system that employs synthetic materials or added hydrostatic stiffness (e.g. using buoys or clump weights) would be a better alternative.

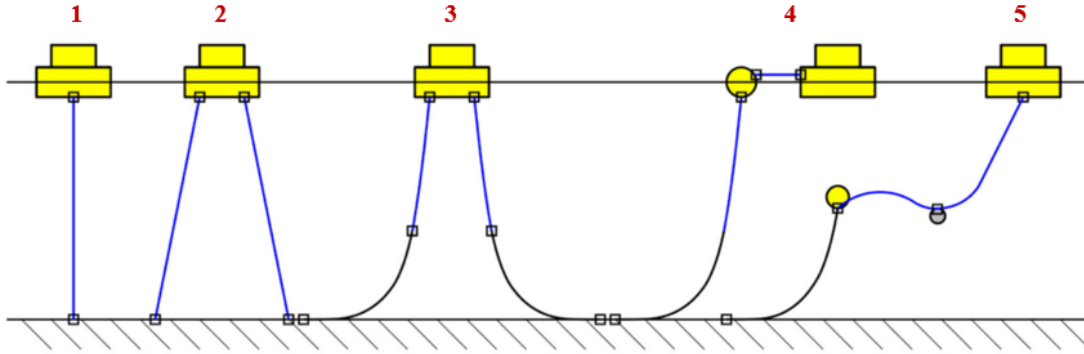


Figure 1-13: Mooring configurations for Marine Energy Converters (MEC): 1- Single taught line (rope); 2- Multiple taught lines (rope); 3- Catenary shape (rope and chain); 4- Catenary shape with surface buoy (fiber rope and chain); 5- Lazy wave (rope and chain) (Karimirad et al., 2014).

In conclusion, a hybrid mooring system that employs chain catenary and synthetic ropes seems to be an effective mooring solution for floating MRE devices.

2.3 Mooring analysis and software applications

Mooring analysis

a, Static catenary equations

For an inextensible, flexible line without bending stiffness, the catenary shape (Figure 1-14) is well known as the static equilibrium configuration of such an element.

The catenary equation for inelastic lines (i.e. those are considered axially un-stretched) can be expressed as (Orcina, 2018).

$$x_{\text{inelas}} = \frac{Th_a}{w} \left[\sinh^{-1} \left(\frac{Tv_a + ws}{Th_a} \right) - \sinh^{-1} \left(\frac{Tv_a}{Th_a} \right) \right] \quad (1.1)$$

$$z_{\text{inelas}} = \frac{Th_a}{w} \left[\sqrt{1 + \left(\frac{Tv_a + ws}{Th_a} \right)^2} - \sqrt{1 + \left(\frac{Tv_a}{Th_a} \right)^2} \right] \quad (1.2)$$

where s is the arc-length from the end A, w is the weight per unit length, Th_a and Tv_a are the horizontal and vertical tension components at the end A respectively.

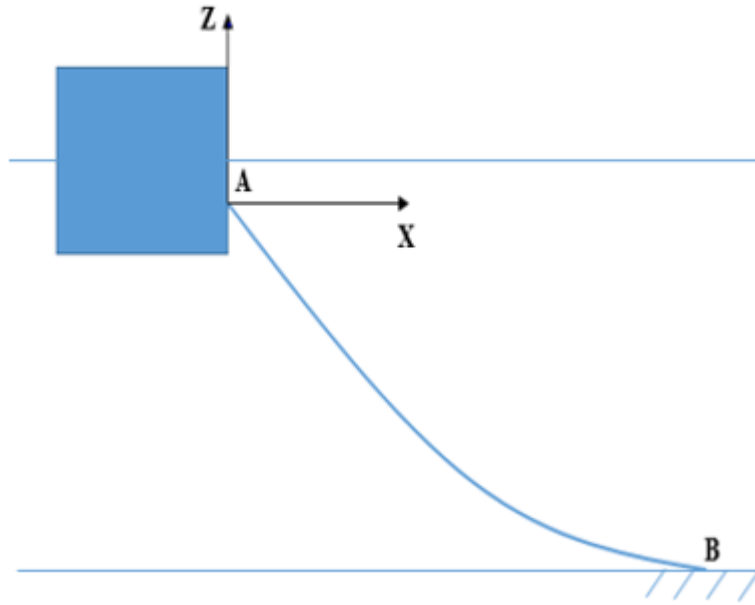


Figure 1-14: The catenary shape of mooring lines.

For synthetic materials with large axial elongation, it is then crucial to consider such an elastic behavior. Therefore, the catenary equations are modified as (Orcina, 2018).

$$x_{\text{elas}} = x_{\text{inelas}} + \frac{Th_a s}{K} = \frac{Th_a}{w} \left[\sinh^{-1} \left(\frac{Tv_a + ws}{Th_a} \right) - \sinh^{-1} \left(\frac{Tv_a}{Th_a} \right) \right] + \frac{Th_a s}{K} \quad (1.3)$$

$$z_{\text{elas}} = z_{\text{inelas}} + \frac{Tv_a s}{K} + \frac{ws^2}{2K} = \frac{Th_a}{w} \left[\sqrt{1 + \left(\frac{Tv_a + ws}{Th_a} \right)^2} - \sqrt{1 + \left(\frac{Tv_a}{Th_a} \right)^2} \right] + \frac{Tv_a s}{K} + \frac{ws^2}{2K} \quad (1.4)$$

where K is the axial stiffness of the elastic line component.

b, Dynamic mooring analysis (DMA)

The tension in mooring lines is the combination of: i- the pre-tension which resulted from the static equilibrium of the floating structure and its mooring system without environmental forces; ii- the static tension induced by the sum of the steady wind, current and wave drift forces; iii- the dynamic tension induced by the sum of the Low Frequency (LF) forces (0-0.02 Hz) induced by the slowly varying wave drift forces, unsteady wind forces, slowly varying tide forces, and the Wave Frequency (WF) forces (0.03-0.3 Hz) induced by the first order wave forces (DNV, 2010).

A coupled analysis considering both the floating structure motions and the mooring system stiffness is required for a full dynamic mooring analysis where the following motion equations must be solved (Barltrop, 1998)

$$\left(M+M_a\right) \frac{d^2 x}{dt^2} + B \frac{dx}{dt} + Kx = F_{\text{Mooring}} + F_{\text{Static}} + F_{\text{WF}} + F_{\text{LF}} \quad (1.5)$$

where M, M_a are the mass and added mass matrices

B is the damping matrix

K is the stiffness matrix (which includes the hydrostatic stiffness of the floating body and the mooring stiffness)

F_{Mooring} - the pre-tension force

F_{Static} - the static forces

F_{WF} - the wave frequency force due to the first order wave

F_{LF} - the low frequency force due to the second order wave drift force

x - the displacement vector

c, Environmental loads

The environmental loads are site-specific and are characterized by combinations of wave, current and wind conditions with an associated return period.

Wind varies with time and with the height from the sea surface. In practice, wind can be modeled either as constant or random in speed and direction. Typically, wind is represented by the mean wind speed calculated for 1 minute, 10 minutes or 1 hour and a gust spectrum to consider fluctuation. The sea current is resulted from the superposition of several flows: the constant current of general circulation of seas, the wind current and tidal stream. Practically, a current profile which considers the current speed and direction corresponding to the water depth is used.

Ocean waves are produced by the wind. The regular waves which never occur in the real ocean environment have a single frequency (wavelength) and amplitude (height). Ocean waves are almost always irregular and can be viewed as the superposition of a number of regular waves (wave components) with different frequencies and

amplitudes. A regular and an irregular wave are illustrated in Figure 1-15. It is admitted that for a duration of 3 hours, the sea conditions remain stationary and the statistical properties of the wave do not change.

There are two types of sea states such as

- Short term sea states which are extreme conditions or Ultimate Limit State (ULS) of wave (plus associated wind and current) during a storm with a duration of 3-6 hours and a return period N (10, 20, 50 or 100 years, etc.). Those are used for the strength design problem.
- Long term sea states are the short term statistical set under normal operating conditions or Fatigue Limit State (FLS) of wave (plus associated wind and current) during one year. Those are used for the fatigue design problem (i.e. to calculate the cumulative fatigue damage of mooring lines).

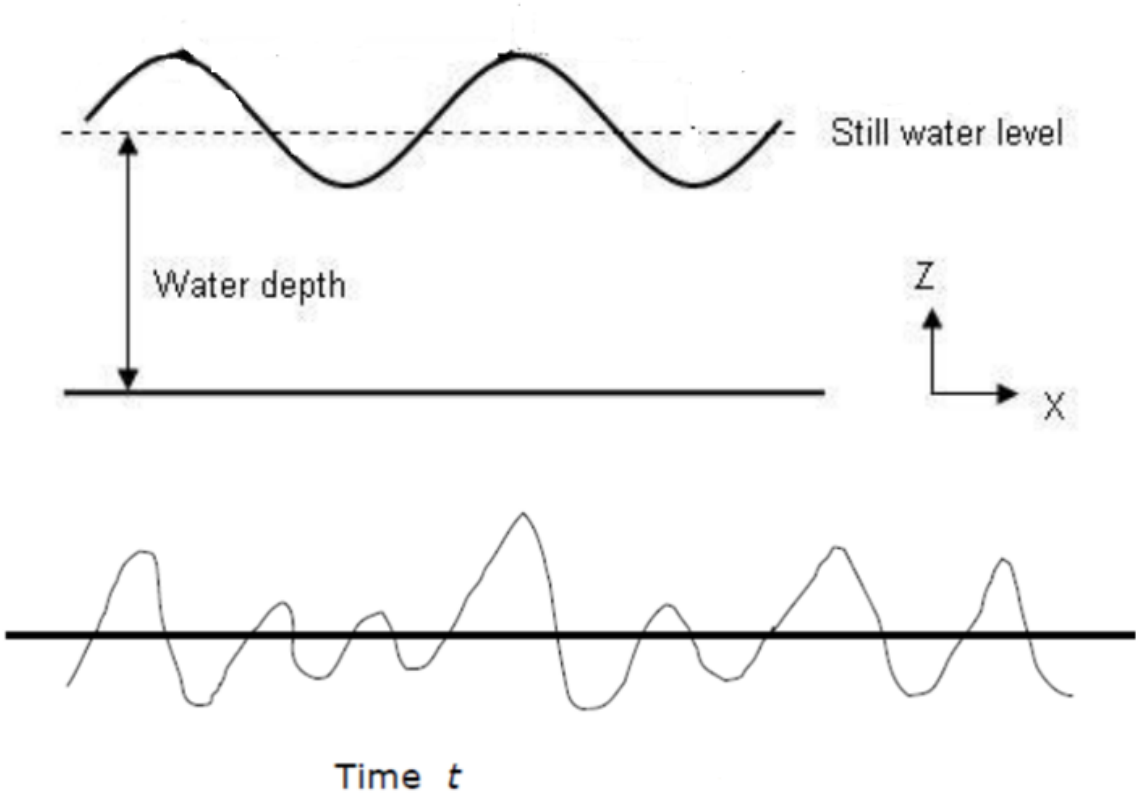


Figure 1-15: A regular wave (up) and an irregular wave (down).

Ocean waves are often described by typical wave spectra for fully developed sea conditions (i.e. after having been blown for a sufficiently long period of time by a wind with constant velocity). In general, the wave energy spectrum derived from an analysis of irregular wave record obtained at a particular place and time in the ocean will be a unique result that will never be exactly repeated. Current practice is to use different

formulae of idealized wave spectra for open oceans and coastal areas (i.e. with limited fetch). The commonly-used JONSWAP formulation is based on an extensive wave measurement program known as the Joint North Sea Wave Project. The spectrum represents wind-generated seas with fetch limitation. The formulation is more general and englobes the spectrum of Pierson- Moskowitz, which is a particular case. It is written as

$$S_{\omega}(\omega) = A \times \frac{5}{16} H_s^2 \omega_p^4 \omega^{-5} \exp \left[-\frac{5}{4} \left(\frac{\omega}{\omega_p} \right)^4 \right] \gamma^{\left[\frac{-(\omega - \omega_p)}{2\sigma^2 \omega_p^2} \right]} \tag{1.6}$$

- where ω – the wave angular frequency
- H_s – the significant wave height
- ω_p – the peak wave angular frequency
- σ – the relative measure of the width of the peak
- γ – the peak-enhancement factor, the effect of increasing the peak of Pierson-Moscowitz spectrum.

For most of the cases $\sigma = 0.07$ for $\omega < \omega_p$ and $\sigma = 0.09$ for $\omega > \omega_p$

$$A = \frac{1}{5(0.065\gamma^{0.803} + 0.135)}$$

A Jonswap spectrum of a random wave is illustrated in Figure 1-16.

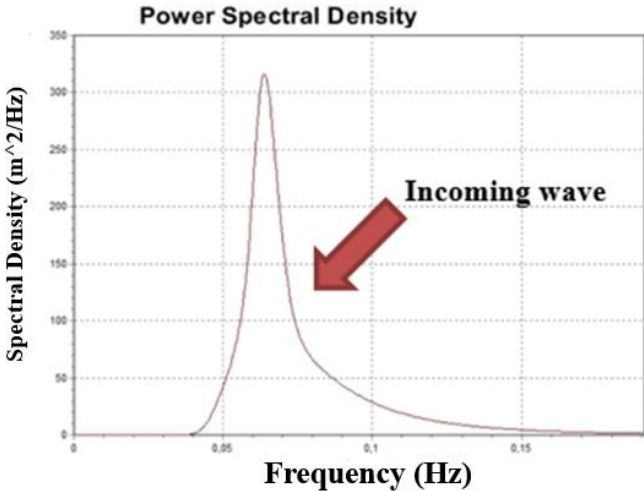


Figure 1-16: A random wave characterized by the Jonswap spectrum.

Software applications

For structural analysis of offshore mooring lines, first, the hydrodynamic properties of the floating structure such as motion Response Amplitude Operators (RAOs), added masses, radiation damping, Quadratic Transfer Functions (QTFs) are calculated for each angular frequency and for each of 6 degrees of freedom based on a diffraction/radiation code such as HydroStar, Wamit, Nehmo, etc. Then, a Finite Element software such as Orcaflex (Orcina, 2012), Deeplines (Principia, 2012), etc. are used to perform the coupled mooring analysis where the mooring lines are considered together with the floating structure. In order to perform such analysis, Orcaflex (or Deeplines) considers the floating structure as a rigid body and requires its hydrodynamic database which can be estimated as mentioned above. The Orcaflex finite element model of a line and a simplified hydrodynamic analysis for mooring analysis of FWT mooring lines are illustrated in Figures 1-17 and 1-18 respectively. For FWT application, a specific modeling tool, FASTlink, has also been developed in order to integrate the aerodynamic load effect in Orcaflex (Masciola, et al., 2011).

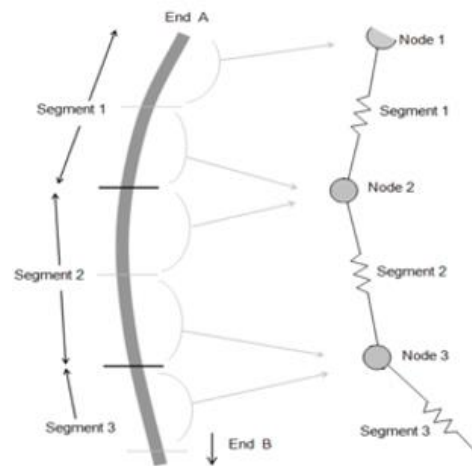


Figure 1-17: The finite element model of a line (Orcina, 2012).

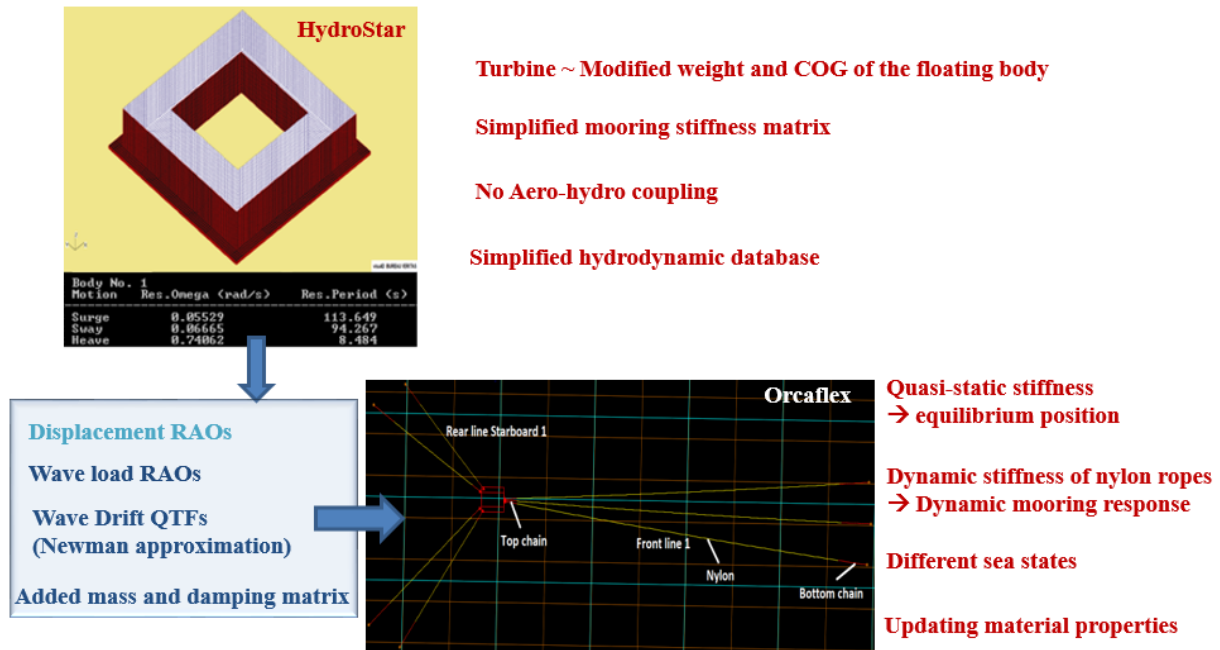


Figure 1-18: A simplified hydrodynamic analysis for mooring analysis of FWT mooring lines.

2.4 Survivability and fatigue analysis

Survivability analysis

A survivability analysis is for ensuring the survivability of mooring systems under extreme conditions (so-called Ultimate Limit State - ULS) where the maximum tension in the mooring lines is designed to remain below the minimum breaking strength of the mooring components, and accidental conditions (so-called Accidental Limit State – ALS) where mooring systems are designed to survive the event of one-line-failure.

Fatigue analysis

A mooring analysis for Fatigue Limit State (FLS) is for ensuring that the individual mooring line have adequate capacity to withstand moderate cyclic loading for a design service life (e.g. 20 to 30 years).

The fatigue analysis of offshore mooring lines is usually based on the Palmgren-Miner's rule (the cumulative damage model or the S-N approach) where fatigue damage is assumed to be linearly accumulated, and the fatigue life is defined at detectable crack initiation (i.e. 1st stage of fatigue) on the structure elements. DNV-OS-301 (DNV, 2010) and API-RP-2SK (API, 2005) recommend S-N curves (Figure 1-19) and T-N curves (Figure 1-20) for calculating the fatigue damage for different mooring materials where failures will occur after a number of cycles N at a particular stress (tension) range S (T).

The fatigue curves are used to calculate the fatigue life of mooring components as

$$N = K.S^{-m} \quad (1.7)$$

where N - the number of cycles to failure under a stress range S

K, m - the parameters of S-N curves

The fatigue damage accumulation is calculated following the Palmgren-Miner's rule as

$$D = \sum_{i=1}^n \frac{1}{N(S_i)} = \frac{1}{K} \sum_{i=1}^n S_i^m \quad (1.8)$$

where S_i - the stress range of the stress cycle number i .

n - the number of stress cycles S_i .

The Fracture Mechanics (FM) approach could be another interesting alternative for fatigue assessment. The approach assumes that failures will occur when dominant cracks have grown to the critical dimension (i.e. 2nd stage of fatigue). The cracks are often resulted from defects that may exist in the material due to an initial manufacturing defect or the initiation of a detectable crack caused by fatigue. The FM approach allows detectable cracks to exist, and thus a longer fatigue life comparing with the S-N approach. However, it also requires an important amount of costly and sophisticated tests.

According to the industry experience, it is require that mooring lines should be inspected every 4-5 years in order to ensure the required safety level. The inspection relies on the detection and measurement of cracks developed in the chain links. The obtained information of crack size can be used to re-evaluate the level of fatigue damage.

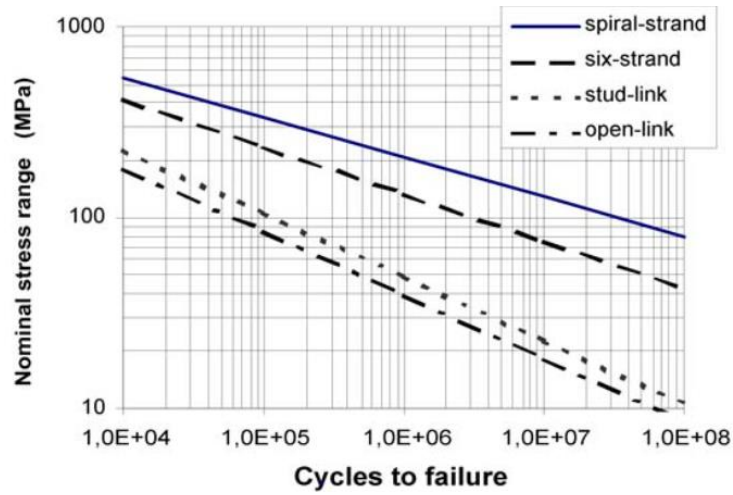


Figure 1-19: Mooring S-N fatigue curves (DNV, 2010).

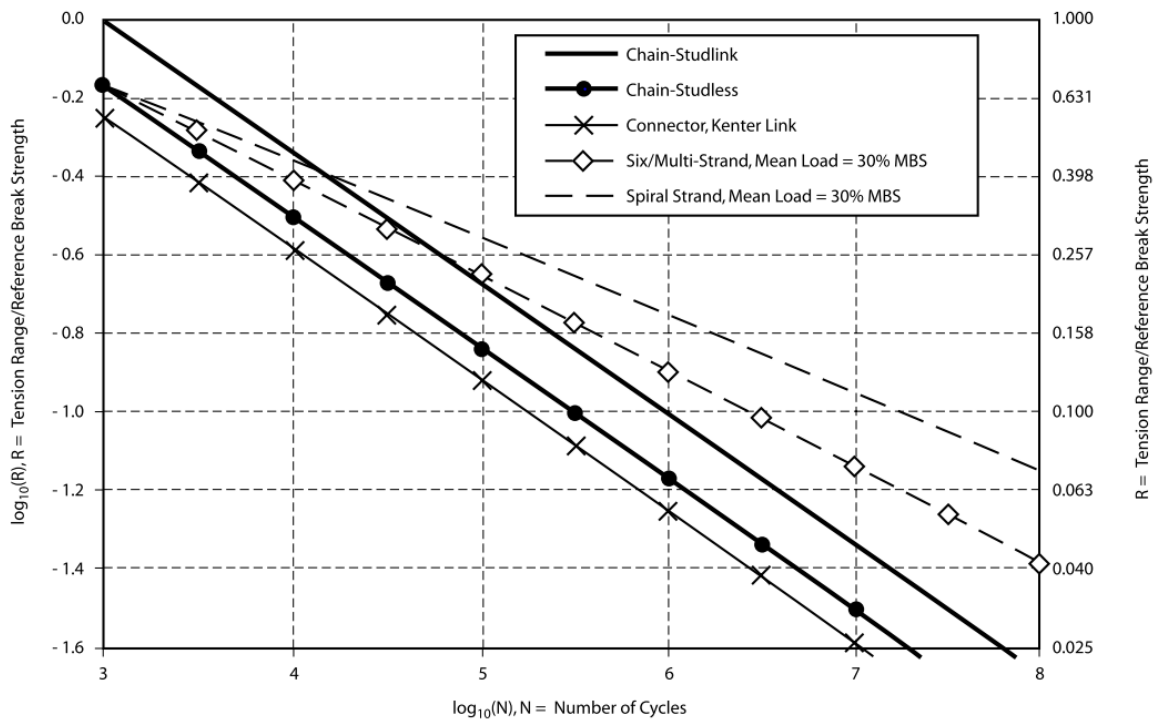


Figure 1-20: Mooring T-N fatigue curves (API, 2005).

Mooring fatigue analysis can be implemented either by time domain method or frequency domain method. The former is considered as the most accurate approach for fatigue analysis but is also time consuming. The later refers to an analytical approach which is very effective in term of computational time. However, cutting-edge approaches for frequency domain fatigue analysis should be investigated in order to ensure reliable fatigue estimate.

Due to the issues mentioned above, in the present work, the S-N approach based on the Palmgren-Miner's rule and the frequency domain fatigue analysis are employed in order to estimate the fatigue damage.

2.5 Methodology for reliability assessment

There are two mooring design approaches developed by the offshore industry: Deterministic (Total Safety Factor Format) and LRFD (Load and Resistance Factor Design) (API, 2005).

The deterministic approach considers a design environmental condition corresponding to a return period and employs a total safety factor on mooring component strength to ensure redundancy against mooring breakage. This approach has been widely used by the offshore industry for over 40 years thanks to its simplicity regarding the design procedure. However, there are still shortcomings since the approach has been developed based on past experience of the offshore industry which may need further effort to ensure sufficient reliability for new applications such as MRE devices. Also, another limitation is that the safety is included in only one safety factor (γ) of the material strength while there must be uncertainties on both environmental conditions and material resistance. Besides, the industry reliability studies also confirmed that mooring designs based on this approach may result in significant difference in term of reliability (API, 2005). The deterministic approach is recommended by API-RP-2SK (API, 2005) as

$$MBL - \gamma T_{\max} \geq 0 \quad (1.9)$$

Where MBL - the Minimum Breaking Load of the mooring component

γ - the safety factor

T_{\max} - the maximum tension in the mooring section

The LRFD approach is referred as a partial safety factor format where a number of load factors for the load components and a number of material factors for the line components strength are employed in the limit state as Eq. (1.10). This concept of partial safety factors (i.e. γ_m , γ_T) allows accounting for the diversity of the effect of uncertainties of loads and material on reliability. The second fundamental quantity involved in the limit state is the characteristic values of load ($T_{\max,k}$) and material (MBL,k) which are quantities of their distribution. It is believed that this approach may yield mooring designs with more consistent reliability since more detailed reliability analysis is required.

$$\frac{MBL,k}{\gamma_m} - \gamma_T T_{\max,k} \geq 0 \quad (1.9)$$

For mooring lines of floating wind turbines where experience is limited or non-existent, it seems preferable to use directly a reliability approach where factors of safety are replaced by the definition of an acceptable probability of failure. The number of simulations required, however, increases dramatically as many parameters are uncertain.

2.6 Methodology for service life monitoring of mooring lines

Health monitoring of mooring lines is essential since many mooring failures have been observed by the offshore industry although guides and specifications for design recommended by standards had been respected. One of the main reasons is that some failure mechanisms may still need further understanding. Therefore, early diagnostic of mooring damage plays a key role for ensuring a safe performance of floating structures (Aqdam et al., 2018). Mooring monitoring should be performed by carefully considering potential failure mechanisms (Ma et al., 2013; Brindley et al., 2014), fatigue damage estimate (Thies et al., 2014), extended-period environmental loads (Huang et al., 2010; Harnois, 2014). Moreover, since maintenance or replacement of mooring lines for MRE devices in shallow water seems simpler and less costly than for deep-water O&G platforms, they could be better options rather than an over-engineered mooring system which would not be commercially viable for large scale deployments.

3. Objectives

The first main objective of this work is to develop a reliability-based methodology for modeling and service life monitoring of mooring lines of FWTs which aims to support making decisions regarding maintenance or replacement of lines based on the reliability levels estimated during the expected service life. It can be done by using numerical model for fatigue estimate and reliability assessment not only a priori (i.e. during the design phase), but also during the operation phase, until the end of the exploitation. The methodology can also be considered as a more detail mooring design approach that could be adopted once the information from similar structures, projects, sites are known.

Secondly, hybrid moorings are likely to be used for commercial applications, for instance FLOATGEN, which justifies the need for better understanding of the load-elongation behaviors and fatigue characteristics of nylon mooring ropes since there is few experience from the offshore industry and current standards on such issues.

The following research questions will be addressed:

- 1, Is mooring monitoring necessary? Which methodology should be employed?
- 2, How to improve the modeling and fatigue damage estimate of nylon mooring ropes?
- 3, How to estimate fatigue damage based on numerical modeling and in-situ measurements? Which approaches?
- 4, How reliability analysis can be performed to support making decisions regarding maintenance or replacement of lines?

4. The research methodology

In order to answer the research questions mentioned above, the following research methodology is used:

- 1, Identify the state-of-the-art in mooring design, mooring material behaviors, fatigue estimate approaches, reliability assessment and mooring monitoring. This is done by reviewing the existing literature and current standards as presented in **Chapter 1**.

- 2, Focus on the modeling and testing procedures in order to capture the non-linear load-elongation behaviors and fatigue damage mechanisms of nylon mooring ropes. Also, for a comprehensive modeling and service life monitoring methodology, there is needs of identifying not only the mechanical behaviors of all mooring components but also the marine environmental factors (e.g., marine growth, corrosion, environmental loads, etc.) that influences such behaviors. These are discussed in **Chapter 2**. An article has been published in the journal of Applied Ocean Research (see Appendix) where a practical modeling procedure was proposed which allows accounting for non-linear dynamic axial stiffness of nylon mooring ropes.

- 3, A methodology for modeling and service life monitoring of mooring lines is proposed based on the reliability approach. In order to select a quick but reliable method to calculate fatigue damage, cutting edge frequency domain approaches have been investigated as an alternative to time domain fatigue analysis. Besides, for reliability assessment of mooring lines in extreme conditions (ULS), it seems necessary to perform an important number of Monte Carlo simulations (MCS) in order to better capture the nonlinearities of mooring responses and to obtain a low probability of failure. In that case, the application of a meta-model such as an Artificial Neural Network (ANN) could be an interesting alternative for nonlinear mooring

response simulation rather than time-consuming time domain modeling. This work is presented in **Chapter 3**. An article has been published in the journal of Ocean Engineering (see Appendix) where the present methodology for modeling and service life monitoring of mooring lines is discussed.

4, Draw conclusions for the present work and outline future work. This is presented in **Chapter 4**.

5. Scope

This work presents a methodology for monitoring of mooring lines of FTWs which can be equally applied to other types of MRE devices and Oil & Gas platforms. However, the methodology is limited to the technical aspects where mooring design and decisions regarding maintenance or replacement of lines are based on strength, fatigue estimate and reliability assessment. The economic aspects are not significantly considered or addressed which would be the subject of separate work.

6. References

ABS (American Bureau of Shipping). Floating Offshore Wind Turbine Installations. 2014.

ABS (American Bureau of Shipping). A History of Advancing Offshore Oil & Gas Technologies, ABS Offshore News, pp 15-21. 2012.

Angulo Á., Edwards G., Soua S., Gan T. Mooring Integrity Management: Novel Approaches Towards In Situ Monitoring. IntechOpen open access peer-reviewed chapter. 2017.

API (American Petroleum Institute). API-RP-2SK. Design and Analysis of Stationkeeping Systems for Floating Structures. 2005.

Aqdam H. Rezaniaiee, Etefagh M.M., Hassannejad R. Health monitoring of mooring lines in floating structures using artificial neural networks, Ocean Eng. 164 (2018) 284–297.

Barltrop N. D. P. Floating Structures: a guide for design and analysis, Ledbury: Oilfield Publications Ltd. (1998).

Bradney. A practical guide to the mooring and anchoring of small boats. UK. 1987.

Bureau Veritas Guidance Note NI 604 DT R00 E. Fatigue of Top Chain of Mooring Lines due to In-plane and Out-of-plane bending. 2014.

Bureau Veritas. Guidance Note NI 432 DTO R01E, Certification of Fibre Ropes for Deepwater Offshore Services. (2007).

Bureau Veritas. NR 493 DT R03 E. Classification of Mooring Systems for Permanent and Mobile Offshore Units. 2015.

Culofsea. SPM (Single Point Mooring) or SBM Operations. <https://cultofsea.com/tanker/spm-single-point-mooring/>. Accessed 2 Mai 2019.

Davies P., Weller S.D., Johanning L., Banfield S.J. A review of synthetic fiber moorings for marine energy applications, 5th Int. Conf. Ocean Energy. (2014) 1–6.

DNV (Det Norske Veritas). DNV-RP-C205: Environmental conditions and environmental loads. 2010.

DNVGL. DNVGL-RP-0286. Coupled analysis of floating wind turbines. Edition May 2019.

DNVGL. DNVGL-OS-E304. Offshore mooring steel wire ropes. 2015.

DNV (Det Norske Veritas). DNV Offshore Standard - Position Mooring. DNV-OS-E301. 2010.

DNV (Det Norske Veritas). DNV-RP-E303. GEOTECHNICAL DESIGN AND INSTALLATION OF SUCTION ANCHORS IN CLAY. 2005.

Engineeringcontent. <https://engineeringcontent.blogspot.com/2015/01/wire-rope.html> (Accessed: Avril 2018).

Flory J.F., Banfield S.J., Ridge I.M.L., Yeats B., Mackay T., Wang P., Hunter T., Johanning L., Herduin M., Foxton P. Mooring systems for marine energy converters. OCEANS 2016. 19-23 Sept. 2016. Monterey, CA, USA

François M., Davies. P, Grosjean F., Legerstee F., Modelling Fiber Rope Load-elongation Properties - Polyester and Other Fibers, (2010) 3–6.

Hanois V. Analysis of highly dynamic mooring systems: peak mooring loads in realistic sea conditions. PhD thesis. University of Exeter, UK. 2014.

Harris R. E., Johanning L., Wolfram J. (2004) Mooring systems for wave energy converters: A review of design issues and choices. MAREC – Conference Proceedings, 3rd International Conference on Marine Renewable Energy, 1st July 2004, Blythe, UK.

Huang C-C, Pan J-Y. Mooring line fatigue: a risk analysis for an SPM cage system. Aquacult. Eng. 42, 8–16. 2010.

Johanning L., Wolfram J. Challenging tasks for floating WECs. In the Proceedings of the International Symposium on Fluid Machinery for Wave and Tidal Energy: State of the Art and New Developments, London, UK, 2005.

Karimirad M., Koushan K., Weller S., Hardwick J., Johanning L. (2014). Applicability of offshore mooring and foundation technologies for marine renewable energy (MRE) device arrays. RENEW – Conference Proceedings, 1st International Conference on Renewable Energies Offshore, Lisbon, Portugal.

LesEchos. <https://www.lesechos.fr/pme-regions/provence-alpes-cote-dazur/eolien-flottant-quatre-technologies-font-surface-1017790>. (Accessed 2 Mai 2019).

Masciola, M., Robertson, A., Jonkman, J., Driscoll, F. (2011) ‘Investigation of a FAST- OrcaFlex coupling module for integrating turbine and mooring dynamics of offshore floating wind turbines’, In the Proceedings of the International Conference on Offshore Wind Energy and Ocean Energy, Beijing, China, 31 October-2 November 2011, Available at: <http://www.nrel.gov/docs/fy12osti/52896.pdf>. Accessed: 4th September 2014.

MC EVOY, P. (2012). Combined Elastomeric & Thermoplastic Mooring Tethers. ICOE – Conference Proceedings, 4th International Conference on Ocean Energy (ICOE). Dublin, Ireland.

McKenna H.A., Hearle J.W. S., O’Hear N., Handbook for fiber rope technology, 2004.

Orcina. Comparison of Orcaflex with theoretical results. <https://www.orcina.com/SoftwareProducts/OrcaFlex/Validation/99-105%20Theoretical%20results.pdf>. (Accessed 29 October 2018).

Orcina. User Manual Online. <http://www.orcina.com/SoftwareProducts/OrcaFlex/Documentation>, (2012).

Parrish D.N. A Novel Mooring Tether for Highly Dynamic Offshore Applications. PhD thesis. University of Exeter, UK. 2015.

Pham H.D., Cartraud P., Schoefs F., Souldard T., Berhault C. Dynamic Modeling of Nylon Mooring Lines for a Floating Wind Turbine. *Appl. Ocean Res.*, 87 (2019), pp. 1-8.

Principia. <http://www.principia-group.com/wp-content/uploads/2016/12/2-DeepLines-Wind-Presentation.pdf>. (Accessed 25 Jan 2019).

Ridge I.M.L., Banfield S.J., Mackay J. Nylon Fibre Rope Moorings for Wave Energy Converters. *OCEANS 2010*; DOI: 10.1109/OCEANS.2010.5663836.

SeaWeb Aquaculture Clearinghouse (2004) At a Crossroads: Will Aquaculture Fulfill the Promise of the Blue Revolution?, Available at: http://www.seaweb.org/resources/documents/reports_crossroads.pdf (Accessed: 7th June 2019).

Tension Technology International (2019). Rope constructions, <https://www.tensiontech.com/tools-guides/rope-constructions>. Accessed: 3 June 2019.

Thies P.R., Johanning L., Harnois V., Smith H.C.M., Parish D.N. Mooring line fatigue damage evaluation for floating marine energy converters: Field measurements and prediction, *Renew. Energy*. 63: 133–144, 2014.

Weller S., Halswell P. Tension-tension testing of a novel mooring rope construction, (2017).

Weller S.D., Davies P., Vickers A.W., Johanning L. Synthetic rope responses in the context of load history: The influence of aging, *Ocean Eng.* 96 192–204. (2015)

Zhao, J., Zhang, L., Wu, H. (2012). Motion Performance and Mooring System of a Floating Offshore Wind Turbine. *Journal of Marine Science and Application*, 11(3), pp 328-334.

CHAPTER 2- MECHANICAL BEHAVIORS OF MOORING COMPONENTS FOR THE MODELING AND SERVICE LIFE MONITORING OF OFFSHORE MOORING LINES

CHAPTER 2- MECHANICAL BEHAVIORS OF MOORING COMPONENTS FOR THE MODELING AND SERVICE LIFE MONITORING OF OFFSHORE MOORING LINES 55

- 1. INTRODUCTION 56
- 2. CHAIN 57
- 3. NYLON 59
 - 3.1 *Load-elongation characteristics* 60
 - 3.2 *Fatigue characteristics* 68
 - 3.3 *Application for numerical modeling of nylon mooring ropes* 79
- 4. MARINE ENVIRONMENTAL IMPACTS 88
- 5. CONCLUSIONS 91
- 6. REFERENCES 93

1. Introduction

For shallow-water offshore floating structures such as semi-submersibles, FPSOs, etc., the mooring lines are usually constituted of long, large diameter chain lines in order to provide necessary catenary offset. For deep-water applications, hybrid mooring lines composed of chain, wire and fiber ropes (e.g. polyester, HMPE, aramid, etc.) are often used in order to reduce the weight of mooring lines and the mooring cost. For Marine Renewable Energy (MRE) devices operating in shallow water, the use of low modulus ropes such as polyester, nylon can provide more compliant and cost-effective design (Weller et al., 2015) (e.g. the unit length cost of nylon is about half that of chain with the same breaking strength). Obviously, longer mooring footprints would be required for polyester in order to reduce extreme tension responses. It is also interesting to highlight that due to the higher stiffness of polyester, the tension responses in fatigue condition are also more important than for nylon. Consequently, that might result in a critically low fatigue life not only for polyester itself but also (more importantly) for the chain sections in the mooring lines. That is to say, nylon could be preferable option for MRE mooring applications.

In the present case study, the mooring configuration is derived from a 2 MW FWT installed at the SEM-REV test site since 2017 as part of the FP7-EU FLOATGEN project (Berhault et al., 2016). The layout of the mooring system connected to a semi-submersible type FWT is illustrated in Figure 2-1 in which a line composed of upper and touchdown chains, with nylon ropes in between. A similar floating structure and mooring configuration have been published by Spraul et al. (2017) based on the publically available information from IDEOL and the Ecole Centrale de Nantes. However, one should be aware that the floater and mooring characteristics used in this case study were selected only for the study purpose and are not representative of the IDEOL's real floating structure and the FLOATGEN mooring system.

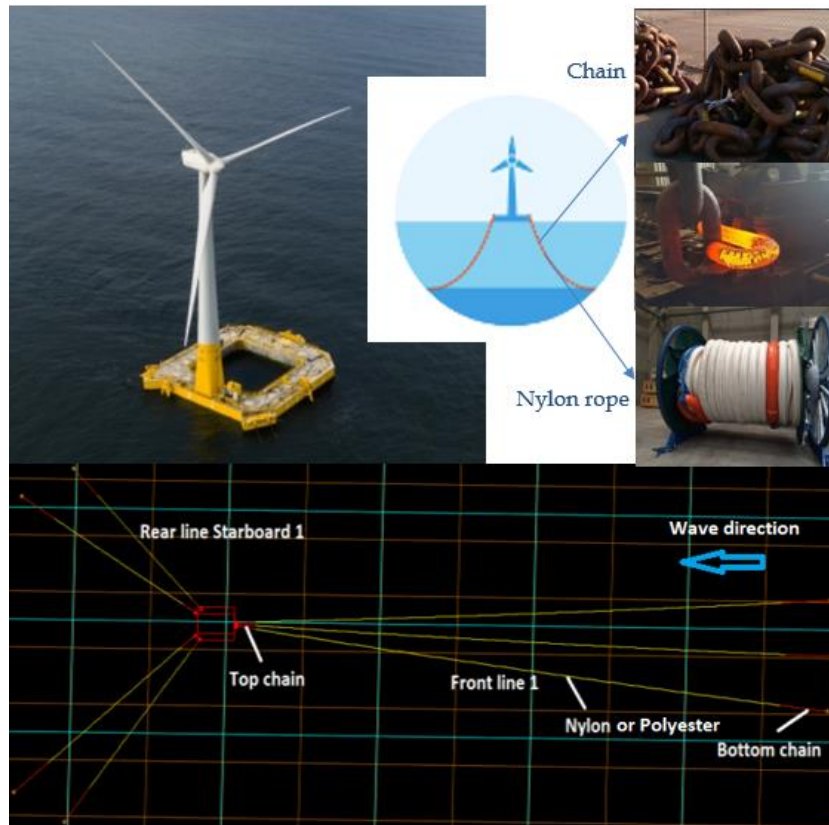


Figure 2-1: The layout of the floating structure and its hybrid mooring lines (chains plus nylon ropes).

This chapter focuses on the mechanical behaviors of the two mooring components, i.e. chain and nylon, and the marine environmental factors that influence such behaviors. The objectives are to identify and calibrate the major factors influencing the modeling and monitoring of mooring lines during operation. Based on such information, the design, modeling and service life monitoring of mooring lines can be better implemented. For these general purposes, the strength and fatigue behaviors of chain and the deteriorating factors will be briefly discussed herein. The mechanical behaviors of nylon mooring ropes have been carefully investigated where modeling and testing issues are addressed for both load-elongation characteristics and fatigue mechanisms. An empirical expression for determining the dynamic stiffness of nylon mooring ropes is drawn based on existing data in the literature. The internal-abrasion fatigue requires further studies where a Non Destructive Test procedure has been proposed. A large part of this chapter is based on one of the authors' published papers (Pham et al., 2019) where the dynamic modeling of nylon mooring ropes is tackled.

2. Chain

With more than 50000 tons in service according to the data from Fernandez et al. (2014), a huge effort has been putting on studying the characteristics and behaviors of chain mooring lines. The outcomes of several JIPs have been integrated to the offshore

standards such as API-RP-2SK (API, 2015), DNV-OS-E301 (DNV, 2010), BV-NI-493 (BV, 2012), etc. Together with wire ropes and connectors (e.g. shackles, H-link, etc.), chain make one of the top three components that caused most incidents in mooring lines. Some failure mechanisms are listed by Ma et al. (2013) such as Out-of-Plane Bending (OPB), chain hockling, flawed flash welds, pitting corrosion, etc. Therefore, it is vital to understand all these mechanisms in order to identify the potential weak points of the lines, why and how the structural responses are modified during operation, and finally how to consider those modifications in mooring strength and fatigue design.

For preliminary design the effective elastic modulus applied in the mooring analysis may be taken as (DNV, 2010)

- Stud chain R3/R4/R5: Not less than 5.6×10^{10} N/m²
- Studless chain R3: $(5.40 - 0.0040 \times d) \times 10^{10}$ N/m²
- Studless chain R4: $(5.45 - 0.0025 \times d) \times 10^{10}$ N/m²
- Studless chain R5: $(6.00 - 0.0033 \times d) \times 10^{10}$ N/m²

where d is the nominal diameter of the chain links in mm.

According to DNV-OS-E301 (DNV, 2010) the Young's Modulus of the chains can be approximated as

$$E = 5.44 \times 10^7 \text{ kN/m}^2 \text{ (studless) or}$$

$$E = 6.40 \times 10^7 \text{ kN/m}^2 \text{ (studlink)} \quad (2.1)$$

The Minimum Breaking Strength (MBS) of the chain can be estimated as

$$MBL = c \times d^2 \times (44 - 0.08 \times d) \quad (2.2)$$

where c is the grade dependent constant, given in the catalogue of Ramnäs (2012).

In addition to the tension-tension fatigue BV-NI-604 (BV, 2014) requires to consider the combined fatigue (i.e. tension-tension plus in-plane and out-of-plane bending) at the top chain when the pre-tension in mooring lines at intermediate draft is higher than 10% of the Minimum Breaking Strength of a chain of the same diameter in Oil Rig Quality (ORQ) grade and when the design life on site is higher than 2 years. The phenomena of in-plane and out-of-plane bending are due to the fact that at fairlead/chain-stopper location, the motions of the vessel are imposed to the fairlead

and the link retained in fairlead pocket whereas the motions of the adjacent links are imposed by the mooring line dynamic motions following mooring line catenary. Due to the angular differences between fairlead and chain and to friction between links, high bending moments are imposed to the first links of the top chain. A mooring system with its underwater fairlead and the in-plane and out-of-plane bending modes are shown in Figures 2-2 and 2-3.

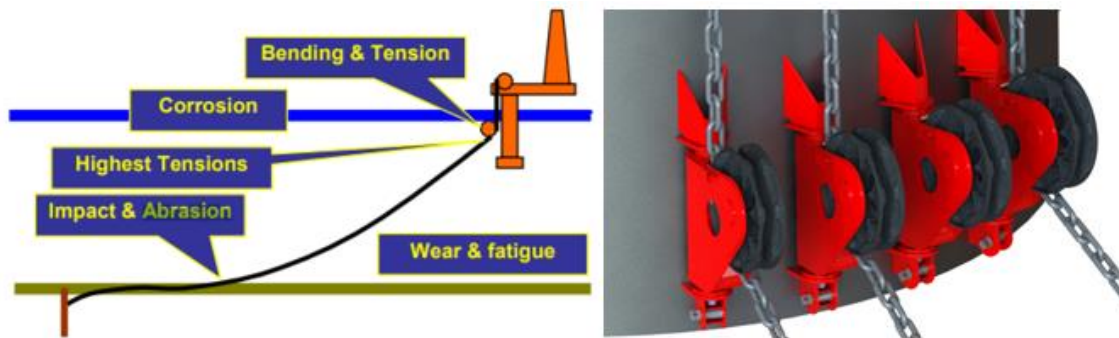


Figure 2-2: A mooring system and the influencing factors (Brown et al., 2012). Right: An underwater fairlead (Royal IHC, 2018).

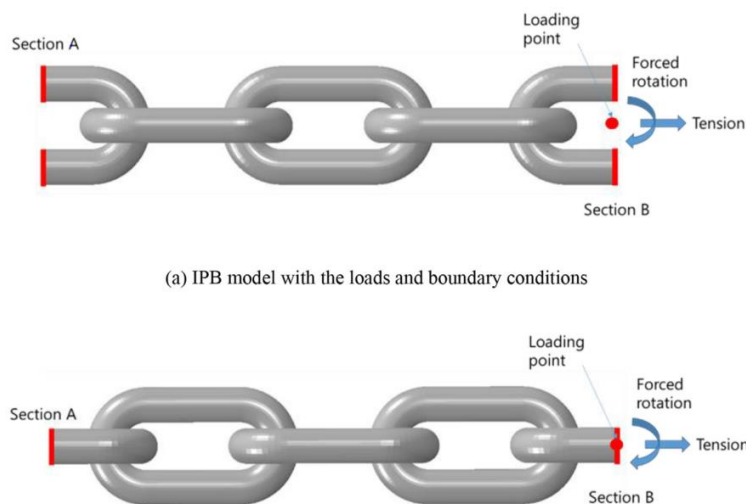


Figure 2-3: In-plane bending and out-of-plane bending modes (Kim et al., 2017).

3. Nylon

Synthetic fibers have been widely used since the deployment of fiber rope offshore moorings for deep-water oil production systems in the late 80's. For deep-water offshore applications, polyester is commonly used thanks to its light weight and good fatigue resistance. For floating wind turbine operating in shallow waters from 50 to 100m, nylon is preferred because of its lower stiffness, reduced mooring footprints and maximum tension. Therefore, The MRE industry shows currently a great interest on developing mooring systems using nylon ropes. Conventional nylon has, however, never been used for permanent mooring applications mostly due to its poor wet fatigue

characteristics. Indeed, typical nylon SPM hawsers are often retired every one or two years. Due to the limit amount of research on the recent nylon ropes, it is therefore crucial to focus on the mechanical behaviors of such material in order to optimize its design and utilization.

3.1 Load-elongation characteristics

Unlike rigid material, synthetic material such as polyester, nylon, etc., exhibit highly nonlinear and time-dependent load-elongation characteristics. Such behaviors should be determined by relevant tests before the design and application of those fiber rope mooring components. The tests should exhibit not only the nonlinear behaviors of ropes as hysteretic materials but also the dynamic loading conditions that ropes undergo during operation (e.g. tension magnitude, the frequency of loading, loading history, etc.).

Testing and modeling methods for polyester have been studied by the offshore industry since the early 80’s. The outcomes of several Joint Industry Projects (JIPs) have been integrated into offshore standards such as API-RP-2SM (API, 2014), DNVGL-RP-E305 (DNV, 2015), ABS (ABS, 2014), BV-NI432-DTO-R01E (BV, 2007). Although the above-mentioned methods are very good examples, they cannot be applied directly on nylon due to its highly non-linear load-elongation and complex fatigue behaviors. Besides, the idea of using nylon ropes for permanent mooring applications is quite new to the offshore industry since conventional nylon has very low fatigue life. It is therefore crucial to focus on the mechanical behaviors of nylon mooring ropes in order to cope with the modeling issue and assure the safety and cost-effectiveness of the mooring design.

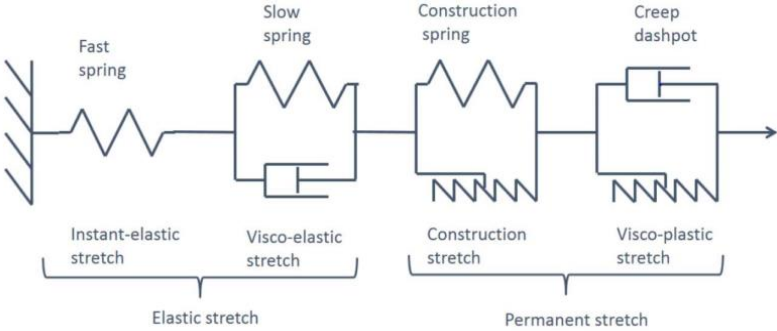


Figure 2-4: The spring-dashpot model (Flory et al., 2007).

Figure 2-4 illustrates the spring-dashpot model proposed by Flory et al. (2007). It can be seen that the elastic stretch includes the instant-elastic stretch and visco-elastic stretch resulting from a fast spring and a damped spring respectively. On the other hand, the permanent stretch comprises the construction stretch represented by a

construction ratchet-spring and the visco-plastic stretch represented by a ratchet-dashpot.

The visco-elastic behavior of synthetic ropes was explained by Flory et al. (2007) and illustrated in Figure 2-5.

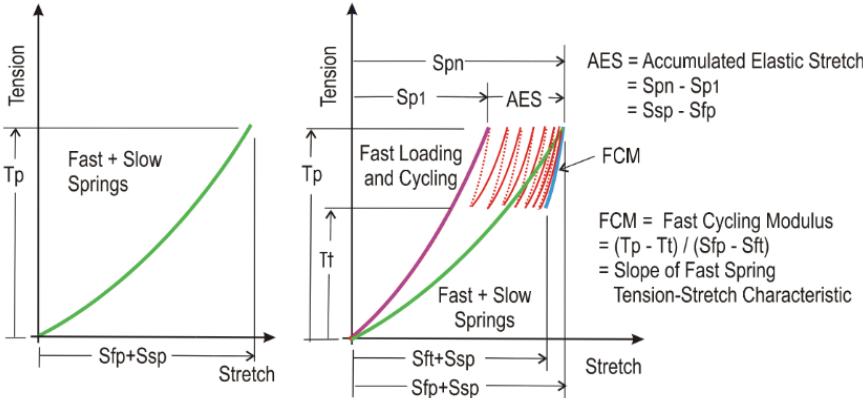


Figure 12 Stretch After Many Cycles is Equivalent to Sum of Fast Plus Slow Spring Stretches
Modulus After Many Cycles is Equivalent to Fast Spring Modulus

Figure 2-5: Fast + slow springs tension-stretch curve (Flory et al., 2007).

DNVGL-RP-E305 (DNVGL, 2015), Falkenberg et al. (2017, 2018) introduce the concept of the Syrope model with the following definitions, which are illustrated in Figure 2-6.

- The original curve: the tension-stretch curve obtained during the very first and quick loading of the new ropes.
- The original working curve: the lower-bound original curve for very slow loading so that visco-elastic stretch can be obtained without delay.
- Working curves: Tension-stretch curves accounting for the historical maximum tension that the rope has been through.
- Instant-elastic (dynamic) stiffness: A stable stiffness (after stabilization of working strain) in response to very fast changes in tension under cyclic loading. The dynamic stiffness results from instant-elastic strain only.

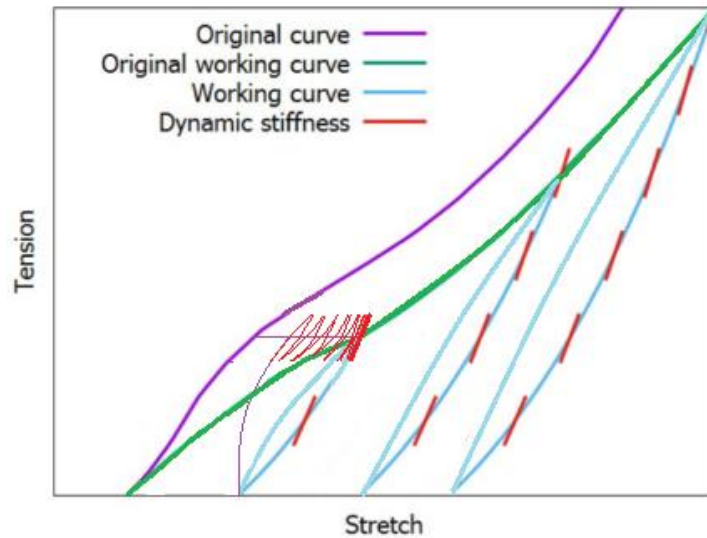


Figure 2-6: The Syrope model (Falkenberg et al., 2017, 2018).

Falkenberg et al. (2017, 2018) recommend selecting a pertinent working curve for static mooring analysis to determine the floating structure excursions (i.e. the excursions at the equilibrium position due to mean environmental loads). This working curve should account for the historical maximum tension that the rope has been through. DNVGL-RP-E305 (DNV, 2015) requires using a correct dynamic stiffness model to calculate the designed tension responses. An earlier research by Bitting (1980) reported an important factor of 3 to 4 times between the dynamic and quasi-static stiffness of nylon ropes. This, again, highlights the importance of using different stiffness models for structure excursions and tension response analysis.

An empirical formula for determining dynamic stiffness of nylon ropes

Offshore standards and researchers have given empirical expressions of dynamic stiffness for synthetic ropes. Generally, the dynamic stiffness of fiber ropes depends strongly on the mean tension, moderately on the tension amplitude and mildly on the frequency of loading (François et al., 2000; Vecchio, 1992). Practically, the loading frequency and tension amplitude impacts are negligible for polyester (François et al., 2010). Nylon, although seems to have closely similar behaviors as polyester, its responses are found to be more nonlinear than the latter. Liu et al. (2014) also studied the main factors influencing the dynamic stiffness of synthetic fiber ropes under cyclic loading. According to their conclusions, the mean tension is the main factor that influences significantly the dynamic stiffness, also the effects of strain amplitude and loading cycles cannot be ignored. Huang et al. (2013) highlighted the importance of understanding the change-in-length properties including creep, hysteresis, recovery, stiffness evolution of synthetic ropes.

Vecchio (1992) and Fernandes et al. (1999) proposed an empirical expression of dynamic stiffness for polyester ropes as

$$\frac{E}{\rho} = \alpha + \beta L_m - \gamma L_a - \delta \log(T_0) \tag{2.3}$$

where $\frac{E}{\rho}$: Specific modulus (N/tex); L_m : Mean load (% of MBL);
 L_a : Load amplitude (% of MBL); T_0 : Period of loading;
 $\alpha, \beta, \gamma, \delta$: Empirical coefficients.

A non-dimensional axial stiffness of ropes can be expressed as

$$K_r = (L_a \cdot l) / (\Delta l \cdot MBL) \tag{2.4}$$

MBL: Minimum Breaking Load La: Tension amplitude
 l: Initial Length of the rope Δl: Stretch

François et al. (2000) proposed empirical expressions of quasi-static and dynamic stiffness for typical polyester ropes depending on the mean tension in the lines (as mentioned above the impacts of tension amplitudes and frequency of loading are considered negligible). These have been integrated into BV-NI432-DTO-R01E (2007) as

Quasi-static stiffness: $K_{rs} = 13 \text{ to } 15$
 Dynamic stiffness: $K_{rd} = 18.5 + 0.33 \cdot L_m$ (2.5)

for normally stiff polyester ropes.

Based on recent dynamic stiffness tests on a wire-lay 3-strand nylon rope from Huntley (2016), it is found that the dynamic stiffness of the nylon rope depends strongly on both the applied mean tension and the tension amplitude. This is illustrated in Figures 2-7 and 2-8.

An expression of dynamic stiffness for nylon can be proposed as,

$$K_{rd} = a \cdot L_m - b \cdot L_a + c \tag{2.6}$$

where a, b, c are determined from a multiple linear regression on the nylon dynamic stiffness testing data reported by Huntley (2016). These values (with 95% of upper-confidence limits) are presented in Table 2-1.

Table 2-1: Empirical coefficients for determining the dynamic stiffness of the nylon rope.

a	b	c
0.39	0.21	2.08

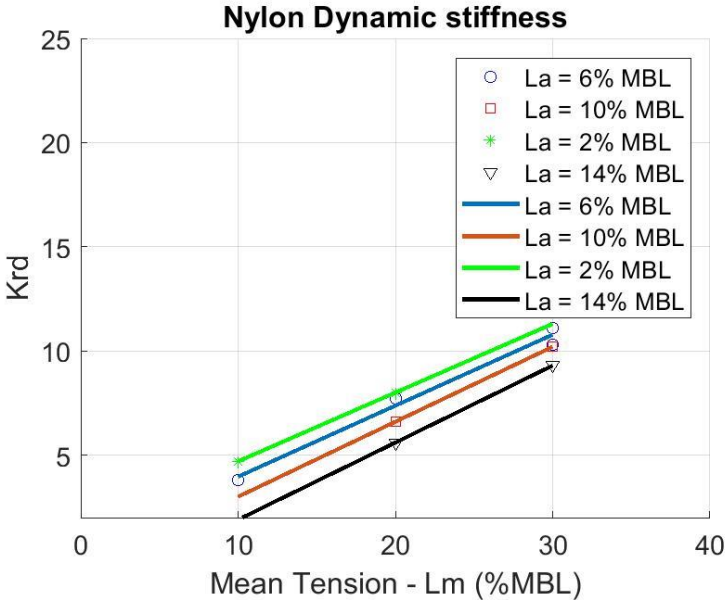


Figure 2-7: Dynamic stiffness of the wire-lay nylon rope depending on the mean tension, Lm (data obtained from Huntley, 2016).

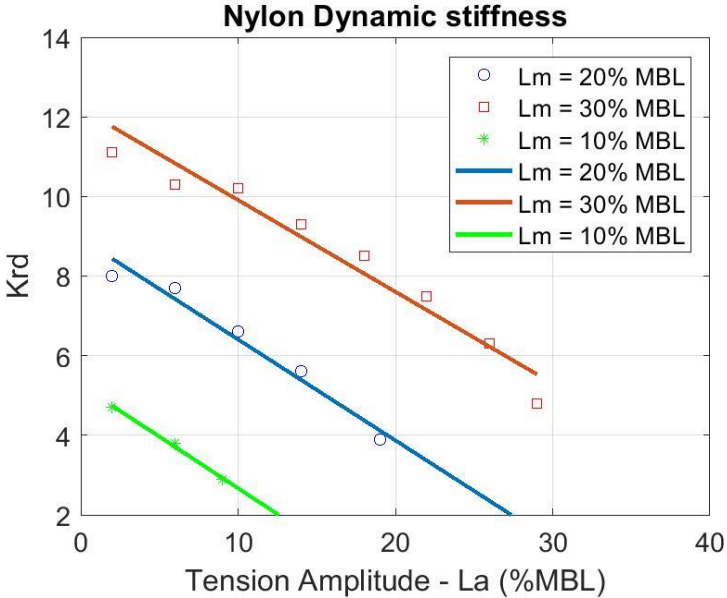


Figure 2-8: Dynamic stiffness of the wire-lay nylon rope depending on the tension amplitude, La (data obtained from Huntley, 2016).

A practical modeling procedure for nylon mooring analysis

A mooring analysis procedure considering the dynamic stiffness of polyester ropes was proposed by Kim et al. (2003) for a SPAR. Since tensions in the mooring lines of a SPAR are often dominated by slow drift motions, this procedure cannot be applied for semi-submersible type floating structures where first-order wave motions are the dominating ones, Arnal et al. (2016). Also, Kim's procedure has its limitation relating the convergent principle since the high-frequency tension component in mooring lines does not result from the motion of the SPAR but more likely from the resonance vibration of the polyester rope. Tahar et al. (2008) extended the traditional elastic rod theory to allow large elongation and nonlinear stress-strain relationships for the modeling of polyester mooring lines. The empirical expression for determining the axial stiffness of polyester proposed by Bosman (1999) was adopted considering a non-constant stiffness depending on the applied mean load. A similar attempt was made by Lin et al. (2015) for the modeling of polyester mooring for a SPAR-type floating wind turbine. The mooring tension responses were validated against the Orcaflex software (Orcina, 2012).

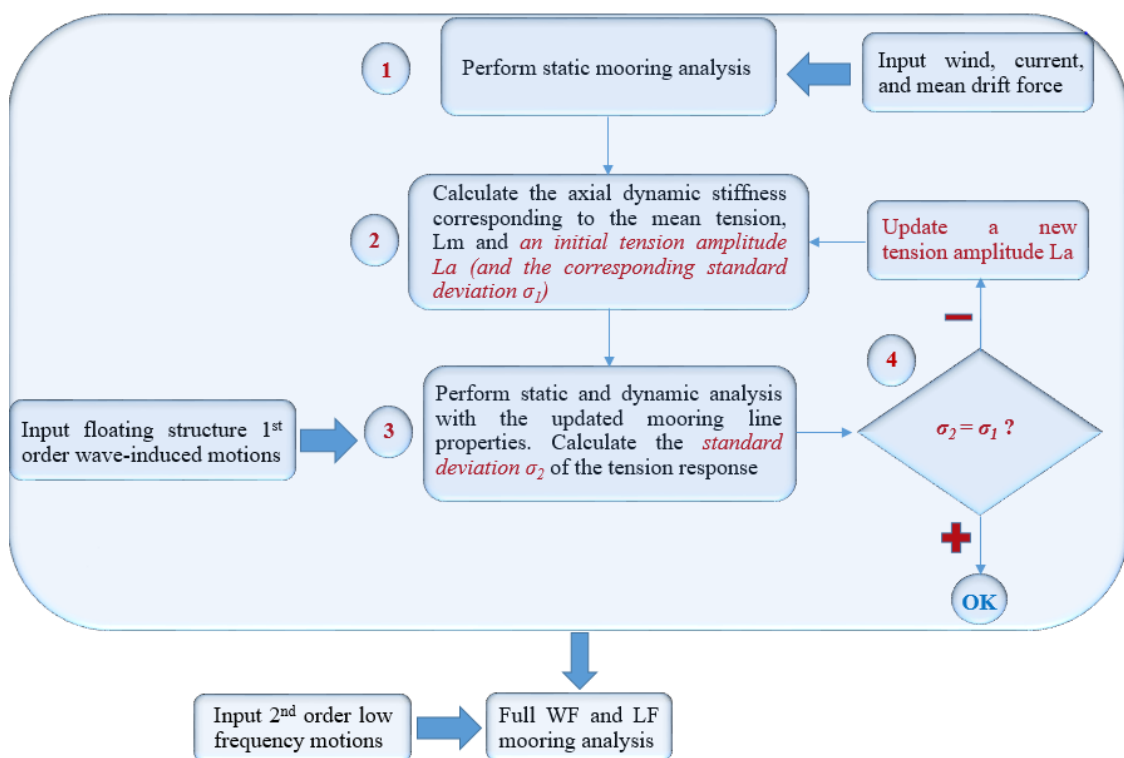


Figure 2-9: Mooring analysis procedure taking into account the impact of tension amplitudes on the dynamic stiffness of nylon ropes.

The recent standard DNVGL-RP-E305 (DNV, 2015) and Falkenberg et al. (2017, 2018) recommend a very practical procedure for fiber rope mooring analysis including the following steps.

- Step 1: Perform the mooring static analysis using the appropriate nonlinear working curves for each mooring line considering the mean environmental loads (i.e. if the mean tension in any of the lines is higher than the preceding highest working tension then the working curve for these lines needs to be updated).
- Step 2: Determine the mean tensions, L_m , at the top of the synthetic lines and update the model with an axial stiffness depending on the mean tension, L_m (the empirical expression as Eq. (2.5) can, therefore, be applied without difficulty). A stress-free length of the lines corresponds to this stiffness and the mass per unit length of the line are also updated.
- Step 3: Perform static and dynamic analysis with the updated mooring line properties.

Since this procedure ignores the tension amplitude effect, it cannot be applied for the dynamic modeling of nylon ropes. Based on that, the author proposed a modified procedure for the numerical mooring analysis of a semi-submersible type floating wind turbine considering the dynamic axial stiffness of nylon ropes. The present procedure composed of the following steps that were basically proposed by DNVGL-RP-E305 (DNV, 2015), Falkenberg et al. (2017, 2018), but some modifications are added (highlighted in red color in Figure 2-9) in order to take into account the impact of the tension amplitude on the dynamic stiffness of nylon.

- Step 1: Same as above.
- Step 2: Determine the mean tension, L_m , at the top of each synthetic line and update the model with an axial stiffness (determined by the Eq. (2.6)) depending on the mean tension, L_m , and an initial tension amplitude, L_a (with the corresponding standard deviation, $\sigma_1 = \frac{L_a}{\sqrt{2}}$), chosen optionally. A stress-free length of the lines corresponds to this stiffness and the mass per unit length of the line are also updated.
- Step 3: Perform static and dynamic analysis with the updated mooring line properties. Calculate the standard deviation σ_2 of the tension response.

- Step 4: Check if the convergent criterion $\sigma_2 = \sigma_1$ is satisfied with a certain tolerance. If not, go back to step 2 and input a new tension amplitude, L_a , and continue the procedure iteratively up to convergence.

The idea is to find a convergent dynamic stiffness for each sea state based on the empirical expression in Eq. (2.6) for the specific mean tension and the convergent tension amplitude determined for each sea state. As can be seen in Figure 2-9, the present procedure works as an iterative process in order to determine a convergent dynamic stiffness of the nylon rope for the sea state by comparing the standard deviation of the input tension amplitude with the standard deviation of the tension response. The compromise is implied, however, by comparing the standard deviation of a deterministic loading process (i.e. with a constant tension amplitude of variation) with the standard deviation of a random tension response process due to the floating structure wave-frequency motions. In fact, it can be seen that the dynamic stiffness tests are performed for regular loading where the tension amplitude is related to its standard deviation as $L_a = \sigma_1 \times \sqrt{2}$. However, due to the fact that the incoming waves are normally irregular processes, the tension responses must have the same characteristics. For that reason, we have to accept a compromise by choosing $L_a = \sigma_2 \times \sqrt{2}$ as tension amplitude of the irregular tension response in order to apply the present empirical dynamic stiffness model for irregular sea states. First, for a harmonic signal, the amplitude is equal to $L_a = \sigma_1 \times \sqrt{2}$. Secondly, an irregular process can be described by the sum of a very large number of sinusoidal processes (with different amplitudes and phases). Therefore, in our opinion, it seems acceptable to assume a tension amplitude, $L_a = \sigma_2 \times \sqrt{2}$, to represent the variation of the tension response for each specific irregular sea state. However, validation with field measurements on nylon mooring lines seems necessary to check the appropriateness of this assumption. Although one might also argue that the convergence check in the present procedure (Figure. 2-9) should be made for both wave frequency and low frequency motions, we believe that it would be difficult and computationally expensive considering them at the same time by using coupled time domain simulations. Moreover, since low frequency motions are small compared to the wave frequency responses for semi-submersible type FWTs (or at least for existing concepts) which is the subject of this study, it seems, therefore, acceptable not to consider low frequency motions in the convergence check. However, the converged dynamic stiffness once determined will be updated in the model in order to calculate the mooring responses considering the coupled wave and low frequency motions.

The present modeling procedure will be applied later in section 3.3 for dynamic modeling of nylon mooring ropes.

3.2 Fatigue characteristics

The main fatigue mechanisms for synthetic ropes are creep, hysteresis heating, internal abrasion, axial compression, etc. (Hearle et al., 1993; Parsey et al., 1982)

Table 2-2: Classification of fatigue characteristics of fiber ropes (Weller et al., 2015)

		Nylon 6	Polyester	Vectran®	Aramid	HMPE
Durability	Ultraviolet light	Good	Good	Poor	Average	Average
	Chemicals	Good	Good	Good	Good	Good
	Temperature	Good	Good	Good	Average	Poor
	Abrasion	Average	Good	Good	Average	Good
	Creep	Average	Good	Good	Good	Poor
	Tension fatigue	Good	Good	Good	Good	Good
	Compression fatigue	Good	Good	Good	Poor	Good

It is believed that hysteresis heating is not a concern for offshore mooring applications where the fiber ropes remain under-water throughout its service life. Likewise, the axial compression fatigue affects only stiff fibers such as aramid and should not be a concern for nylon. However, the design practice for polyester mooring lines recommended by Bureau Veritas NI 432 (BV, 2007) is to keep the minimum tension in mooring lines not lower than 2% of MBS to avoid axial compression fatigue. The internal abrasion and creep, therefore, remain two critical fatigue modes for nylon ropes. Table 2-2 (Weller et al., 2015) illustrates the classification of the durability characteristics of fiber ropes for offshore mooring applications.

Creep

Creep is a static fatigue damage mode that the rope fails after a certain duration of time at a constant tension. Creep is either recoverable (primary creep - at low tension) or non-recoverable (secondary creep – at high tension). The latter is relevant to creep fatigue failure of fiber ropes. Creep fatigue failure can be critical for typical nylon that might fail in less than 5 hours being tensioned at 80% of its breaking strength (McKenna et al., 2004). For wet nylon 66, the creep process is the dominating fatigue mechanism for load levels above 30% its breaking strength. For cyclic loading, the creep effect is the same as if the peak load (i.e. maximum load) has been applied continuously. The creep fatigue mechanism is independent of the frequency of loading

and can be predicted by the linear relationship between the maximum load and the log time to failure in second. Creep effect doesn't lead to the reduction of strength of ropes at least up to 75 to 80% of the fatigue life time (Mandell, 1987). Figure 2-10 illustrated the static (i.e. creep) fatigue and cyclic fatigue of polyester yarns. It can be seen that the two curves are closely similar, therefore, it confirms that at high load levels creep is the dominant fatigue mechanism.

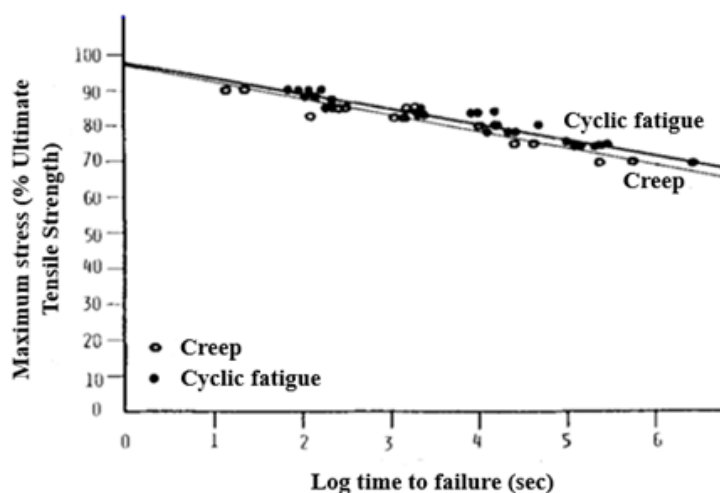


Figure 2-10: Failure time vs. maximum stress for polyester yarns under creep rupture ($Ra=1$) and cyclic fatigue ($Ra=0.1$, $f=1\text{Hz}$) – $Ra = \text{Minimum Load} / \text{Maximum Load}$ (Mandell et al., 1987).

Internal abrasion

Internal abrasion is a dynamic fatigue damage mode that the rope fails after a certain number of cycles under cyclic loading. Internal abrasion is caused by relative motions between strands which are directly related to the tension range and inversely related to the mean tension. Therefore, it can be concluded that the severity of internal abrasion is directly related to the tension amplitude and inversely related to the mean tension (Flory et al., 2006). Internal abrasion is a serious problem for highly structured, wet nylon ropes at moderate tension (McKenna et al., 2004). Severe internal abrasion can lead to significant loss of strength of ropes during operation and, therefore, might modify mooring system behaviors and even lead to failure in ultimate and fatigue conditions. The severity of internal abrasion can be reduced by using long-lay-length stranded subrope in parallel construction and special marine finish (Ridge et al., 2010; Banfield et al., 2017). Some rope constructions that may improve internal abrasion fatigue behaviors other than the braided construction such as parallel ropes or wire-lay ropes are illustrated in Figure 2-11.

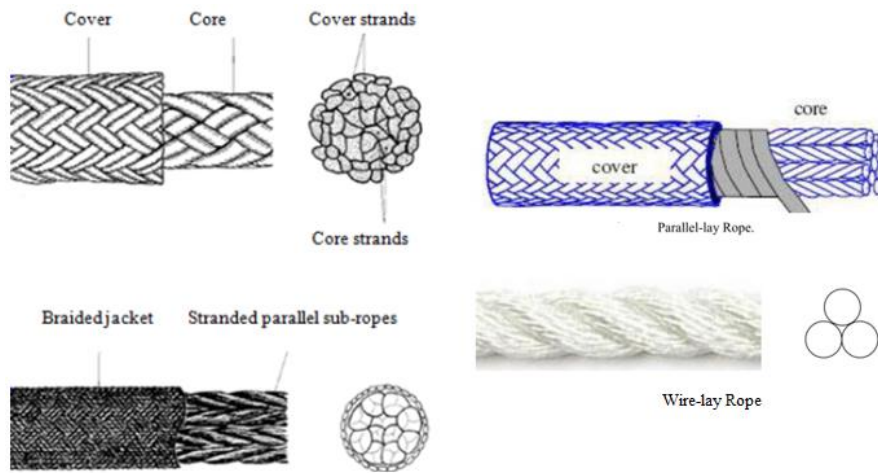


Figure 2-11: Some rope construction (Ridge et al., 2010; Banfield et al., 2017; Huntley, 2016).

If the design tension is kept at low levels (i.e. under 30% of the nylon breaking strength), it is believed that internal abrasion should be the only fatigue damage mode of concern for nylon. Internal abrasion can be avoided or reduced by proper design (by increasing mean tension and reducing tension amplitude). While the mean tension can be simply increased by modifying the line length or positions between the anchor points and the fairlead, the tension amplitude depends strongly on the floating structure motions due to the first and second order excitation wave loads and the rope stiffness. It has also been shown that rope stiffness and creep fatigue are directly related to the mean (or maximum static) tension. Therefore, an over-increasing mean tension might be unfavorable for mooring behaviors. An integrated mooring-floater design seems to be preferred over the uncoupled design in order to reduce the tension amplitude in fiber rope mooring components. Figure 2-12 illustrates inter-strand abrasion damage in a polyester rope after a 48-million-cycles fatigue test and a nylon subrope after ten-million-cycles fatigue tests.



Figure 2-12: Inter-strand damage in a polyester rope (left) after a 48-million-cycle fatigue test (Banfield et al., 2018) and a nylon subrope (right) after a ten-million-cycles fatigue tests (Banfield et al., 2017).

A review of existing fatigue tests on nylon mooring ropes

Unlike polyester that several JIPs have proven its very good fatigue and abrasion characteristics for mooring application, the adequacy of nylon for permanent mooring application stay still questioned for many people. However, there are actually a lack of long cycle fatigue tests for nylon ropes. Currently, fiber rope fatigue testing methods in offshore standards are still limited and focused on specific applications. The method “Thousand Cycle Load Levels” (TCLL) (OCIMF, 2000) is commonly applied by rope producers. However, this accelerated fatigue testing method was proposed specifically for Single Point Mooring (SPM) hawsers and does not seem appropriate for a permanent mooring application. Also, since low load level fatigue tests are costly and time-consuming, most tension-tension fatigue tests have been done at high load levels. This, however, can give misleading results when extrapolated to low load levels (Flory, 1989). For instance, the load levels tested to establish the T-N fatigue curve for the nylon subrope proposed by the Tension Technology International (TTI) (Ridge et al., 2010; Banfield et al., 2017) Figure 2-13) are at the mean tension of 40% of MBL with the tension ranges vary from 40% to 70% of MBL where creep is believed to be the dominating effect. Indeed, when extrapolated to low load level (e.g. 10 to 15% of breaking load as for nylon SPM hawsers), the fatigue curve proposed by the TTI gives a number of cycles to failure of 1000 times greater than the field data retirement value (about 2.5 million cycles) of the nylon hawsers operated by the Whitehill Manufacturing Corporation as illustrated in Figure 2-14 (Huntley, 2016).

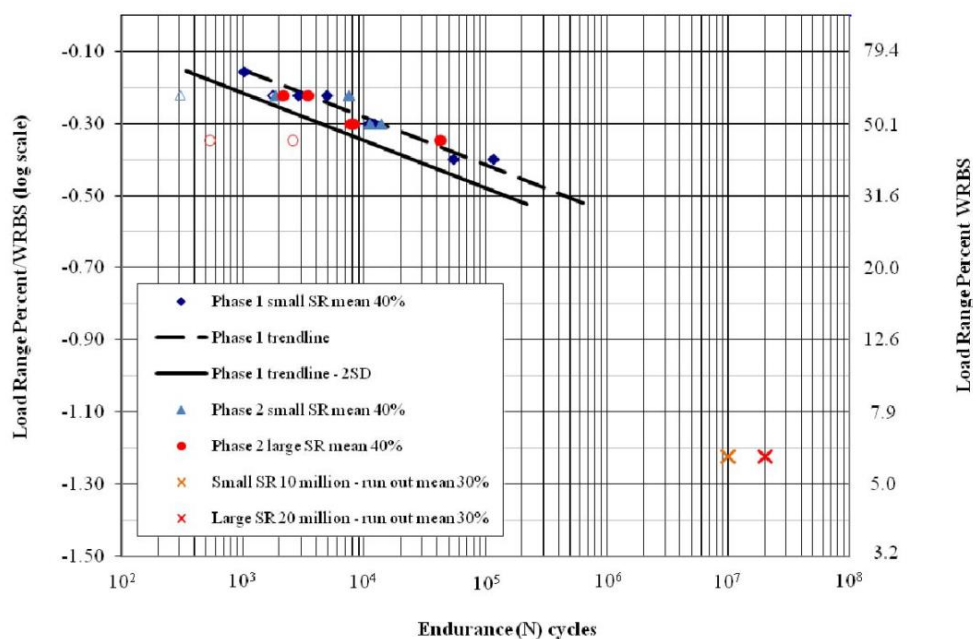


Figure 2-13: A nylon fatigue curve based on the testing data of the TTI (Ridge et al.2010, Banfield et al., 2017).

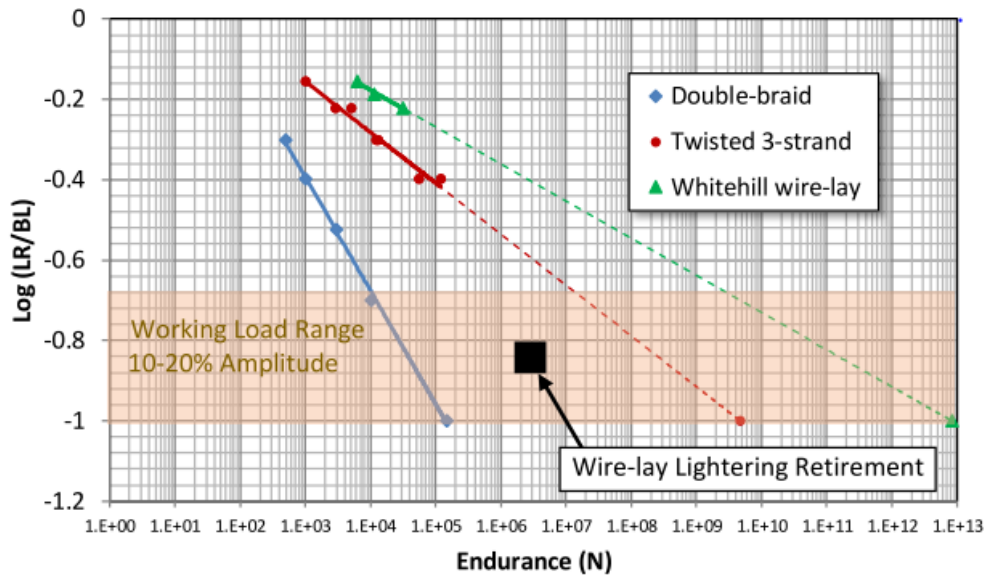


Figure 2-14: Comparison of nylon fatigue characteristics (Huntley, 2016) (the red line is the fatigue curve obtained from the nylon subrope tests performed by the Ridge et al., 2010) (LR- Load Range, BL: Breaking Load).

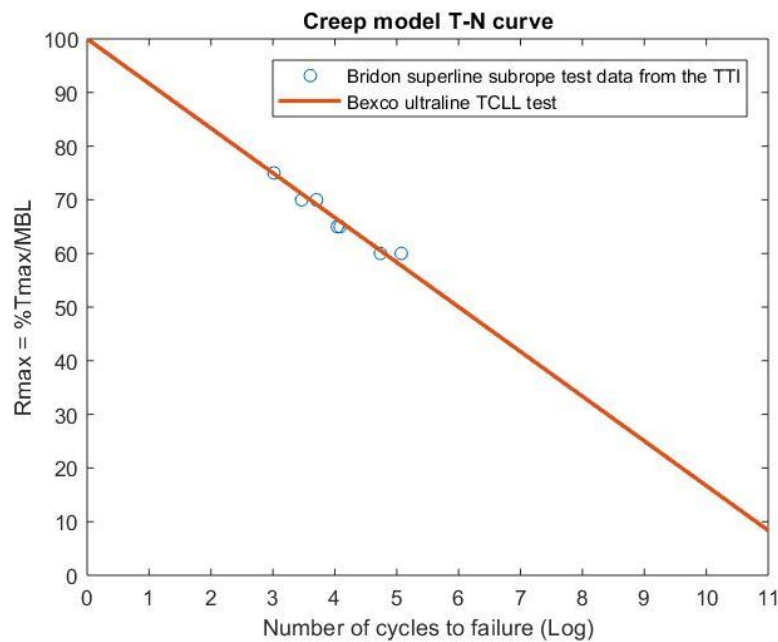


Figure 2-15: A creep model fatigue curve, T_{max} - maximum tension in the rope.

Figure 2-15 shows a semi-log relationship between the maximum tension ratio, $R_{max} = \% \frac{T_{max}}{MBS}$ and the number of cycles to failure. The data of the high load level fatigue tests on the Bridon's superline nylon subrope (Ridge et al., 2010) where the dynamic tension ranges are recalculated as the maximum static tension ratios, R_{max} , and the TCLL fatigue curve of the Bexco's ultraline nylon rope are plotted together showing very good match. This explains again the domination of creep fatigue behavior at high load levels, and proves that the high load level fatigue tests seem only capture the creep fatigue behavior of the ropes.

The ten million and twenty million cycles fatigue tests performed by the Tension Technology International (Banfield et al., 2017; Flory et al., 2016) which show almost no loss of strength for the Bridon’s nylon subrope can be explained by the high mean tension (30% of MBS) and low tension range (6% of MBS). Indeed, it seems obvious that at such a tension level the relative motions between strands are locked and as a consequence, resulting in no abrasion damage. Also, as mentioned above creep fatigue is not a concern at around 30% of MBS. Therefore, these fatigue tests doesn’t seem to cover all the critical tension ranges for fatigue behaviors of nylon ropes.

Another approach to study the inter-strand abrasion behavior of synthetic ropes is based on the yarn-on-yarn abrasion tests. These tests have been performed for nylon yarns of Bridon and Bexco (Flory et al., 2016; Chevillotte et al., 2018). Although an excellent improvement in abrasion resistance is observed for both the nylon yarns where new coating technologies (i.e. marine finish) are applied, it is difficult to extrapolate the testing results to full-scale ropes. A yarn-on-yarn abrasion machine is illustrated in Figure 2-16.

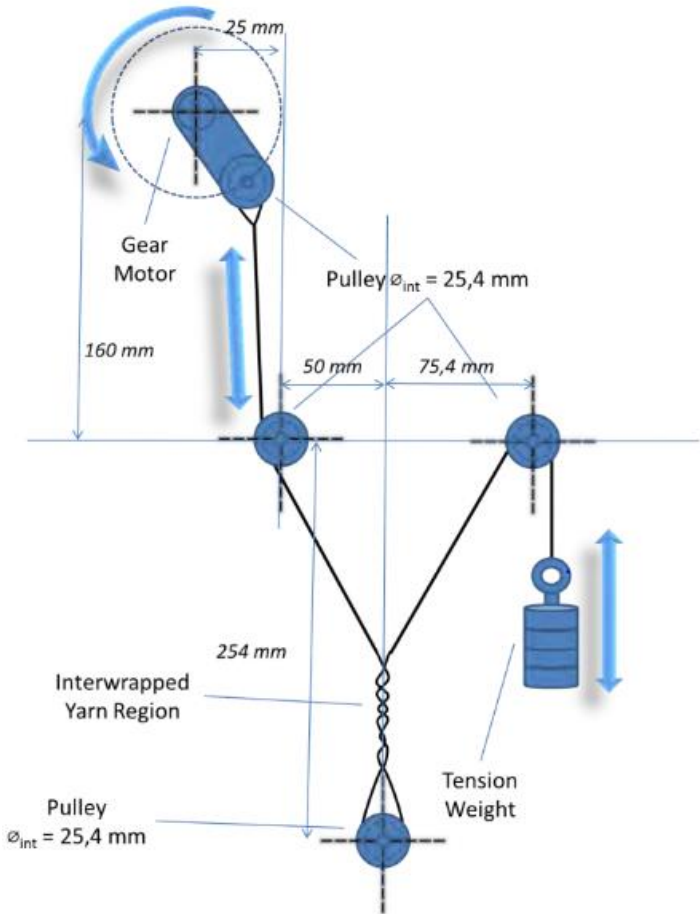


Figure 2-16: A yarn-on-yarn abrasion machine (Chevillotte et al., 2018).

It seems important to stress that in current standard fatigue testing approaches there has been no clear precision and distinction of which mechanisms of fatigue causing

rope failure (Lechat, 2007). The author would argue that creep and internal abrasion fatigue should be considered separately as two different fatigue criteria when it comes to fatigue estimate of nylon mooring ropes. Also, internal abrasion fatigue should be carefully assessed since it induces not only strength reduction but also modified structural responses due to material loss. Indeed, besides the strength reduction due to inter-strand damage, it is also crucial to investigate the residual stiffness of the ropes since a modified rope stiffness might result in modified structure behaviors. The issue has been studied by Bandfield et al. (2018) where the residual stiffness of a polyester rope that has been through 15 million cycles of at the mean tension of 40% of MBL and the tension range of 20% of MBL is compared with its as new stiffness as in Figure 2-17. It is noted that only 8% loss of strength was found after 15 million cycles due to inter-strand abrasion. The curves are shown to be closely matched up to around 50% of break load. It proves that the 10 cycles of bedding-in from 1% to 50% of break load is sufficient to remove most of the construction stretch. The deviation from 50% of the breaking load to failure is most likely due to the additional structural bedding-in of both rope and splices of the fatigued rope.

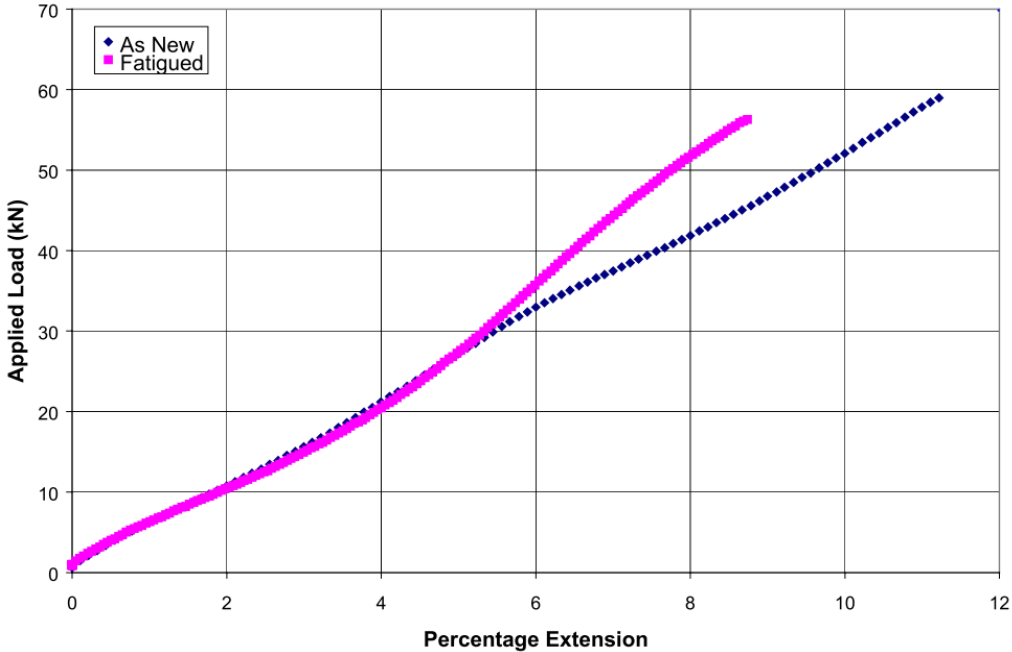


Figure 2-17: 6t sub-rope load/extension curves up to break for new rope (after 10 conditioning cycles) and after fatigue testing (Bandfield et al., 2018).

Liu et al. (2015) investigated the influence of the internal abrasion damage on the dynamic stiffness of polyester ropes and found significant dynamic stiffness reduction due to material loss. Their results are illustrated in Figure 2-18 where dynamic stiffness of polyester ropes corresponding to different damage levels are compared.

An empirical expression of dynamic stiffness for damaged ropes is expressed as (Liu et al., 2015)

$$K_r = \alpha (1-D)^\omega + \beta (1-D)^\psi L_m - \gamma \varepsilon_a - \delta L_m \exp(-\kappa N) \quad (2.7)$$

where

α , ω , β , ψ , γ , δ and κ are coefficients related to the material and structure of the fiber ropes;

D is the damage levels (% of MBS);

L_m is the mean tension (% of MBS);

ε_a is the amplitude of strain;

N is the number of loading cycles.

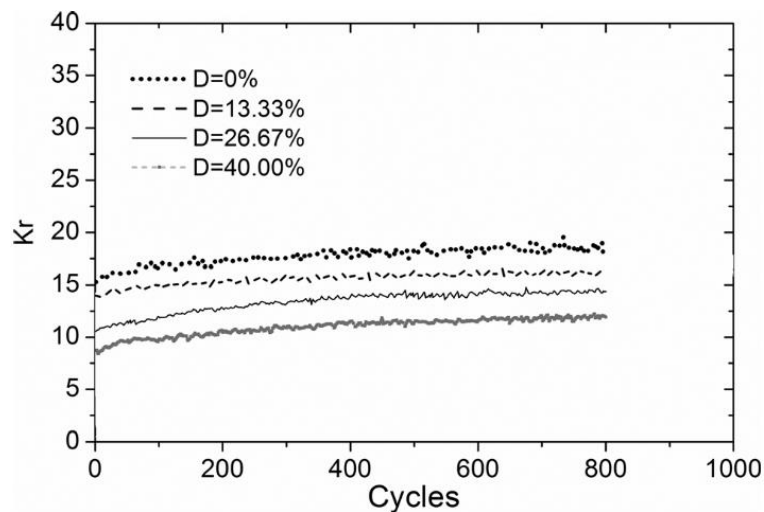


Figure 2-18: The influence of material loss on the residual dynamic stiffness of polyester ropes (Liu et al., 2015) (D - the damage level in % of MBS)

A non-destructive testing approach to characterize internal abrasion fatigue

Although internal abrasion fatigue tests are costly and time consuming, a comprehensive procedure for fatigue testing of fiber ropes that can be applied for every levels of loading is of great interest. Therefore, the author proposes, as an alternative, a non-destructive testing approach as in the following in order to capture the internal abrasion damage effects on nylon ropes without having to perform fatigue tests until failure. The present non-destructive fatigue test procedure is presented in Figure 2-19 where the aim is to characterize the residual strength and stiffness of damaged ropes as a function of the levels of loading (i.e., mean tension and tension

amplitude) and the corresponding number of effective cycles. Ultimately, the author expects that the testing results could be extrapolated in order to determine the number of cycles to failure at every level of loading. The tests are to be performed on nylon subropes in wet condition.

In the following, in order to characterize the internal-abrasion fatigue, a tension ratio R_a ($R_a = \frac{T_{\min}}{T_{\max}}$) is used to represent the level of loading. The relationship between R_a and the number of Cycles to Failure (CTF) – N should be determined for every load level (i.e. R) (DNVGL, 2015). The rope failure is defined as a complete loss of load-carrying capacity, i.e. the Residual Breaking Strength (RBS) equals to 0. However, one might argue that only the ratio R_a would not be enough to represent every load ranges (i.e. different mean tensions and tension amplitudes may result in the same R). The author suggests to verify this assumption by performing the same tests (i.e. same number of cycles) for the same ratio R_a but with different mean tensions and tension amplitudes (e.g. $R_a = 0.25$ at the mean tension, $L_m = 10\%$ of MBL, and the tension amplitude, $L_a = 6\%$ of MBL, comparing with $R = 0.25$ at the mean tension, $L_m = 20\%$ of MBL, and the tension amplitude of $L_a = 12\%$ of MBL).

The following fatigue cyclic tests should be performed

- $N_1 = 100,000.00$ cycles ($f = 0.65\text{Hz}$) ≈ 1.78 days
- $N_2 = 200,000.00$ cycles ($f = 0.65\text{Hz}$) ≈ 3.56 days
- $N_3 = 300,000.00$ cycles ($f = 0.65\text{Hz}$) ≈ 5.34 days
- $N_4 = 400,000.00$ cycles ($f = 0.65\text{Hz}$) ≈ 7.12 days
- $N_5 = 800,000.00$ cycles ($f = 0.65\text{Hz}$) ≈ 14.24 days
- $N_6 = 1,600,000.00$ cycles ($f = 0.65\text{Hz}$) ≈ 28.48 days

Then break test to check the residual strength and stiffness of ropes.

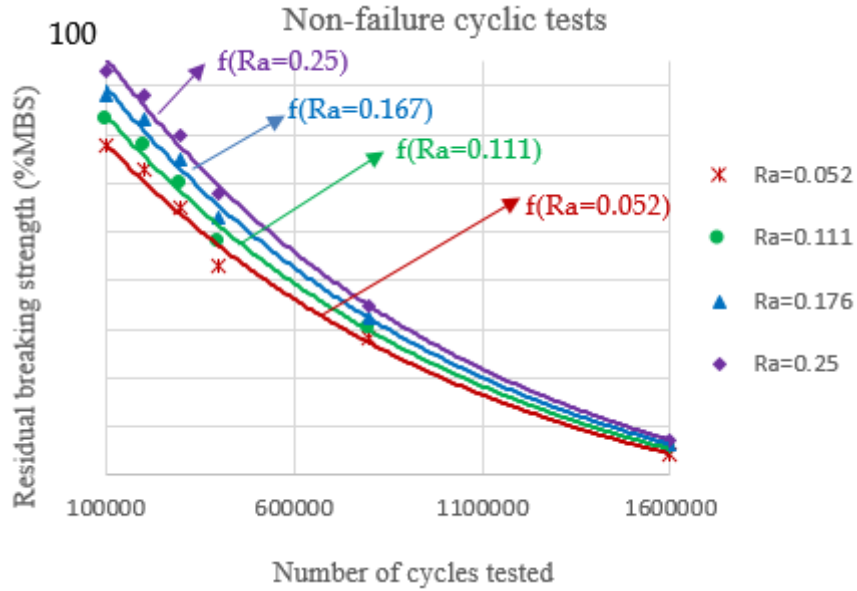


Figure 2-19: Non-destructive fatigue tests on nylon subropes (MBS: Minimum Breaking Strength).

4 levels of loading are chosen as in the Figure 2-19 at the mean tension equals to 10% of MBL and the corresponding tension amplitude of 6% (Ra= 0.25), 7% (Ra= 0.176), 8% (Ra= 0.111), 9% (Ra= 0.052). The expected testing results are presented in Figure 2-19 where a function that represents the residual breaking strength of ropes considering the effective cycles could be obtained for each level of loading such as $f(Ra= 0.25)$, $f(Ra= 0.176)$, $f(Ra= 0.111)$, $f(Ra= 0.052)$. Based on that, a function of the residual breaking strength of ropes at every level of loading together with the number of effective cycles can also be obtained as Eq. (2.8)

$$RBS = f(Ra, N) \quad (2.8)$$

where Ra- the ratio defining the tension level, $(Ra = \frac{T_{min}}{T_{max}})$

N- the number of effective cycles corresponding to the ratio Ra

Also, the testing results presented in Figure 2-19 and Eq. (2.8) could be extrapolated to determine the number of cycles to failure at each level of loading as in Figure 2-20. Based on that, an internal abrasion fatigue curve could be obtained for every levels of loading as illustrated in Figure 2-21. Basically, the greater Ra gets, the lower effect of inter-strand damage is expected. Also, there should be a minimum value of Ra where no damage due to internal abrasion fatigue would be found. This is illustrated as the red horizontal line in Figure 2-21.

$f(Ra=0.25) \rightarrow N(R=0.25)$ at which the RBS = 0
 $f(Ra=0.176) \rightarrow N(R=0.176)$ at which the RBS = 0
 $f(Ra=0.111) \rightarrow N(R=0.111)$ at which the RBS = 0
 $f(Ra=0.052) \rightarrow N(R=0.052)$ at which the RBS = 0

Figure 2-20: Extrapolating the non-failure fatigue test results.

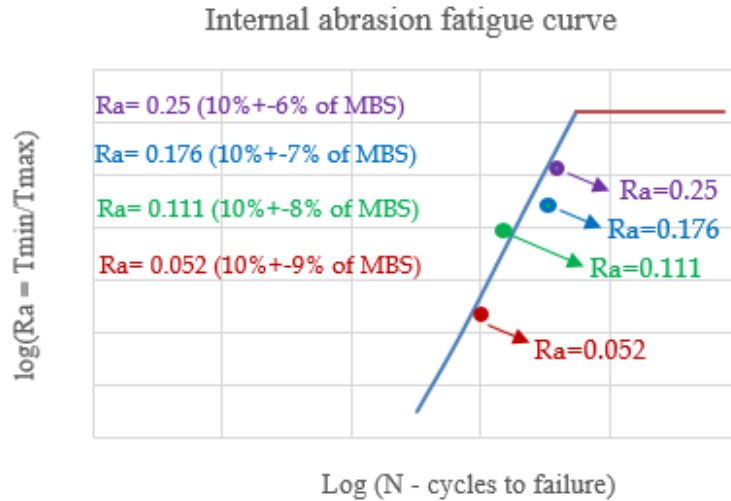


Figure 2-21: An internal abrasion fatigue curve.

The quasi-static and dynamic stiffness tests (as discussed in Figure 2-6, section 3.1) are to be re-performed on damaged ropes. An empirical expression of dynamic stiffness for damaged rope could be obtained as in the Eq. (2.9).

$$K_{rd} = \alpha(1-D)^\omega + \beta L_m - \gamma L_a \quad (2.9)$$

where

- D- the damage level (%MBS);
- L_m- the mean tension (%MBS);
- L_a- the tension amplitude (%MBS);
- α, β, ω, γ- empirical coefficients

In conclusion, the present internal abrasion fatigue tests could be considered for substituting current testing approaches in the literature which are costly and time-consuming but still cannot cover every possible levels of loading. Moreover, for hybrid mooring lines with applications of nylon mooring ropes, the methodology for modeling and service life monitoring of mooring lines presented in **Chapter 3** of this manuscript requires a sound understanding of the residual breaking strength and stiffness of nylon ropes during exploitation.

3.3 Application for numerical modeling of nylon mooring ropes

The results discussed in this section have been published in one of the authors’ papers (Pham et al., 2019) where the primary objective is to assess the impact of the dynamic stiffness of nylon mooring ropes on the dynamic mooring behaviors in real sea conditions. It is done by applying the suggested nylon mooring analysis procedure described in Figure 2-9 and the empirical expression of nylon rope dynamic stiffness in Eq. (2.6).

Dynamic mooring analysis is performed for both ULS and FLS cases in order to investigate the impact of the present nylon dynamic stiffness model on both strength and fatigue design of mooring lines. A chain-polyester-chain mooring system and a chain-nylon-chain system are also compared to study the impact of the different stiffness cases corresponding to the two synthetic materials on the design motions and tension responses of the system.

Floating structure and mooring line properties

The mean water depth of the site is taken as 36 m in this case study. The considered FWT has a total mass of about 5000 t and a draft of approximately 7 m. The floater is considered as a square ring with a 36 m width, a height of 10 m, and a 21 m wide moonpool. The wind turbine’s nacelle is located 60 m above the free surface. The floating structure model is illustrated in Figure 2-22.

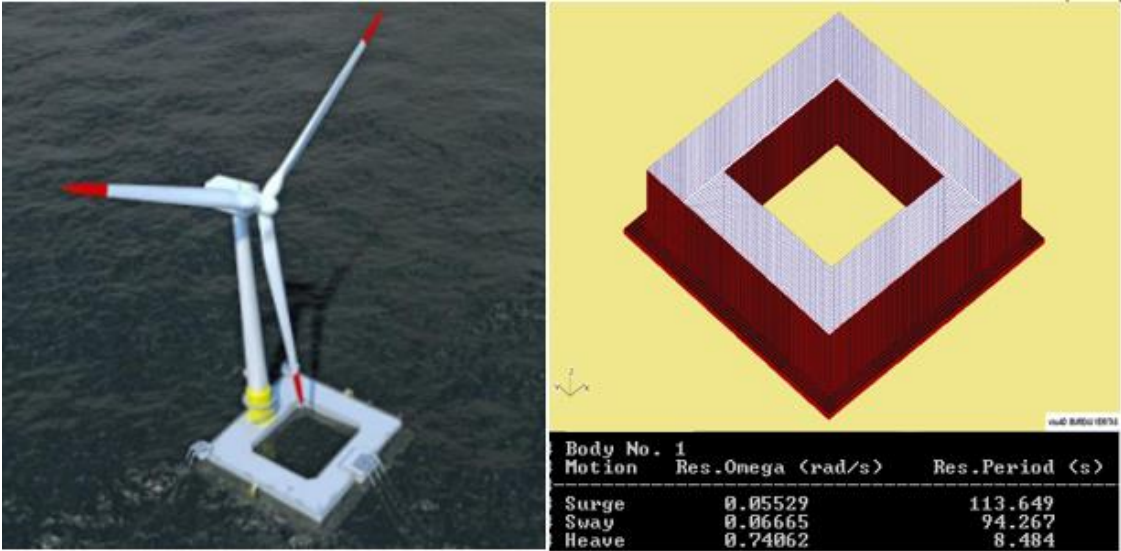


Figure 2-22: Left- The FLOATGEN FWT (ECN, 2018); Right- The floating structure modeled by HydroStar (BV, 2016).

The mooring line properties are presented in Table 2-3 in which the same minimum breaking strength is chosen for all the mooring components.

Table 2-3: Mooring line properties.

Materials/Properties	Diameter (m)	Axial stiffness EA_dynamic (kN)	Minimum Breaking Strength (kN)
Nylon	0.216	Determined by the Eq. (2.6) and the procedure Fig. 6	10.000E3
Polyester	0.188	Determined by the Eq. (2.5) and the DNVGL's procedure	10.000E3
Chain/R4S	0.095	1.10E6	9.987E3

Dynamic mooring analysis

For simplification, wind and current loads are approximated as a steady contribution included in the mean tension. The mooring lines dynamic analysis is performed using OrcaFlex with a simulation duration set to 3 hours. The hydrodynamic database is calculated using HydroSTAR. The wave-frequency and low-frequency floating-body motions are then computed within OrcaFlex using a coupled analysis with the mooring system. Although no dynamic wind forces are considered, the wind turbine assembly has an influence on the mass and inertia of the system. Quadratic viscous damping on the structure is also included in order to achieve realistic vertical motions.

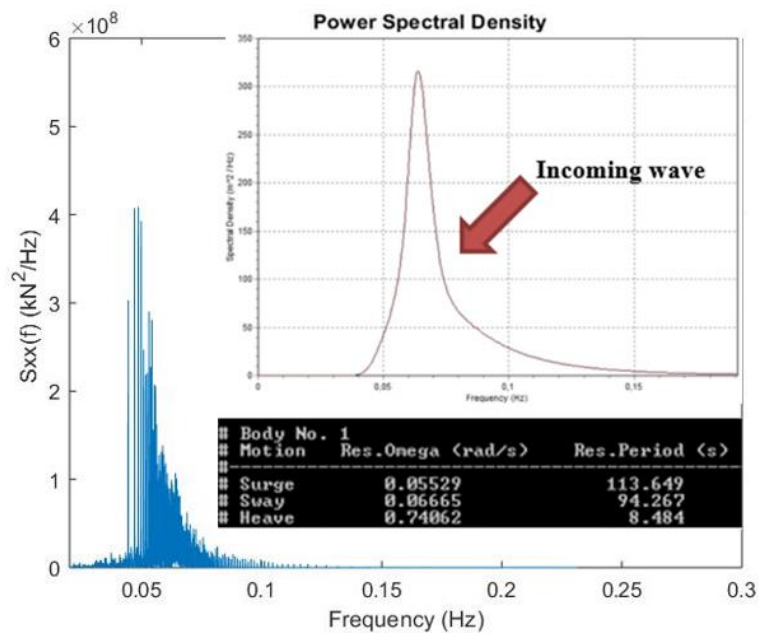


Figure 2-23: Power spectral density of the incoming wave and the tension response.

Table 2-4: Extreme and moderate sea states at the SEMREV sea test site.

Sea state	Spectra type	Hs (m)	Tp (s)	Gamma
Extreme	Jonswap	10	15.7	3.3
Moderate - Fatigue	Jonswap	2.61	13.8	3.3

The extreme and moderate sea states at the SEMREV sea test site (as presented in Table 2-4) are used in the calculation.

The Power Spectral Density (PSD) of the tension response in a mooring line is presented in the Figure 2-23 showing clear dominance of wave frequency responses.

Dynamic modeling of nylon mooring ropes

Table 2-5: Different dynamic stiffness cases of the nylon rope and the resulting standard deviation of the tension response.

Sea state	Mean Tension (% of MBL)	Tension Amplitude (% of MBL)	Axial stiffness EA_dynamic (kN)	Standard deviation of the tension response (kN)
Extreme -100 year return period	30	30	74.8E3	0.571E3
Extreme -100 year return period	30	26	83.2E3	0.655E3
Extreme -100 year return period	30	21	93.7E3	0.757E3
Extreme -100 year return period	30	15.32	105.628E3	1.0833E3
Moderate - Fatigue	10	10	38.8E3	0.045E3
Moderate - Fatigue	10	7	45.1E3	0.052E3
Moderate - Fatigue	10	5	49.3E3	0.056E3
Moderate - Fatigue	10	0.9	57.91E3	0.064E3

Table 2-6: Different dynamic stiffness cases of the nylon rope and the resulting platform motions.

Stiffness case / Motions	30 +- 30 % MBL				30 +- 26 % MBL			
	Mean	STD	Min	Max	Mean	STD	Min	Max
Surge (m)	-0.58	5.84	-25.4	13.8	-0.62	6.2	-25.7	14.56
Sway (m)	-0.01	0.02	-0.08	0.06	-0.01	0.02	-0.1	0.09
Heave (m)	0.02	2.53	-9.93	8.34	0.03	2.53	-9.93	8.31
Roll (deg)	0	0.01	-0.02	0.02	0	0.01	-0.02	0.02
Pitch (deg)	-0.51	2.58	-8.89	7.14	-0.51	2.57	-8.87	7.13
Yaw (deg)	0.06	0.01	0.02	0.09	0.06	0.01	0.02	0.09
	30 +- 21 % MBL				30 +- 15.32 % MBL			
	Mean	STD	Min	Max	Mean	STD	Min	Max
Surge (m)	-0.69	6.54	-27.5	15	-0.81	6.98	-30.30	15.40
Sway (m)	-0.01	0.02	-0.12	0.11	-0.01	0.02	-0.16	0.16
Heave (m)	0.03	2.53	-9.94	8.27	0.04	2.54	-9.96	8.23
Roll (deg)	0	0.01	-0.02	0.02	0.00	0.01	-0.02	0.03
Pitch (deg)	-0.52	2.55	-8.85	7.01	-0.53	2.51	-8.81	6.68
Yaw (deg)	0.06	0.01	0.01	0.1	0.06	0.01	0.01	0.11

The fiber rope mooring analysis procedure presented in Figure 2-9 is applied to determine the dynamic tensions in mooring lines based on the convergent dynamic stiffness determined for each specific sea state. The procedure starts with a tension amplitude, L_a , that is equal to the mean tension, L_m (the lowest realistic stiffness case in our experience), then converges very quickly after a few iterations. For instance, the dynamic stiffness case, 30 % +- 15.32 % of MBL, determined for the ULS case represents the mean tension, L_m , at 30 % of MBL and the convergent tension amplitude, L_a , equals to 15.32 % of MBL, determined by the procedure. The corresponding convergent dynamic stiffness of 10 % +- 0.9 % of MBL is found for the FLS case. The results presented in Table 2-5 show the important impact of the tension amplitude on the dynamic stiffness of nylon and the resulting dynamic tension

responses in the mooring lines. The corresponding platform motion statistics are presented in Table 2-6.

Figures 2-24 and 2-25 show the tension time histories at the fairlead point of the front line 1 comparing different cases of stiffness (i.e. with the same mean tension but different tension amplitudes). It can be seen that at the same mean tension, with a lower tension amplitude, the rope gets stiffer which results in more severe tension responses in the line (both in peak and trough values). This confirms the important impact of the tension amplitude on the dynamic stiffness of nylon ropes and the resulting dynamic tension in both strength and fatigue conditions.

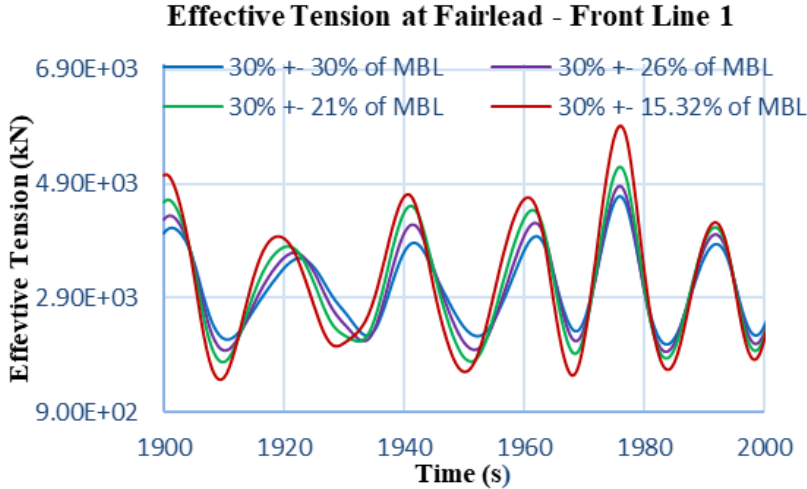


Figure 2-24: Dynamic tension of a mooring line in ULS condition applied the present fiber rope mooring analysis procedure presented in Figure 2-9.

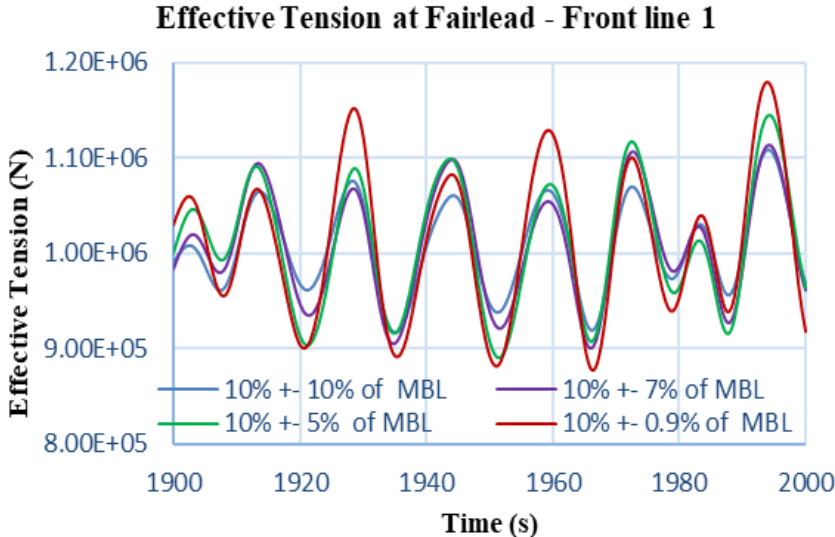


Figure 2-25: Dynamic tension of a mooring line in FLS condition applied the present fiber rope mooring analysis procedure presented in Figure 2-9.

The maximum design tension of the mooring component is chosen as

$$T_{max_design} = \frac{MBL}{SF} \tag{2.10}$$

where MBL - The Minimum Breaking Load of the mooring component.

SF – The minimum safety factor of the mooring components taken as 1.67 according to API-RP-2SK (API, 2005).

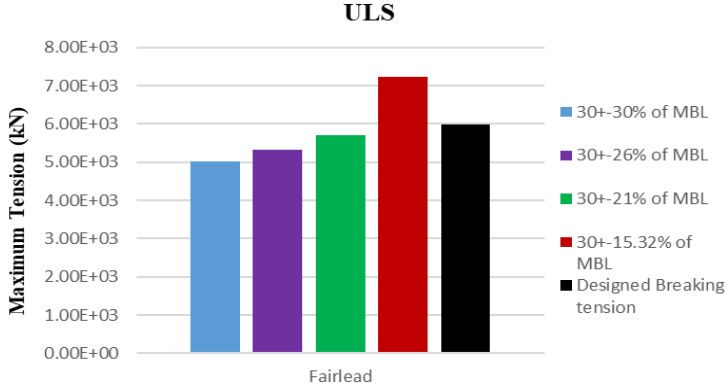


Figure 2-26: Comparison of maximum tensions for different cases of stiffness with the design breaking tension (i.e. which considers the safety factor of 1.67 according to API-RP-2SK (API, 2005)).

It can be seen in Figure 2-26 that if the tension amplitude is not correctly considered while determining the rope stiffness, the maximum tension in the mooring lines can be underestimated. Indeed, the line is still considered correctly designed for the three stiffness cases (30 % +- 30 % of MBL, 30 % +- 26% of MBL, 30 % +- 21 % of MBL) whereas it has already failed if the convergent dynamic stiffness (i.e. determined following the procedure in Fig. 6), 30 % +- 15.32 % of MBL is considered.

As there is currently limited publically available research on the fatigue behavior of nylon ropes, the fatigue analysis will be performed hereafter for only the chain section at the fairlead point. This, however, shows the importance of the present dynamic stiffness model on the global fatigue responses of the mooring lines.

The T-N fatigue curve approach according to API-RP-2SK (API, 2005) is applied as

$$N = K \cdot T_R^{-m} \tag{2.11}$$

where N - the number of cycle to failure under a tension range T_R

$K = 1000, m = 3$ for studlink chain (API, 2005)

The fatigue damage accumulation is calculated following the Palmgren-Miner’s rule,

$$D = \sum_{i=1}^n \frac{1}{N(T_{Ri})} = \frac{1}{K} \sum_{i=1}^n T_{Ri}^m \tag{2.12}$$

where T_{Ri} - the tension range at tension cycle number i .

n - the number of tension cycles T_{Ri} .

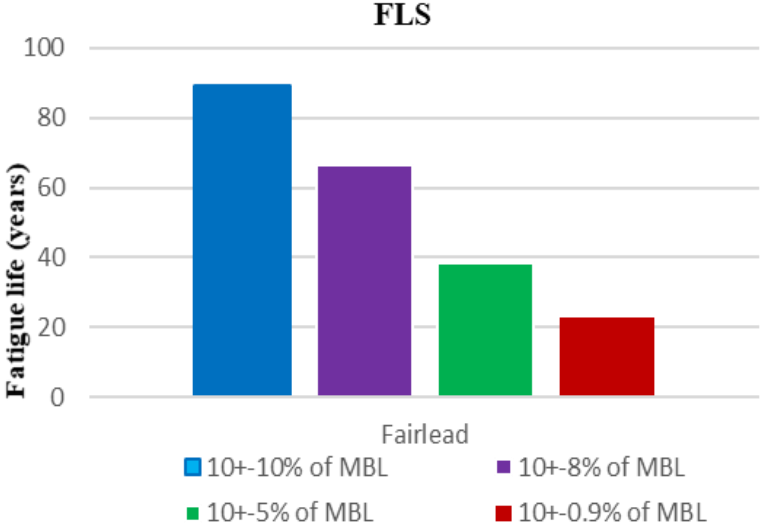


Figure 2-27: Expected fatigue lives for different stiffness cases (a safety factor of 3 according to API-RP-2SK (API, 2005) is already consider for the fatigue life in each case).

The time domain fatigue analysis is performed by Orcaflex. Figure 2-27 compares the fatigue life of the front line 1 at the fairlead point for different cases of stiffness. It shows that the convergent dynamic stiffness model gives a more conservative fatigue life estimate. For instance, the fatigue life considering the dynamic stiffness equivalent to the case 10 +- 10% of MBL is about 89 years whereas it is only about 22 years for the convergent dynamic stiffness case, i.e. 10% +- 0.9% of MBL.

Comparison of chain-nylon-chain and chain-polyester-chain mooring systems

Two mooring systems composing of chain-nylon-chain and chain-polyester-chain are compared to study the impact of the different cases of stiffness for the two synthetic materials on mooring line responses. The same MBL (as presented in Table 2-3) and the same mean tensions in each sea state are chosen for the two mooring systems in order to investigate the required fiber rope lengths and the resulting tension responses. The un-stretched lengths of polyester and nylon ropes are chosen according to the mean tension for each sea state. For this, the quasi-static stiffness (as in Eq. (2-5)) and

the static modulus reported Varney et al. (2013) are used for polyester and nylon respectively.

Table 2-7: Mooring line properties.

Materials/Properties	Mean Tension	Axial Stiffness EA_dynamic (kN)	Un-stretched length (m)
Nylon	30 % of MBL	105.628E3	681.195
Polyester	30 % of MBL	284E3	722.530
Nylon	10 % of MBL	57.91E3	713.896
Polyester	10 % of MBL	218E3	732.362

The line characteristics and motion statistics of the floating structure are presented in Tables 2-7 and 2-8. It can be seen that at the same mean tension significantly higher stiffness is found for polyester. Consequently, that results in not only longer required un-stretched lengths of the lines but also restricted levels of motions corresponding with more severe dynamic tension responses. In the following example, it is the author’s intention to choose the same mean tension for different mooring configurations (i.e. with nylon and with polyester). This allows to investigate the un-stretched length required for each mooring component for the same footprint and the corresponding mooring responses.

The tension responses in both ULS and FLS conditions are also compared in Figures 2-28 and 2-29. The significant increases in tension extremes (i.e. peak and trough) is found in the chain-polyester-chain mooring system. This confirms the advantage of nylon for reducing the extreme tension responses in mooring lines, which is favorable for both extreme and fatigue designs.

In conclusion, the numerical results show the advantages and conservativeness of the present nonlinear dynamic stiffness model for nylon mooring modeling in both ULS and FLS cases. However, comparison with field measurements on real nylon mooring lines or dynamic stiffness tests under irregular loading are necessary in order to validate and improve the model. Furthermore, the coupled aero-hydrodynamic analysis could be of great importance for the modeling of FWT responses but is not considered

in this work. The results show also the advantage of nylon on reducing the required mooring line lengths and tension responses which are favorable for both strength and fatigue design.

Table 2-8: Motion statistics.

Stiffness cases / Motions		Surge (m)	Sway (m)	Heave (m)	Roll (deg)	Pitch (deg)	Yaw (deg)
Nylon 30% of MBL	Mean	-0.81	-0.01	0.04	0.00	-0.53	0.06
	STD	6.98	0.02	2.54	0.01	2.51	0.01
	Min	-30.30	-0.16	-9.96	-0.02	-8.81	0.01
	Max	15.40	0.16	8.23	0.03	6.68	0.11
Polyester 30% of MBL	Mean	-1.35	0.00	-0.40	0.00	-0.56	0.06
	STD	6.98	1.11	2.55	0.18	2.16	0.47
	Min	-27.80	-5.83	-9.31	-1.06	-6.95	-3.39
	Max	16.31	4.82	7.17	1.18	6.54	2.35
Nylon 10% of MBL	Mean	-0.04	0.00	-0.01	0.00	0.00	0.00
	STD	0.98	0.00	0.77	0.00	1.43	0.00
	Min	-4.03	-0.01	-2.50	-0.01	-4.09	0.00
	Max	2.65	0.01	2.30	0.01	4.13	0.00
Polyester 10% of MBL	Mean	-0.30	0.00	-0.08	0.00	-0.14	0.06
	STD	2.07	0.01	0.72	0.00	1.37	0.02
	Min	-6.23	-0.04	-2.24	-0.01	-3.55	0.01
	Max	4.84	0.03	1.87	0.01	3.18	0.13

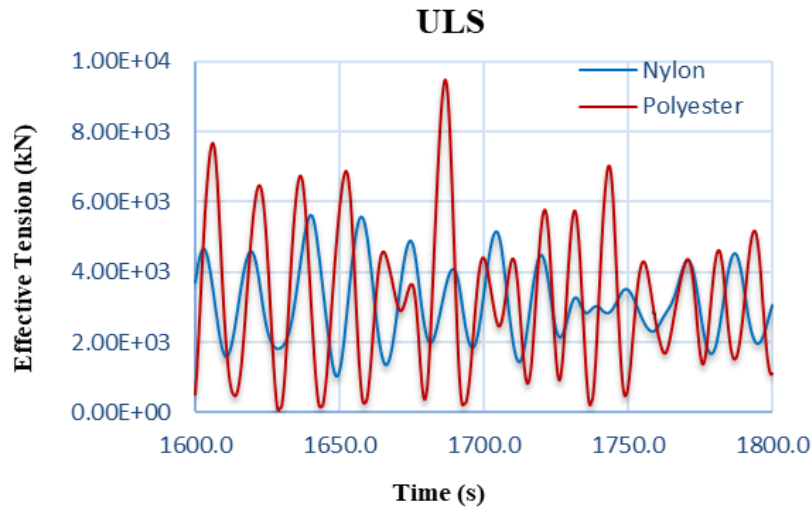


Figure 2-28: Tension responses, ULS.

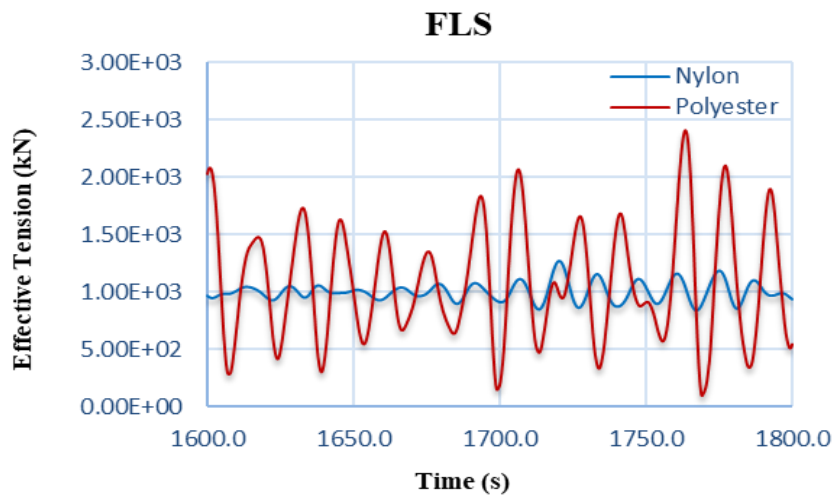


Figure 2-29: Tension responses, FLS.

4. Marine environmental impacts

For the present in-service monitoring methodology, it is also important to understand and consider the marine environmental factors that influence the modeling and health monitoring of mooring lines. These environmental factors include the water depth, the environmental loads (e.g. wind, current, wave), marine species, etc.

Spraul et al. (2017), Yang et al. (2017) and Wright et al. (2016) studied the effects of marine growth on the mooring lines of marine renewable energy devices. According to their conclusions, the biofouling has an important impact on the tension responses and thus on the fatigue life of mooring lines. For fiber rope mooring without covering and filters, junior harsh marine species such as mussels can even penetrate and growth inside the ropes, then accelerate the inter-strand abrasion (Weller et al., 2015). The marine species colonization measured at the Ecole Centrale Nantes/SEM-REV test site (Spraul et al., 2017) is shown in Figure 2-30 for illustration.

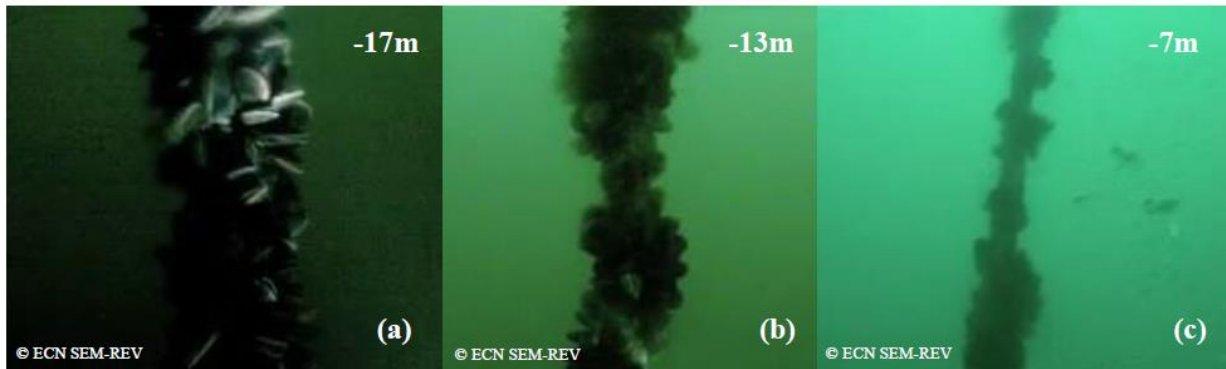


Figure 2-30: Biofouling colonization survey using under-water camera at the SEM-REV test site (Spraul et al., 2017).

Others marine environmental effects such as accelerated corrosion of chain links in sea water, wear at the fairlead connection point and seabed touchdown sections of the lines, etc. should be listed and understood for a comprehensive modeling and service life monitoring approach. Indeed, experiences from the Oil & Gas industry show several mooring line failures due to the fatigue damage induced by the crack propagation which can be accelerated by corrosion in marine environment and wear between chain links or at connection points (Lardier et al., 2008). Corrosion results in the reduction of steel surface, variation in residual stresses, therefore, influences both strength and fatigue design of mooring lines. Corrosion in sea water of chains is a complex phenomenon since it depends on both the mooring material properties and the marine environment characteristics (the composition of sea water, temperature, salinity, dissolved oxygen, etc.). Most of corrosion models are simply based on a constant rate of corrosion. For instance, API-RP-2SK (API, 2005) recommends an industry practice to increase the chain diameter in the splash zone and the dip or thrash zone on hard bottom by 0.2 to 0.4 mm/year, this increasing diameter is reduced to 0.1 to 0.2 mm/year for the remaining length. Bureau Veritas Guidance Note NI-493 (BV, 2015) requires a 0.4 mm/years of corrosion and wear allowance for the chain section in splash zone and the bottom length, and 0.3mm/year in the remaining length. DNV OS-E301 (DNV, 2010) recommends considering a corrosion rate of 0.4 mm/year in chain diameter in the catenary and bottom parts and a higher rate of 0.8 mm/year for the splash zone. Melchers et al. (2007) proposed a probabilistic model for fully submerged chains with the mean value of corrosion rate about 0.44mm/year with a standard deviation of 0.1mm/year. Schoefs et al. (2009) suggested an inspection model of the steel loss in view to account for the variability of the corrosion rate with time.



Figure 2-31: Corroded chain mooring lines of a met-ocean buoy at the SEM-REV sea test site (Berhault, 2017).

The corrosion observed in the catenary mooring lines of a met-ocean buoy operated at the Ecole Centrale Nantes/SEM-REV sea test site (Berhault, 2017) is illustrated in Figure 2-31.

During their design life-time, material loss in synthetic ropes can also be induced and accelerated by some external factors such as,

- Harsh granular and shell marine species penetration inside the ropes, and the forming of salt crystal (i.e. a phenomenon that happens when the ropes undergo regularly through consecutive dry-wet cycles, e.g. at the splash zone section) that induce and accelerate inter-strand abrasion. These problems can be avoided by proper design such as the use of rope jacket and filter, and by keeping the fiber rope section always underwater during operation.
- Excessive wear at the top-connection point and sea-bed connection. This can be avoided by using additional chain sections at the upper and touch-down part of the lines.

For the safety operating objectives discussed above, a clump weight is applied near the top connection point of the nylon rope in order to keep it always underwater during operation. Also, the distributed buoys are applied to avoid contact between the fiber ropes with the sea-bed.

5. Conclusions

This chapter discusses the mechanical behaviors of the two mooring components, i.e. chain and nylon, and the marine environmental factors influencing such behaviors. The objectives are to identify and calibrate major factors influencing the modeling and monitoring of mooring lines during operation. Based on the information mentioned previously, the design, modeling and service life monitoring of mooring lines can be improved. Indeed, it can be seen that monitoring and inspection should focus on the first link of the top chain that is more vulnerable due combined fatigue damage (i.e. tension-tension plus in-plane and out-of-plan bending). Corrosion and wear were found more severe at splash zone and sea-bed contact sections of the chain whereas lower rate of corrosion was found for fully submerged sections.

The critical parameters for monitoring and investigating should be floating structure motions, mooring tensions and the angle differences between fairlead and chain, marine growth, corrosion and wear, etc. Those parameters should be carefully investigated and monitored in order to update the structure behaviors and reliability, and to forecast necessary maintenance or replacement of lines.

As for the nylon rope, an empirical expression of axial dynamic stiffness depending on both the mean tension and the tension amplitude is drawn based on rope stiffness tests in the literature. A practical procedure for dynamic modelling of nylon mooring ropes is proposed (Pham et al., 2019). Moreover, creep and internal abrasion are identified as two major fatigue mechanisms for nylon ropes which should be studied separately. Internal-abrasion fatigue, however, is a non-linear and complex fatigue mode which may induce severe material loss and modified stiffness of nylon ropes. In order to fully understand internal abrasion fatigue without having to perform exhausting long-cycle fatigue tests, a non-destructive fatigue testing approach is proposed which will be among the authors' future scope of work.

The marine environmental factors such as marine growth, corrosion and environmental loading are also discussed in order to identify and calibrate factors influencing the modeling and monitoring of mooring lines during exploitation. This is important for the methodology presented in **chapter 3** where a sound understanding of the actual states of the mooring system during exploitation is required in order to improve the accuracy of the mooring resistance check, fatigue estimate via reliability assessment.

6. References

ABS (American Bureau of Shipping). Guidance Notes on the Application of Fiber Rope for Offshore Mooring. (2014).

API (American Petroleum Institute). API-RP-2SM. Design, Manufacture, Installation, and Maintenance of Synthetic Fiber Ropes for Offshore Mooring, (2014).

API (American Petroleum Institute). API-RP-2SK. Design and Analysis of Stationkeeping Systems for Floating Structures. 2005.

Arnal V., Soulard T., Berhault C. Etude De Sensibilite Aux Chargements Hydrodynamiques Et Aerodynamique Pour Les Eoliennes Offshores Flottantes, Dans Des Conditions Extremes. 15eme journée d'hydrodynamique, 22-24 novembre 2016, Brest, France.

Banfield S., Ridge I.M.L. Fatigue durability of nylon rope for permanent mooring design. (2017). OCEANS 2017, 19-22 June 2017.

Banfield S.J., Casey N. FATIGUE MECHANISMS AND RESIDUAL PROPERTIES OF POLYESTER ROPES. https://www.tensiontech.com/_app_/resources/documents/www.tensiontech.com/fatigue_mechanisms_and_residual_props_polyester.pdf. (Accessed: 10 March 2018).

Berhault C. SEM-REV: Corrosion et Usure. Le Croisic/France - West Atlantic Coast. https://www.weamec.fr/wp-content/uploads/2017/10/4_SEM-REV-WeAMEC-Corrosion.pdf (2017).

Berhault C., Le Crom I., Le Bihan G., Rousset J.M. SEM-REV, de 2007 à 2016, du projet au site opérationnel: retour d'expérience. 14èmes Journées Nationales Génie Côtier – Génie Civil, Toulon, 2016.

Bitting K.R. The dynamic behavior of nylon and polyester line. Coast Guard Research and Development Center, USCG-D-39-80, Apr. (1980).

Bosman R.L.M., Hooker J. The Elastic Modulus Characteristics of Polyester Mooring Ropes. OTC 10779 (1999) 2–6.

Brown M.G., Hall T. D., Marr D.G., M. English M., Snell R.O. Floating Production Mooring Integrity JIP – Key Findings. Offshore Technology Conference, 2-5 May, Houston, Texas. OTC-17499-MS (2005).

BV (Bureau Veritas). HydroStar for expert user manual. June 2016.

BV (Bureau Veritas). NR-493-DT-R03-E. Classification of Mooring Systems for Permanent and Mobile Offshore Units. 2015.

BV (Bureau Veritas). Bureau Veritas Guidance Note NI-604-DT-R00-E. Fatigue of Top Chain of Mooring Lines due to In-plane and Out-of-plane bending. 2014.

BV (Bureau Veritas). Guidance Note NI 432 DTO R01E, Certification of Fibre Ropes for Deepwater Offshore Services. (2007).

Chevillotte Y., Marco Y., Davies P., Bles G., Arhant M. Fatigue of polyamide mooring ropes for floating wind turbines. MATEC Web of Conferences 165, 10002 (2018) 1–7.

Del Vecchio C.J.M. Light Weight Material for Deepwater Mooring. PhD thesis. University of Reading, UK. (1992).

DNV. DNV Offshore Standard - Position Mooring. DNV-OS-E301, 2010.

DNVGL. RP-E305. Design, testing and analysis of offshore fibre ropes, (2015).

Ecole Centrale de Nantes. Floatgen, la première éolienne en mer en France. <https://www.ec-nantes.fr/actualites/floatgen-la-premiere-eolienne-en-mer-en-france-170471.kjsp> (accessed 29 October 2018).

ECN (Ecole Centrale de Nantes). Floatgen, la première éolienne en mer en France. <https://www.ec-nantes.fr/actualites/floatgen-la-premiere-eolienne-en-mer-en-france-170471.kjsp> (accessed 29 October 2018).

Falkenberg E., Ahim V., Yang L., DNVGL. Best Practice for Analysis of Polyester Rope Mooring Systems. Offshore Technology Conference. OTC-27761-MS, Houston, Texas, USA, 1–4 May (2017).

Falkenberg E., Yang L., Ahim V. The Syrope Method for Stiffness Testing Of Polyester Ropes. Proceedings of the ASME 2018 37th International Conference on Ocean, Offshore and Arctic Engineering. (2018) 3782–3787.

Fernandes A.C., Del Vecchio C.J.M, Castro G.A.V. Mechanical properties of polyester mooring cables. *International Journal of Offshore and Polar Engineering*. (1999). 9:208–213.

Fernández J., Storesund W. Fatigue Performance of Grade R4 and R5 Mooring Chains in Seawater Omae2014-23491, Omae2014-23491. (2014) 1–6.

Flory J., Ahjem V., Bandfield S.J. A New Method of Testing for Change-in-Length Properties of Large Fiber-Rope Deepwater Mooring Lines, *Offshore Technology Conference*, 30 April-3 May, Houston, Texas, U.S.A, 2007.

Flory J., Banfield S. J. Durability of polyester ropes used as deepwater mooring lines. 0197-7385 *OCEANS* 2006, 18-21 Sept.

Flory J., Parsey M., Leech C. A method of predicting rope life and residual strength. *OCEAN* 1989. 18-21 Sept. 1989. Seattle, WA, USA, USA.

Flory J.F., Banfield S.J., Ridge I.M.L., Yeats B., Mackay T., Wang P., Hunter T., Johanning L., Herduin M., Foxtton P. Mooring systems for marine energy converters. *OCEANS* 2016. 19-23 Sept. 2016. Monterey, CA, USA.

François M., Davies P. Fibre rope for Deepwater Mooring: A Practical Model for The Analysis of Polyester Mooring Systems. *Proc. of Rio O&G conf. Rio de Janeiro, Brazil*, (2000).

François M., Davies P., Grosjean F., Legerstee F. Modelling fibre rope load–elongation properties – polyester and other fibres. *OTC 20846*. Houston, USA. 2010.

Huang W., Liu H., Lian Y., Li L. Modeling nonlinear creep and recovery behaviors of synthetic fiber ropes for deepwater moorings, *Appl. Ocean Res.* 39 (2013) 113–120.

Hearle J.W.S., Parsey M.R., Overington M.S., Bandfield S.J. Modelling the long-term fatigue performance of fibre rope. *Proceedings of the Third International Offshore and Polar Engineering Conference*, Singapore, 6-11 June 1993.

Huntley M.B. Fatigue and Modulus Characteristics of Wire-Lay Nylon Rope. *MTS/IEEE Oceans Conference Proceedings*. Monterey, CA, USA. (2016).

Kim Y., Kim M-S., Park M-Y. Fatigue analysis on the mooring chain of a spread moored FPSO considering the OPB and IPB. *International Journal of Naval Architecture and Ocean Engineering*. 2017.

Kim M., Ding Yu., Zhang Jun. Dynamic simulation of Polyester Mooring Lines. Deepwater Mooring Systems Concepts, Design, Analysis, and Material. Houston, Texas, 101-114, 2003.

Lardier J., Moan T. Fatigue Reliability of Catenary Mooring Lines Under Corrosion Effect. Proceedings of the ASME 27th International Conference on Offshore Mechanics and Arctic Engineering OMAE2008. June 15-20, 2008, Estoril, Portugal (2008).

Lechat C. COMPORTEMENT MECANIQUE DE FIBRES ET D'ASSEMBLAGES DE FIBRES EN POLYESTER POUR CABLES D'AMARRAGE DE PLATES-FORMES OFFSHORE, PhD thesis. Ecole des Mines de Paris. 2007.

Lin Z., Sayer P. An enhanced stiffness model for elastic lines and its application to the analysis of a moored floating offshore wind turbine. Ocean Eng. 109 (2015) 444–453.

Liu H., Lian Y., Li L., Zhang Y. Experimental Investigation on Dynamic Stiffness of Damaged Synthetic Fiber Ropes for Deepwater Moorings, J. Offshore Mech. Arct. Eng. 137 (2015) 061401.

Liu H., Huang W., Lian Y., Li L. An experimental investigation on nonlinear behaviors of synthetic fiber ropes for deepwater moorings under cyclic loading, Appl. Ocean Res. 45 (2014) 22–32.

Ma K., Energy C., Company T., Duggal A., Smedley P., Exploration B.P. A Historical Review on Integrity Issues of Permanent Mooring Systems. OTC 24025, 2013.

Mandell J. Modelling of marine rope fatigue behavior. Textile Research Journal. Volume: 57 issue: 6, page(s): 318-330. June 1, 1987

Mandell J., STECKEL M.G., CHUNG S.-S., KENNEY M.C. Fatigue and environmental resistance of polyester and nylon fibers. POLYMER ENGINEERING AND SCIENCE, AUGUST, 1987, Vol. 27, No. 75.

McKenna H.A., Hearle J.W. S., O'Hear N., Handbook for fiber rope technology, 2004.

Melchers R.E., Moan T., Gao Z. Corrosion of working chains continuously immersed in seawater. Journal of Marine Science and Technology; Vol. 12, No. 2, pp. 102-110. (2007).

OCIMF. OCIMF Guidelines for The Purchasing and Testing of SPM Hawsers, 2000.

Orcina. User Manual Online.
<http://www.orcina.com/SoftwareProducts/OrcaFlex/Documentation>. 2012.

Parsey M. Fatigue of SPM Mooring Hawsers. Proceedings of Offshore Technology Conference, OTC 4307, Houston, May 1982.

Pham H.D., Cartraud P., Schoefs F., Soulard T., Berhault C. Dynamic Modeling of Nylon Mooring Lines for a Floating Wind Turbine. *Appl. Ocean Res.*, 87 (2019), pp. 1-8.

Ramnäs. Quality Chains and Accessories. https://www.offshore-europe.co.uk/__novadocuments/30275?v=635060256952870000. (2013).

Ridge I.M.L., Banfield S.J., Mackay J. Nylon Fibre Rope Moorings for Wave Energy Converters. OCEANS 2010.

Royal IHC. UNDERWATER FAIRLEAD.
<https://www.royalihc.com/en/products/offshore/fpso-equipment/underwater-fairlead>.
(Accessed: 12 Mai 2018).

Schoefs F., Clément A., Nouy A. Assessment of ROC curves for inspection of random fields, *Struct. Saf.* 31 (2009) 409–419.

Spraul C., Pham H.D, Arnal V., Reynaud M. Effect of Marine Growth on Floating Wind Turbines Mooring Lines Responses. In AFM 2017 23ème Congrès Français de Mécanique, 28 Aug – 1 Sept, 2017.

Tahar A., Kim M.H. Coupled-dynamic analysis of floating structures with polyester mooring lines, *Ocean Eng.* 35 (2008) 1676–1685.

Varney A., Taylor R., Seelig W. Evaluation of Wire-Lay Mooring Lines in a Wave Energy Device Field Trial. MTS/IEEE Oceans 2013 Conference Proceedings, 2013.

Weller S.D., Johanning L., Davies P., Banfield S.J. Synthetic mooring ropes for marine renewable energy applications, *Renew. Energy.* 83 (2015) 1268–1278.

Weller S.D., Johanning L., Davies P., Banfield S.J. Synthetic mooring ropes for marine renewable energy applications. *Renewable Energy* 83 (2015) 1268-1278.

Weller S.D., Davies P., Vickers A.W., Johanning L. Synthetic rope responses in the context of load history: The influence of aging, *Ocean Eng.* 96 (2015) 192–204.

Wright C., Pakrashi V., Murphy J. The dynamic effects of marine growth on a tension moored floating wind turbine. Proceedings of Renew 2016, 2nd International Conference on Renewable Energies Offshore, Lisbon, Portugal, 2016.

Yang S-H., Ringsberga J W., Johnsona E., Huc Z. Biofouling on mooring lines and power cables used in wave energy converter systems—Analysis of fatigue life and energy performance. Applied Ocean Research 65 (2017) 166–177.

CHAPTER 3 – METHODOLOGY FOR MODELING AND SERVICE LIFE MONITORING OF MOORING LINES OF FLOATING WIND TURBINES

CHAPTER 3 – METHODOLOGY FOR MODELING AND SERVICE LIFE MONITORING OF MOORING LINES OF FLOATING WIND TURBINES . 100

- 1. INTRODUCTION 101
- 2. STATE-OF-THE-ART IN MOORING LINE FATIGUE ANALYSIS 103
 - 2.1 *Time domain fatigue analysis* 104
 - 2.2 *Frequency domain (spectral) fatigue analysis*..... 105
 - 2.3 *Comparison of fatigue damage calculated by spectral fatigue approaches and time domain analysis*..... 109
- 3. METHODOLOGY FOR MODELING AND SERVICE LIFE MONITORING OF MOORING LINES 110
- 4. METHODOLOGY FOR RELIABILITY ASSESSMENT 112
 - 4.1 *Reliability in strength condition (ULS)*..... 113
 - 4.2 *Reliability in fatigue condition (FLS)* 114
 - 4.3 *Reliability assessment for the case study*..... 114
- 5. SIMULATION OF NON-GAUSSIAN PROCESSES BASED ON ARTIFICIAL NEURAL NETWORK..... 123
 - 5.1 *Artificial Neural Network (ANN) for simulation of nonlinear mooring response*..... 127
 - 5.2 *Comparison and application for reliability assessment* 134
- 6. CONCLUSIONS..... 142
- 7. REFERENCES 145

1. Introduction

The modeling and monitoring of offshore mooring lines require a sound understanding of both the relating mechanical behaviors of all the mooring components (i.e. load-strain behaviors, breaking strength, critical modes of failure, etc.) and the marine environmental factors (i.e. environmental loading, corrosion, abrasion, colonization of marine species, etc.) that influence such behaviors. The design of offshore mooring lines are often checked against three limit states (DNV, 2010).

- Ultimate Limit State (ULS) where the lines maximum tension are designed to remain below the minimum breaking strength of the mooring components. A good estimate of the working tension is, therefore, mandatory for a reliable design. It also means that in order to perform a detailed mooring design, the mechanical properties (i.e. load-strain properties, breaking strength, etc.) of all the mooring components and the relating deterioration factors must be well understood.
- Fatigue Limit State (FLS) where mooring lines are designed for a certain service life (usually between 20 and 25 years for FWTs). The fatigue life of a mooring line is affected by not only the mechanical fatigue behaviors of the materials composing that line but also the material deterioration due to the marine environmental factors.
- Accident Limit State (ALS) where the mooring system is designed with a certain redundancy in order to ensure their capability of surviving against the failure of one line.

The previous issues have been subjects of a large amount of research work (Aqdam et al., 2018; Xue et al., 2018; Wu et al., 2015). Ma et al. (2013) investigated several accidental events in permanent mooring systems and found that many line failures occurred in early service years of mooring lines. Even if fatigue is generally the dominant cause, Gryphon incident (Finucane, 2012) teaches us a case of failure due to a combination of failure of heading control and overload. Moreover, the failure mechanisms have surprised the industry experts. A limit number of known failures for mooring lines of marine renewable energy devices (e.g. Oceanlinx in 2010 and Wavedragon in 2004) has been discussed by Christensen et al. (2005), but the reasons of failure stay still unclear. Brindley et al. (2014) stressed that only strength requirements do not fully reflect the system reliability. Pham et al. (2004), Pham (2018) studied the interaction between the reliability in the ULS and FLS. According

to their conclusions, the total reliability should be considered either by multiplying the reliability of the two design criteria (for the reliability in the ULS case) or by adding the fatigue damage caused by extreme sea states that might probably occur at any point during the expected service life of structures (for the reliability in the FLS case).

Unlike O&G platforms, MRE devices are generally small compared to the incident wave length and thus will tend to dynamically respond to first-order and second-order wave loading as well as the combined effects of wind and currents. There is usually strong coupling between the device and mooring system responses and hence complex motions can occur which may be large if the system response is resonant (Weller et al., 2013). For the FLOATGEN project that the present case study is based on, nylon is used as a principal mooring component and the modeling of mooring responses lacks validation. It is mainly due to the non-linear load-elongation behavior and fatigue characteristics of nylon mooring ropes that cannot be captured following the same testing and modeling procedures for polyester as recommended by the present O&G standards.

Thies et al. (2014) argued that numerical modeling seems still scantily validated for new applications such as floating marine renewable energy devices. They proposed, as an alternative, an approach to predict fatigue damage using directly in-situ load measurements. Their approach has been concluded to allow a better fatigue assessment and an optimization of safety factors at the design state where on-site measurements are available. Also, the approach may be used for the in situ monitoring in order to predict the fatigue damage and the remaining service life of the structure during deployment. However, the author believe that only load measurements are not enough to characterize the actual state of mooring lines that actually includes the likely modified mooring line mechanical behaviors (e.g. strength and stiffness reduction, etc. due to material loss (Gao et al., 2005; Liu et al., 2015), modified mass and hydrodynamic damping due to biofouling (Spraul et al., 2017; Yang et al., 2017; Wright et al., 2016) and other marine environmental factors such as corrosion, wear, extreme environmental conditions, etc. (DNV, 2010; API, 2005; BV, 2015; Lardier et al., 2008; Melchers et al., 2007; Schoefs et al., 2009). These mechanical behaviors of mooring materials and marine environmental factors should be fully understood and accounted for. Indeed, it is vital to clarify the mechanics of the mooring line responses, to understand why and how they might be modified during deployment, and how those can be accounted for in order to update the actual fatigue damage and predict the remaining allowable service life of the system. That is why, in the author's opinion, modeling and monitoring should be implemented in parallel in order to better control

and update the actual state of mooring lines, better estimate the fatigue damage and reliability of the system during deployment. Based on that, decisions regarding required maintenance or replacement of lines can be made.

This chapter focuses on the service life monitoring of mooring lines. For this general objective, first, fatigue damage estimate based on cutting-edge frequency domain approach has been investigated in order to select a quick but reliable approach for fatigue analysis as an alternative to time domain fatigue analysis. Secondly, a methodology for modeling and service life monitoring of mooring lines of FWTs is proposed based on the reliability approach. The methodology can be applied for the Ultimate Limit State (ULS) in order to check if the mooring lines can still sustain the design extreme load case after years of operation. Also, by applying the methodology for the Fatigue Limit State (FLS), the remaining allowable service life can be predicted based on the information obtained from the previous operating years. Furthermore, the present methodology can also be considered for a more detailed mooring design once the information from similar structures, projects, sites, etc. are known. Finally, in order to perform a more accurate reliability assessment for extreme conditions (ULS) the application of a meta-model such as an Artificial Neural Network is investigated for nonlinear mooring response simulation. The aim is to avoid time-consuming time domain mooring modeling by building an identification system based on field measurements.

The selected frequency domain fatigue analysis approach and the present methodology for modeling and monitoring of mooring lines have been presented in another under-review paper of the author (Pham et al., 2019-b).

2. State-of-the-art in mooring line fatigue analysis

For mooring lines of offshore structures subjected to irregular and nonlinear loadings, time domain analysis is the most accurate method for simulating tension time histories. However, the method is also computationally expensive since it requires many lengthy realizations of responses in order to assure reliable statistical estimations. In addition, it also requires an appropriate cycle counting method and a damage accumulation hypothesis (e.g. Palmgren-Miner rule, etc.) for fatigue damage estimate. Thus, the frequency domain fatigue analysis (or spectral method) seems to be an efficient alternative (Mršnik et al., 2013). Besides, in order to ensure the safety integrity level of structures and the cost-effectiveness of the design, structural reliability analysis is often required. In that case, the analytical spectral method is preferable since it can be applied to reliability analysis by considering directly the randomness of the structural

responses due to environmental loadings together with the material uncertainties. However, the conventional frequency-domain fatigue analysis cannot capture the actual wide-band and nonlinear behaviors of the mooring responses. The comparison between time-domain and conventional frequency-domain fatigue analysis is illustrated in Figure 3-1.

<div style="border: 1px solid black; border-radius: 50%; padding: 5px; width: fit-content; margin: 0 auto;">Time-domain fatigue analysis</div> <ul style="list-style-type: none"> ✓ The most accurate method for fatigue analysis ✓ Being able to capture all non-Gaussian effects x Require accurate counting technique (e.g. RFC, etc.) x Time consuming 	<div style="border: 1px solid black; border-radius: 50%; padding: 5px; width: fit-content; margin: 0 auto;">Conventional frequency-domain fatigue analysis</div> <ul style="list-style-type: none"> x Fail to capture the actual bi-modal effects x Fail to capture non-Gaussian effects ✓ Do not require a counting technique ✓ Time efficiency
--	--

Figure 3-1: Comparison of time-domain and frequency-domain fatigue analyses.

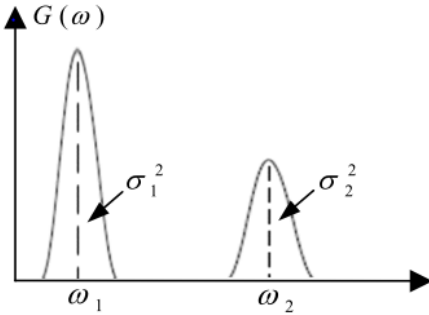


Figure 3-2: A bi-modal spectrum (Gao et al., 2010).

Several research has been focused on improved frequency domain methods that can take into account the wide-band effect of structural responses. One of the pioneered methods was proposed by Jiao et al. (1990), in which they presented a combination rule for two well-separated narrow-band Gaussian processes (as illustrated in Figure 3-2) based on the statistical properties of the combined process. The method proposed by Tovo (2002), Benasciutti et al. (2004, 2005) has been recognized as one of the most accurate method. Moreover, since mooring response is in principle non-Gaussian random process, conventional frequency domain method often lead to bias results (Sarkani, 1994). The use of a corrective coefficient multiplying with the Gaussian fatigue damage (D_g) in order to account for non-Gaussian effect seems to be an effective solution (Winterstein, 1988; Yu et al., 2003; Cianetti et al., 2017; Preumont, 1994).

2.1 Time domain fatigue analysis

It is commonly accepted that during a short-term sea state, mooring response is considered as a stationary random process which can be represented by samples of

time history thanks to the Monte Carlo simulation method. On the one hand, the duration of each sample of time history must be long enough to ensure the stationarity (i.e. the unconditional joint probability distribution does not change when shifted in time. As a consequence, statistical parameters such as mean and variance do not change over time) and ergodicity (i.e. its time average is the same as its average over the probability space). On the other hand, it is necessary to simulate for each sea state a set of tension time history samples (10 to 30 samples) in order to ensure good statistical estimate, (API, 2005). For each sample of stress time history, a counting method is applied to determine the number of cycles corresponding to the stress variation, $S = S_{\max} - S_{\min}$, where S_{\max} and S_{\min} are the consecutive maximum and minimum stress respectively. Among several counting methods, the rainflow counting (RFC) method (Rychlik, 1987) illustrated in Figure 3-3, is the most commonly used.

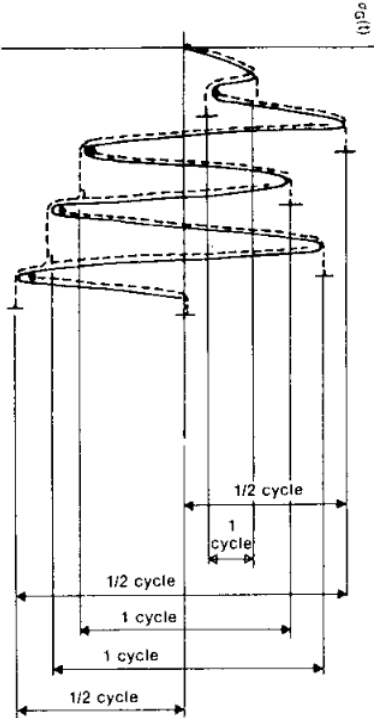


Figure 3-3: The rainflow counting method (Pham, 2010).

2.2 Frequency domain (spectral) fatigue analysis

Random processes and spectral density

In frequency domain analysis, a random process is represented by its Power Spectral Density (PSD) which is used to estimate both the cycle distribution and fatigue damage (Preumont, 1994; Bendat, 2000). Mooring response is often combined of Wave Frequency (WF) and Low Frequency (LF) tension components. In principle, due to the motions of the floating structures, the drag force acting on mooring lines and the geometrical nonlinearity of lines, the combined WF and LF mooring response is usually a wide-band non-Gaussian process.

Let $X(t)$ represent a stationary random process, the spectral moments of its spectral density $W_X(\omega)$ can be calculated as

$$\lambda_n = \int_0^{\infty} \omega^n W_X(\omega) d\omega \quad (3.1)$$

The standard deviation of $X(t)$: $\sigma_X = \sqrt{\lambda_0}$ (3.2)

The mean up-crossing rate: $v_0 = \frac{1}{2\pi} \sqrt{\frac{\lambda_2}{\lambda_0}}$ (3.3)

The frequency of peak: $v_p = \frac{1}{2\pi} \sqrt{\frac{\lambda_4}{\lambda_2}}$ (3.4)

The band-width parameters: $\alpha_1 = \frac{\lambda_1}{\sqrt{\lambda_0 \lambda_2}}$ $\alpha_2 = \frac{\lambda_2}{\sqrt{\lambda_0 \lambda_4}}$ (3.5)

The spectral parameter: $\delta = \sqrt{1 - \frac{\lambda_1^2}{\lambda_0 \lambda_2}}$ (3.6)

For different mooring line components, the corresponding fatigue S-N curves are used to estimate fatigue damage of such components. A typical single-slope S-N fatigue curve can be seen in Eq. (3.7).

$$N = KS^{-m} \quad (3.7)$$

where N - the cycle number to failure under constant stress range, S ($S = S_{\max} - S_{\min}$).

K, m - the S-N-curve parameters.

The fatigue damage accumulation is followed the Palmgren-Miner's rule and is described as

$$D = \sum_{i=1}^n \frac{1}{N(S_i)} = \frac{1}{K} \sum_{i=1}^n S_i^m \quad (3.8)$$

where S_i is the stress range at stress cycle number i
 n - is the number of stress cycles S_i

The expected damage \bar{D} is then estimated as

$$\bar{D} = \frac{1}{K} E \left[\sum_{i=1}^n S_i^m \right] = \frac{N_0}{K} \bar{S}^m \quad (3.9)$$

where N_0 is the mean number of stress cycles.

\bar{S}^m is defined as: $\bar{S}^m = \frac{1}{N_0} \sum_{i=1}^n S_i^m = \int_0^{\infty} S^m f_S(s) ds$ (3.10)

Narrow-band process

If $X(t)$ is a narrow-band Gaussian process, its amplitude, A , follows a Rayleigh distribution

$$f_A(a) = \frac{a}{\sigma_x^2} \exp\left(-\frac{a^2}{2\sigma_x^2}\right) \quad (3.11)$$

The stress range S is then exactly $2A$ and is written as

$$\bar{S}^m = \int_0^\infty (2a)^m f_A(a) da = \left(2\sqrt{2}\sigma_x\right)^m \Gamma\left(\frac{m}{2}+1\right) \quad (3.12)$$

where Γ - Gamma function

$$\Gamma(z) = \int_0^\infty y^{z-1} e^{-y} dy$$

The expected damage due to $X(t)$ in a time period T (s) is estimated as

$$\bar{D}_{NB} = \frac{v_0 T}{K} \left(2\sqrt{2}\sigma_x\right)^m \Gamma\left(\frac{m}{2}+1\right) \quad (3.13)$$

Wide-band process

For a wide-band Gaussian process, however, the Rayleigh distribution assigns larger probabilities to larger stress ranges, the fatigue damage estimated by Eq. (3.13) might result in too conservative estimation (Jiao et al., 1990). The idea is, first, to estimate the fatigue damage based on the narrow-band assumption, then multiply with a correction coefficient to find the damage of the actual wide-band process:

$$\bar{D}_{WB} = \rho \bar{D}_{NB} \quad (3.14)$$

A bimodal process which includes two separated narrow-band contributions can be represented as:

$$X(t) = X_1(t) + X_2(t) \quad (3.15)$$

where $X_1(t)$ and $X_2(t)$ represent the Low-Frequency (LF) and Wave-Frequency (WF) narrow-band Gaussian process respectively.

The fatigue damage due to $X(t)$ is assumed to be a combination of the envelop $P(t)$ of $X(t)$ (as determined by Eq. (3.16)) and the envelop of the WF process $X_2(t)$.

$$P(t) = X_1(t) + R_2(t) \quad (3.16)$$

where $R_2(t)$ is the envelop of the WF process $X_2(t)$.

The closed-form expression of ρ proposed by Jiao and Moan (Jiao et al., 1990):

$$\rho_{JM} = \frac{\bar{D}_{X,WB}}{\bar{D}_{X,NB}} = \frac{\bar{D}_P + \bar{D}_{WF}}{\bar{D}_{X,NB}} = \frac{v_{0,P}}{v_{0,Y}} \left[\lambda_1^{*\frac{m}{2}+2} \left(1 - \frac{\lambda_2^*}{\lambda_1^*} \right) + \sqrt{\Pi \lambda_1^* \lambda_2^*} \frac{m \Gamma\left(\frac{m}{2} + \frac{1}{2}\right)}{\Gamma\left(\frac{m}{2} + 1\right)} \right] + \frac{v_{0,2}}{v_{0,Y}} \lambda_2^{*\frac{m}{2}} \quad (3.17)$$

$$\text{where} \quad \lambda_i^* = \frac{\lambda_{0,i}}{\lambda_{0,1} + \lambda_{0,2}}; \quad i = 1, 2$$

The closed-form expression in Eq. (3.17) can give very good fatigue estimation comparing with time domain simulations and RFC technique for well-separated bimodal spectrum. For the case of closely-spaced spectrum, however, it may lead to too conservative fatigue estimation (Jiao et al., 1990). In that case, an alternative approach is preferable.

According to Tovo (2002) and Benasciutti et al. (2004), The rainflow damage can be estimated as

$$\bar{D}_{X,WB} = \bar{D}_{X,RFC} = b \bar{D}_{X,NB} + (1-b) \bar{D}_{X,RMC} = (b + (1-b)\alpha_2^{m-1}) \cdot \bar{D}_{X,NB} = \rho_{TB} \cdot \bar{D}_{X,NB} \quad (3.18)$$

where $\bar{D}_{X,RMC}$ is the damage given by range-mean counting, which can determined as (Preumont, 1994).

$$\bar{D}_{X,RMC} \approx \frac{v_0 \Gamma}{K} \left(\sqrt{2\lambda_0} \alpha_2 \right)^m \Gamma\left(1 + \frac{m}{2}\right) = \alpha_2^{m-1} \bar{D}_{X,NB} \quad (3.19)$$

b is the weighting index depends on the spectral density $W_x(\omega)$ approximated as (Benasciutti et al. (2004)):

$$b \approx \frac{(\alpha_1 - \alpha_2) \left[1.112 (1 + \alpha_1 \alpha_2 - (\alpha_1 + \alpha_2)) e^{2.22\alpha_2} + (\alpha_1 - \alpha_2) \right]}{(\alpha_2 - 1)^2} \quad (3.20)$$

Non-Gaussian process

Sarkani et al. (1994) showed that the main error between non-Gaussian and Gaussian fatigue estimate is related to the kurtosis of the process and the slope, m , of the material fatigue curve. Winterstein (1988) demonstrated the relationship between the non-Gaussian and Gaussian fatigue damage depending on the kurtosis of the process and m as following:

$$\lambda_{NG} = \frac{\bar{D}_{NG}}{\bar{D}_G} = 1 + m(m+1) \frac{(k_u - 3)}{24} \quad (3.21)$$

where k_u is the kurtosis (fourth order moment of the Probability Distribution Function - PDF) of the process.

Others formula of λ_{NG} are also proposed by Cianetti et al. (2017) and Braccesi et al. (2009):

$$\lambda_{NG} = \exp\left(\frac{m^{3/2}}{\pi} \left(\frac{k_u - 3}{5} - \frac{s_k^2}{4}\right)\right) \quad \text{for low } k_u \text{ (i.e. small than 5)} \quad (3.22)$$

$$\lambda_{NG} = \exp\left(\frac{m^{3/2}}{(0.156 + 0.416k_u)\pi} \left(\frac{k_u - 3}{5}\right)\right) \quad \text{for high } k_u \text{ (i.e. greater than 5)} \quad (3.23)$$

where s_k is the skewness of the process.

Wide-band non-Gaussian process

The wide band non-Gaussian fatigue damage is then determined by

$$\bar{D}_{NG} = \lambda_{NG} \cdot \bar{D}_G = \lambda_{NG} \cdot \bar{D}_{WB} = \lambda_{NG} \cdot \rho \cdot \bar{D}_{NB} \quad (3.24)$$

2.3 Comparison of fatigue damage calculated by spectral fatigue approaches and time domain analysis

Table 3-1: Comparison of fatigue damage calculated by time domain analysis and different frequency domain fatigue analysis approaches for different sea states (Pham et al., 2019-b).

Sea states		Fatigue damage				
Hs	Tp	D_TimeDomain	D_TB+C	D_TB+W	D_NB	D_JM+W
1.25	4.5	5.78E-05	5.36E-05	5.51E-05	6.35E-05	6.86E-05
4.75	10.5	1.27E-02	1.33E-02	1.26E-02	1.44E-02	1.56E-02
2.71	13.8	2.93E-03	2.92E-03	2.93E-03	3.15E-03	3.40E-03
4.25	9.5	8.91E-03	9.11E-03	8.80E-03	1.01E-02	1.09E-02
4.75	12.5	1.72E-02	1.75E-02	1.78E-02	1.89E-02	2.05E-02
3.75	16.5	1.62E-02	1.64E-02	1.69E-02	1.76E-02	1.91E-02
2.25	16.5	3.05E-03	3.03E-03	3.08E-03	3.32E-03	3.59E-03
3.75	13.5	8.79E-03	8.37E-03	8.47E-03	8.86E-03	9.58E-03
3.75	18.5	2.04E-02	2.03E-02	2.02E-02	2.15E-02	2.33E-02
2.25	18.5	4.03E-03	3.80E-03	3.88E-03	4.23E-03	4.58E-03

Table 3-1 and Figure 3-4 show a comparison of fatigue damage calculated by time domain fatigue analysis and different frequency domain fatigue analysis approaches for different sea states observed at the SEM-REV sea test site (Pham et al., 2019-b). It can be seen that, the method of Tovo and Benasciutti (Benasciutti et al., 2004; Tovo et al., 2002) with the non-Gaussian corrected coefficient proposed by Cianetti et al.

(2009) or Braccresi et al. (2017) gives the most accurate fatigue estimate comparing with time domain fatigue analysis. This spectral fatigue approach is selected in the following for fatigue analysis based on field measurements.

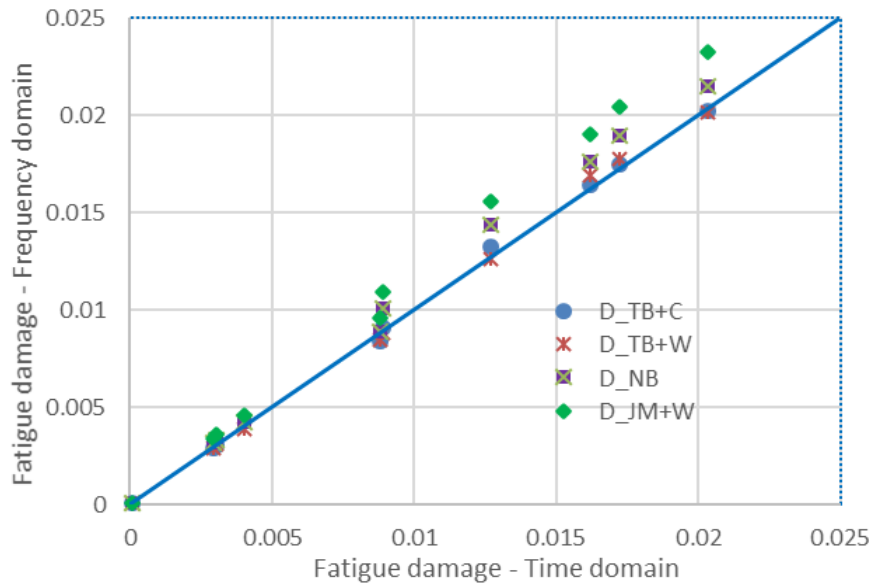


Figure 3-4: Comparison of different improved frequency-domain fatigue analysis methods with time domain simulations (Pham et al., 2019-b). (D_{TB+C} : the Tovo & Benasciutti approach (Benasciutti et al., 2004; Tovo et al., 2002) with the non-linear coefficient proposed by Cianetti et al. (2009) or Braccresi et al. (2017). D_{NB} : The narrow-band approach. D_{TB+W} : the Tovo & Benasciutti approach (Benasciutti et al., 2004; Tovo et al., 2002) with the non-linear coefficient proposed by Winterstein (1988). D_{JM+W} : the Jiao & Moan approach (Gao et al., 2007) with the non-linear coefficient proposed by Winterstein (1988).

3. Methodology for modeling and service life monitoring of mooring lines

A methodology for modeling and service life monitoring of mooring lines is discussed in the following based on reliability approach. On the one hand, the reliability approach allows accounting for the uncertainties of the materials and environmental loading (Pham et al. (2004); Pham (2018), Bitner-Gregersen et al., 1995; Horn et al., 2019; Rendón-Conde et al., 2015). On the other hand, based on the corresponding required reliability level, the design safety coefficients can be optimized for a more cost-effective but reliable design. Finally, decisions regarding the required maintenance or replacement of mooring lines can be made based on the level of reliability predicted during operation.

The methodology is presented in Figure 3-5 where the mechanical behaviors of all mooring components (i.e. strength, stiffness, fatigue characteristics, etc. as presented in block 2 of the flowchart) and the environmental factors that influence such behaviors (i.e. water depth, environmental loading, marine species, corrosion and wear, etc. as presented in block 1 of the flowchart) are identified. The measured

environmental factors (block 1) and mechanical properties of mooring components (block 2) are input to the mooring analysis tool to calculate the mooring response which is then checked against the measured one. Basically, for the present methodology, it is very important to determine and clarify which changes will occur (i.e. material deterioration, modified mass and damping due to bio-colonization, modified length or pretension due to creep of the synthetic mooring components, etc.), and how to update those changes in the modeling and fatigue life monitoring of mooring lines. For instance, after years of exploitation, the material loss (e.g. due to corrosion for chain or internal abrasion for nylon) may induce significant modifications on not only stiffness but also strength and fatigue characteristics of mooring components. Finally, the collecting information is updated in the mooring analysis tool in order to assess the reliability of the mooring lines following their expected service life. As a consequence, a full control of the actual state of mooring lines, and a better estimate of fatigue and reliability can be achieved. In the present methodology, the probabilities of failure (P_f) in the ULS and FLS are calculated following the expected service life of mooring lines considering modified mechanical behaviors of mooring components and relating environmental factors. The P_f for ULS (P_{f_ULS}) is calculated to ensure a sufficient level of reliability to sustain the design extreme sea states that might probably happen at any moment during the service life. The P_f for FLS (P_{f_FLS}) is estimated to ensure a sufficient level of reliability that the cumulative fatigue damage is minor than the critical damage. Moreover, the author also predicts the reliability level in the FLS considering the added damage due to the design extreme sea states (e.g. with a return period of 100, 50, 20, 10 years, etc.) assuming that they might probably happen at any moment during the expected service life of mooring lines. These probabilities of failures in ULS and FLS are used to support making decisions regarding maintenance or replacement of lines.

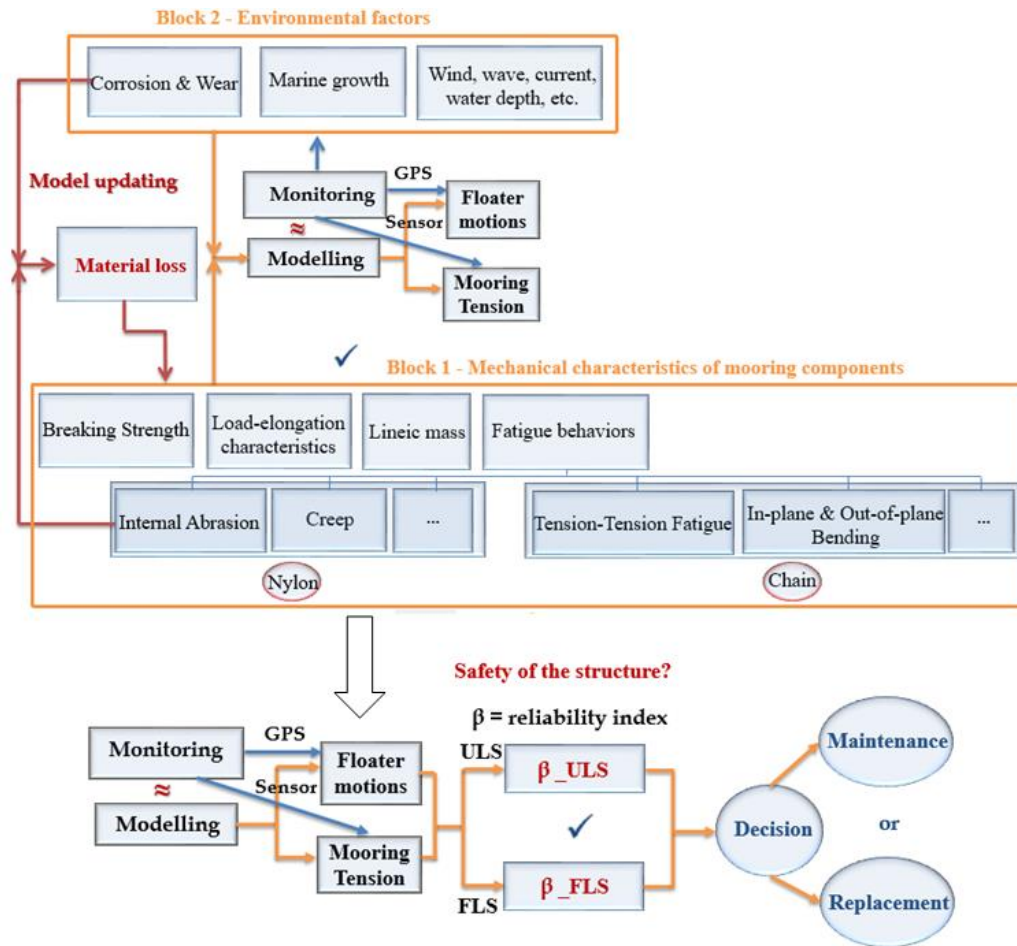


Figure 3-5: Methodology for modeling and service life monitoring of mooring lines

4. Methodology for reliability assessment

It is commonly known that reliability plays a key role in the cost-effectiveness of design where uncertainties are important. In structural reliability analysis, it's about estimating uncertainties in the predictions of structural resistance and applied loads. These uncertainties include the randomness of the environmental impacts and loadings, the material uncertainties, the statistical uncertainties and the modeling uncertainties, etc. In fact, any prediction of environmental loadings and the structural resistance is based on a certain model which approximates the reality. Therefore, it is of great importance to assess the uncertainties of the adopted model since they influence directly the accuracy of the reliability analysis (Gao, 2008).

For reliability assessment, the probability of failure is estimated as

$$P_f = P(G < 0) = P(R - S < 0) \quad (3.25)$$

where

- G- the failure function
- R- the structural resistance
- S- the load effect

Reliability analysis can be solved by using analytical methods such as First and Second Order Reliability Methods (FORM and SORM) and simulation methods such as crude Monte Carlo simulation, importance sampling, Latin Hypercube simulation, etc. (Hasofer et al., 1974; Rackwitz et al., 1978; Liu et al., 1961; Fiessler et al., 1979; Breitung, 1984; Der Kiureghian et al., 1987; Tvedt, 1990). Time-invariant and time-variant reliability analyses have been studied by Thoft-Christensen et al. (1982), Madsen et al. (1986), Melchers (1987), Hagen et al. (1991), Marley et al. (1992), and Ayala-Uraga et al. (2007). In the DEEPMOOR project, the mooring reliability analysis has been studied for two type of floating structures (i.e. FPSO and semi-submersible) considering three limit states, i.e. Ultimate Limit State (ULS), Fatigue Limit State (FLS) and Accidental Limit State (ALS) (Hørte et al., 1998; Mathisen et al., 1998; Mathisen et al., 2005). The outcomes of the project has been integrated in DNV-OS-E301 (DNV, 2010). The mooring reliability analysis is also adopted in several international standards such as API-RP-2SK (API, 2005), BV-NR-493 (BV, 2015), etc. where partial safety factors have been recommended based on reliability analyses. Mooring reliability analysis has also been the subject of an important amount of research (Brindley et al., 2014; Pham, 2010; Pham et al., 2014; Pham, 2018; Rendón-Conde et al., 2015; Luo et al., 1991; Larsen et al., 1996; Snell et al., 1999; Vazquez-Hernandez, 2006).

For mooring lines of floating wind turbines, in this work, the author focuses on two limit states, i.e. ULS and FLS. The time-variant reliability analysis is performed based on the modeling and service life monitoring methodology presented in the previous section.

4.1 Reliability in strength condition (ULS)

The time-dependent failure function in strength condition (ULS) can be written as

$$G_{\text{ULS}}(t) = T_{\text{BS}}(t) - T_{\text{smax}}(t) \quad (3.26)$$

where $T_{\text{BS}}(t)$ - the time-dependent breaking strength of the mooring components

t - the number of operating years

$T_{\text{smax}}(t)$ - the time-dependent maximum tension in the mooring components

The time-dependent probability of failure in strength condition is calculated as

$$P_{\text{f_ULS}}(t) = P(G_{\text{ULS}}(t) < 0) \quad (3.27)$$

4.2 Reliability in fatigue condition (FLS)

The probability of failure in fatigue condition can be calculated as

$$P_{f_FLS} = P(G_{FLS}(t) < 0) \quad (3.28)$$

where

$$G_{FLS}(t) = G_{FLS,l}(t) = \Delta - D_{cumulative}$$

$D_{cumulative}$ – the cumulative fatigue damage

Δ – the critical damage

4.3 Reliability assessment for the case study

As an illustration, in the following case study, the author considers corrosion in chain sections of the mooring lines as an annual constant reduction of diameter of chain links. This phenomenon leads to material loss and likely modified mooring response. The same exercises have been done by Gao et al. (2005) and Lardier et al. (2008) for the reliability of chain links accounting for their reduced breaking strength and the increased stress due to corrosion. The frequency domain fatigue analysis is chosen to calculate the fatigue damage directly from the measured tension responses. The advantages are two-fold: first, the fatigue damage can be estimated without having to perform RFC technique as in time domain analysis, second, the analytical formula of the fatigue damage can be used directly for reliability analysis considering the uncertainties of the environmental loading and the S-N fatigue curves of mooring components.

It's worth to acknowledge that standards DNV-OS-E301 (DNV, 2010), API-RP-2SK (API, 2005), Bureau Veritas NR 493 (BV, 2015) recommend to consider an additional thickness of chain links at the initial design stage in order to compensate the material loss due to corrosion. In our opinion, this is a good practice for Oil & Gas platforms mooring lines in deep-water where maintenance or replacement of lines are difficult and costly. However, that also increases the cost and the tension in the mooring system as they become heavier and stiffer. For mooring systems of MRE devices where it seems easier and less costly to maintain or replace damage lines, the present monitoring methodology discussed in section 3 of this chapter might be a promising alternative to ensure cost-effective design and safe operation.

In the following example, instead of choosing a greater diameter of chain links to account for the corrosion effect, the mooring system is designed for the expected fatigue life of 20 years with a safety factor of 3 (Lardier et al., 2008). The probabilities of failure in ULS and FLS are calculated following the expected service life in order to

investigate how material loss (e.g. due to corrosion as in the present case study) influences the modeling and service life monitoring of mooring lines, and how decisions on maintenance or replacement of lines can be made based on the estimated levels of reliability. Although the material loss due to the internal abrasion fatigue damage of the nylon rope is not considered here due to the lack of available data for this fatigue mechanism, it can be accounted for in the same manner by following the present methodology. For the sake of simplification, we do not consider marine growth and the additional damage due to In-Plane and Out-of-Plane Bending (IPB and OPB) in this example either. However, it should be stressed that in shallow water and at high pretension (i.e. greater than 10% of the Minimum Breaking Strength of the top chain) IPB and OPB are important and the combined fatigue (i.e. tension-tension plus IPB and OPB) should be investigated (BV, 2014).

The time-dependent diameter of the chain links considering the corrosion effect is determined as (Lardier et al., 2008)

$$d(t) = d_0 - t.rc \quad (3.29)$$

where t - the operation time in years; d_0 - the diameter of chain links at $t=0$,

rc - the annual corrosion rate;

The time-dependent axial stiffness of the chain sections considering the corrosion effect is determined as (Orcina, 2016)

$$\begin{aligned} EA(t) &= 0.854 \times 10^8 \times (d(t))^2 \text{ (kN)} \quad \text{for studless chain} \\ EA(t) &= 1.01 \times 10^8 \times (d(t))^2 \text{ (kN)} \quad \text{for studlink chain} \end{aligned} \quad (3.30)$$

The instantaneous stress response process, $X(t)$, of the chain links is calculated from the tension process $T_s(t)$ as

$$X(t) = \frac{T_s(t)}{A(t)} \quad (3.31)$$

where $A(t)$ – the time-dependent cross section of the chain links, $A(t) = 2. \pi \times \frac{(d(t))^2}{4}$

The corrosion in the chain sections are considered as a reduction in the diameter of chain links and the axial stiffness of the sections as in Eq. (3.29) and Eq. (3.30). Those are updated in the Orcaflex model to calculate the modified mooring response. The

same mooring configuration and floating body as presented in section 3.3 of **chapter 2** is used for the present case study.

The time-dependent Minimum Breaking Strength (MBS) of the chain links is determined as

$$\text{MBS}(t) = c^2 \cdot (d(t))^2 \cdot (44 - 0.08 \cdot d(t)) \quad (3.32)$$

where c is the grade dependent coefficient (Ramnäs, 2013).

In the following example, due to the small discrepancy for comparativeness of the probability of failure, another estimate of reliability, i.e. the reliability index, is compared. The reliability analysis is performed based on the First Order Reliability Method (FORM) using the open source initiative OpenTURN (2016).

Reliability in strength condition (ULS)

It is commonly accepted by the offshore industry that for the duration of 3 to 6 hours (i.e. corresponding to the duration of an extreme sea state), the tension response process, $T_s(t)$, can be considered as stationary. Assuming that the process is normally distributed, the probability density function of the maximum tension, T_{smax} , is expressed as

$$p(T_{smax}) = \frac{1}{\sigma_{T_s}^2 \sqrt{2\pi}} \exp\left(-\frac{T_{smax}^2}{2\sigma_{T_s}^2}\right) \quad (3.33)$$

Where σ_{T_s} is the standard deviation of the tension response process $T_s(t)$.

The time-dependent breaking tension of the chain links, $T_{BS}(t)$, is assumed to be log-normally distributed with the mean value equals to $1.2 \times \text{MBS}(t)$ and the Coefficient of Variation (COV) equals to 0.05 (Gao et al., 2005). These are presented in Tables 3-2 and 3-3 where the material loss in the chain links due to corrosion is considered as an annual reduction in diameter, rc , equals to 0.4 mm/year and 0.8 mm/year respectively.

Table 3-2: The time-dependent Breaking Tension of chain link at the fairlead connection point considering an annual reduction in diameter, $r_c = 0.4 \text{ mm/year}$.

t (years)	Residual thickness (mm)	Residual MBS (kN)	Mean BS (kN)	Variance of BS
0	95	9.987E3	11.984E3	359.043E3
1	94.6	9.911E3	11.894E3	353.655E3
5	93	9.613E3	11.535E3	332.655E3
8	91.8	9.391E3	11.269E3	317.476E3
10	91	9.244E3	11.093E3	307.624E3
13	89.8	9.025E3	10.830E3	293.243E3
15	89	8.88E3	10.657E3	283.917E3
18	87.8	8.665E3	10.398E3	270.313E3
20	87	8.523E3	10.227E3	261.498E3

Table 3-3: The time-dependent Breaking Tension of chain links at the fairlead connection point considering an annual reduction in diameter, $r_c = 0.8 \text{ mm/year}$.

t (years)	Residual thickness (mm)	Residual MBS (kN)	Mean BS (kN)	Variance of BS
0	95	9.987E3	11.984E3	359.043E3
1	94.2	9.836E3	11.804E3	348.323E3
5	91	9.244E3	11.093E3	307.624E3
8	88.6	8.809E3	10.570E3	279.331E3
10	87	8.522E3	10.227E3	261.498E3
13	84.6	8.101E3	9.721E3	236.246E3
15	83	7.824E3	9.389E3	220.382E3
18	80.6	7.416E3	8.899E3	197.996E3
20	79	7.149E3	8.579E3	183.984E3

In this exercise, as an example, the time domain dynamic mooring analysis is performed using OrcaFlex in order to get the time histories of the tension responses that will be latter considered as measured signals. The effect of corrosion is considered by reducing the diameter of the chain links and the stiffness of the chain sections which are updated in the model. The time history and the Power Spectral Density of $T_s(t)$ due to an extreme sea state (as presented in Table 2-4, section 3.3 of **chapter 2**) are shown in Figure 3-6. It must also be highlighted that the assumption of Gaussian distribution may lead to an under-estimate of the extreme maximum tension response and a corresponding unrealistically low probability of failure, which will be discussed further in section 5 of this chapter. However, it is acceptable here as the purpose of the case study is to illustrate the present methodology by showing the importance of updating the material loss during the expected service life in order to better estimate the reliability of the system.

The time-dependent failure function and probability of failure in strength condition is written as Eq. (3.26) and Eq. (3.27).

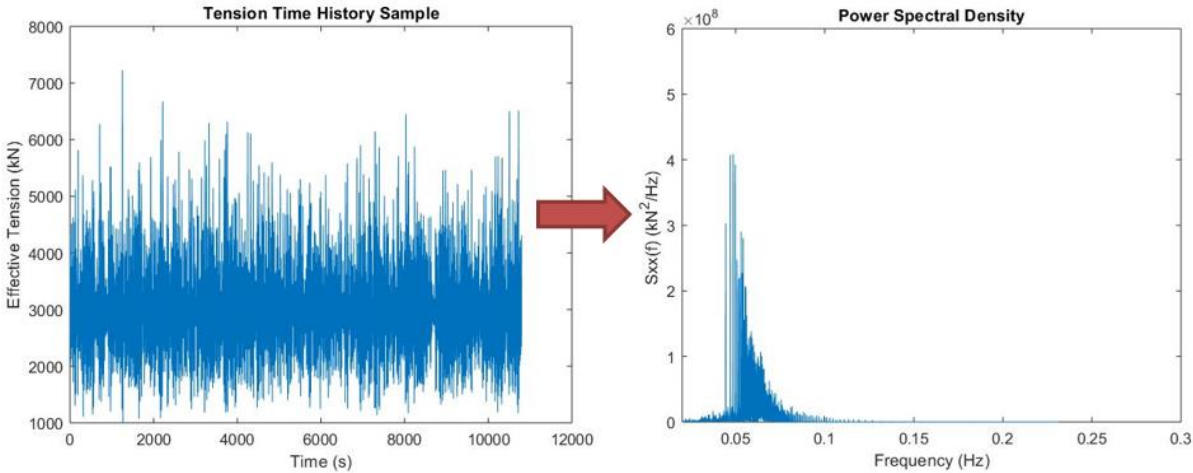


Figure 3-6: Time history and PSD of the tension response, $T_s(t)$, in the design extreme sea state.

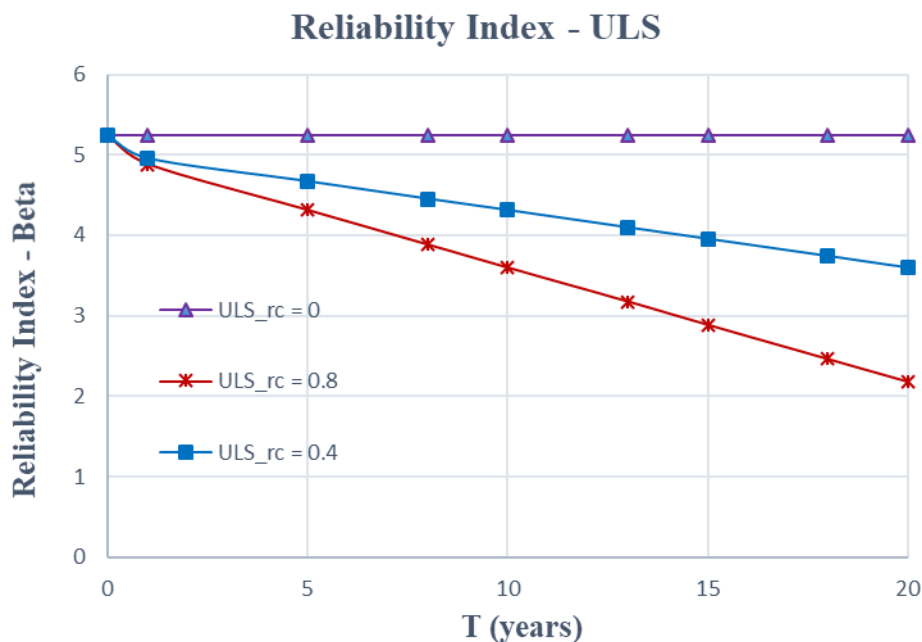


Figure 3-7: Time-dependent reliability index in strength condition of the chain link.

The time-dependent reliability index of the chain link connected to the fairlead for the extreme sea state are presented in Figure 3-7. It can be seen that due to corrosion, the reliability index decreases as the breaking strength of the chain links decreases over time. Therefore, if corrosion is not considered in the design (e.g. by increasing the diameter of chain links (DNV-OS-E301, 2010; API-RP-2SK, 2005; BV-NR-493, 2015), it might be possible that after a few years of deployment, the structure would no longer be able to withstand the initial extreme design sea state. For instance, if we consider that a reliability index of 3.7 (Schulze, 2006; Vazquez-Hernandez et al., 2006) is acceptable, the mooring line is then considered failed under the same design extreme sea state only after 10 years of deployment with an annual reduction in diameter of 0.8 mm/year. In other words, maintenance or replacement of lines should be done after 10 years of operation in order to ensure the safety requirement in extreme condition.

Reliability in fatigue condition (FLS)

The time history and the Power Spectral Density of $T_s(t)$ due to a moderate sea state (as presented in Table 2-4, section 3.3 of **chapter 2**) are shown in Figure 3-8.

The DNV's S-N fatigue curve for chain links (DNV-OS-E301, 2010) is used to calculate the fatigue damage. The estimated fatigue life is 20 years with a safety factor equals to 3 (Lardier et al., 2008). The objective for this setting is to investigate the added effect of corrosion on the cumulative fatigue damage by calculating the time-

dependent reliability index of the chain links taking into account an annual reduction in diameter of the chain links (Lardier et al., 2008).

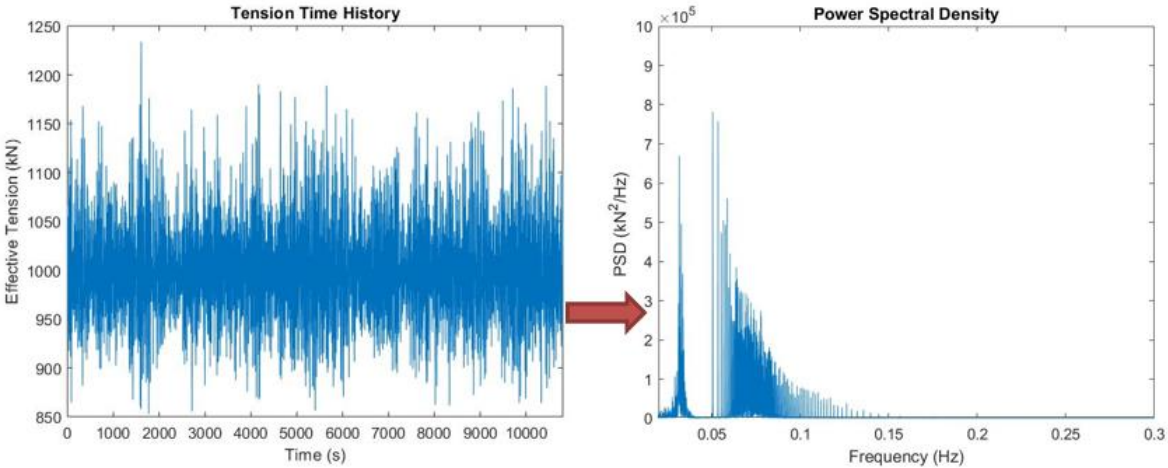


Figure 3-8: The tension response PSD obtained from the tension time history calculated by Orcaflex using Fast Fourier Transformation (FFT).

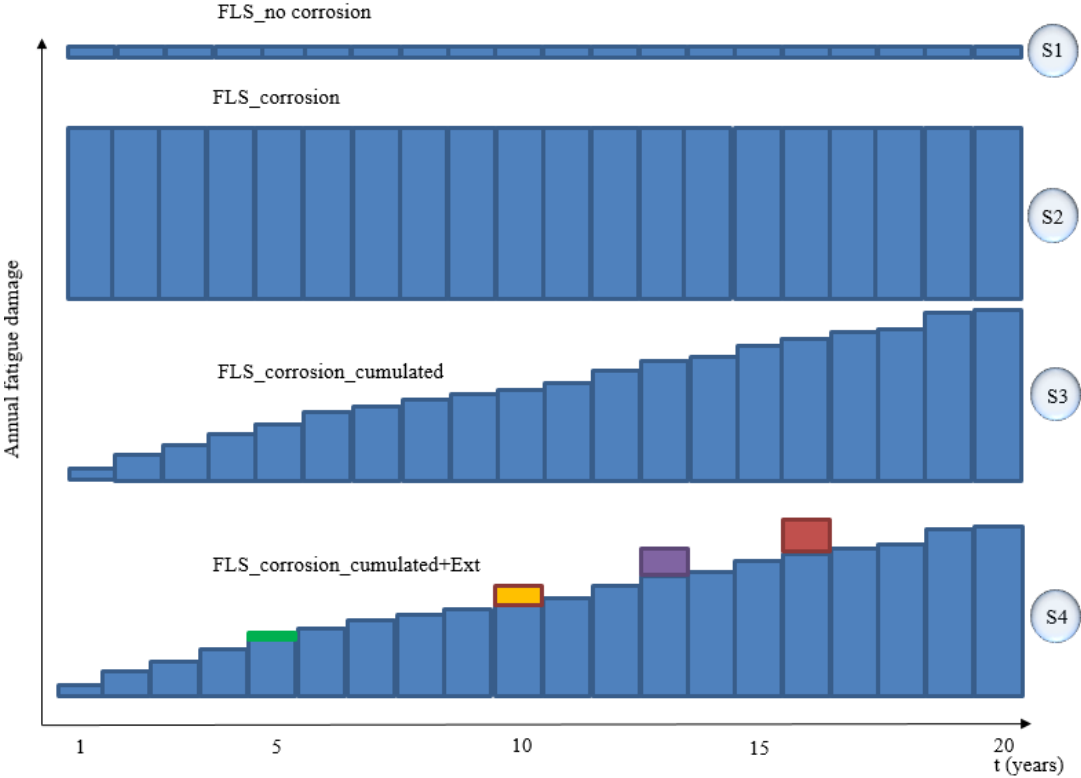


Figure 3-9: Different approaches to calculate the fatigue damage of the chain links highlighting the effect of corrosion. The added damage due to extreme sea states (e.g. those with a return period of 10, 20, 50 or 100 years that might probably happen during operation) are illustrated in green, yellow, violet and red color of the case S4.

Figure 3-9 illustrates different approaches for calculating the cumulative fatigue damage of the chain links considering corrosion effect. S1: the cumulative fatigue damage is calculated without corrosion. S2: the cumulative fatigue damage is calculated with the same quantity of material loss (reduced diameter) as it would be at

the end of 20 years of deployment. S3: the cumulative fatigue damage is calculated considering an annual reduction in diameter of the chain link. S4: the cumulative fatigue damage is calculated in the same manner as the case S3 but the added fatigue damage due to the design extreme sea states (e.g. with a return period of 100, 50, 20, 10 years, etc.) that might probably happen at any moment within the expected service life of the mooring lines is also considered. As we consider here an annual reduction in diameter of the chain links, the stress response is considered unchanged within one year for the same sea states, so as the fatigue damage D_{annual} . With a more frequent measurement, the cumulative fatigue damage can be determined by summing the damage calculated from the measured data for every month or couple of months.

The probability of failure of the chain links can be calculated as

$$P_{f_FLS} = P(G_{FLS}(t) < 0) \tag{3.34}$$

where $G_{FLS}(t) = G_{FLS_1}(t) = \Delta - t \cdot D_{\text{annual}}$ for the cases S1 and S2

$$G_{FLS}(t) = G_{FLS_3}(t) = \Delta - \sum_{k=1}^t D_{\text{annual}} \quad \text{for the case S3}$$

$$G_{FLS}(t) = G_{FLS_4}(t) = \Delta - \left(\sum_{k=1}^t D_{\text{annual}} + D_{\text{ULS}} \right) \quad \text{for the case S4}$$

Δ - the model uncertainty in the Palmgren-Miner rule, presented in Table 3-4.

Table 3-4: The uncertainties of the Palmgren-Miner rule and the DNV's S-N curve (Lardier et al., 2008; Mathisen et al., 2005).

Parameters	Distribution	Mean value	Standard deviation
Model uncertainty in the Palmgren-Miner rules, Δ	Log-normal	1	0.3
Log(K) (where K, the S-N curve parameter)	Normal	11.55	0.24
m	Fixed	3	-

The time-dependent reliability index of the chain link connected to the fairlead is shown in Figures 3-10 and 3-11 considering the effect of corrosion as an annual reduction in diameter of the chain links of 0.4 mm/year and 0.8 mm/year respectively. It is observed in the Figure 3-10 that the reliability index is more precisely calculated in the case $FLS_{rc} = 0.4_Cumulated$ (case S3) where the fatigue damage is cumulatively summed considering an annual reduction in diameter of chain links. By

contrast, the case $FLS_{rc} = 0.4$ (case S2) seems overly conservative since only the final reduced diameter at the end of the 20 years is considered to calculate the annual damage, then multiplied with the number of operating year. With the assumption that there might be an sea state happen during the expected service life, the reliability index is calculated as $FLS_{rc} = 0.4_{Cumulated+Ext}$ (case S4) by summing the added damage caused by this extreme sea state into the cumulative fatigue damage. The added damage caused by the extreme sea states is an interesting view that allows forecasting the level reliability of structures in FLS considering disadvantage events such as extreme sea states. This can be useful to inform stake-holders about the probable risk and to support making decisions regarding maintenance or replacement of lines.

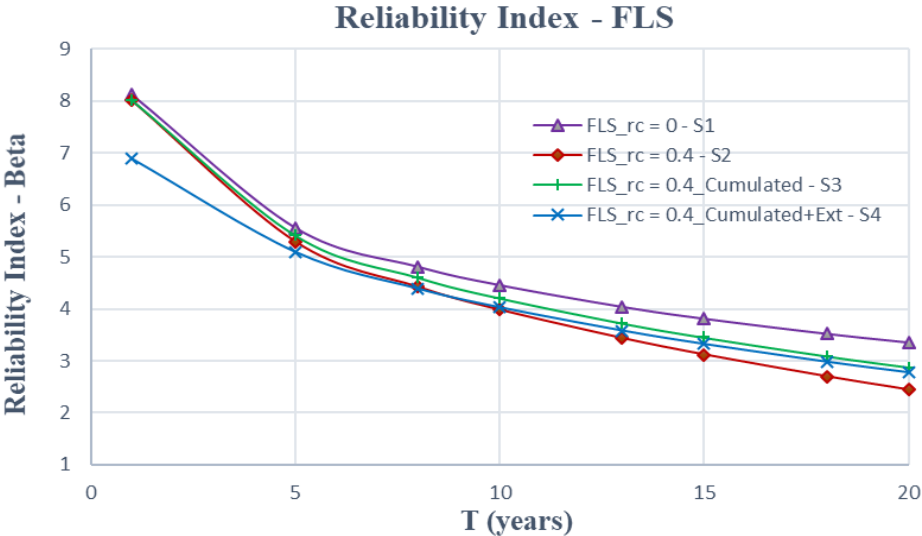


Figure 3-10: Time-dependent reliability index calculated based on different approaches, $rc = 0.4$ mm/year.

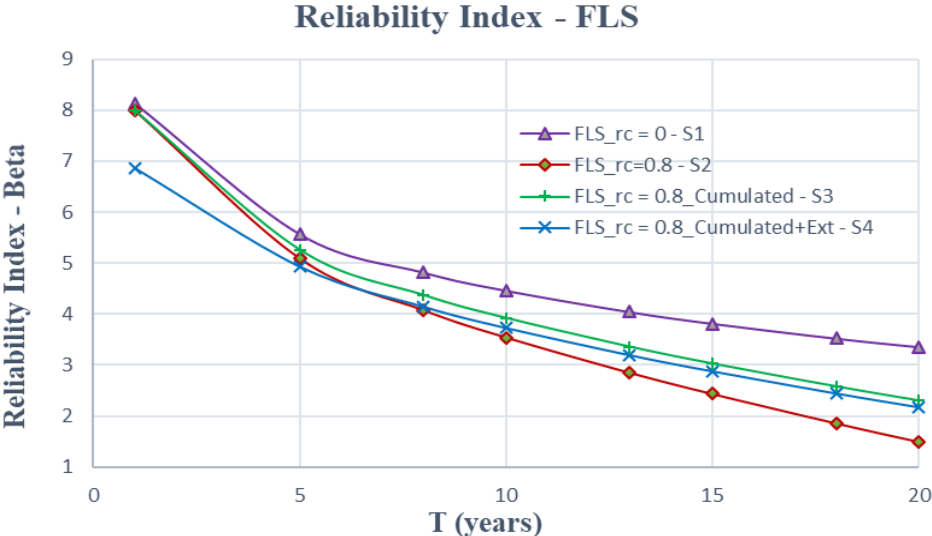


Figure 3-11: Time-dependent reliability index calculated based on different approaches, $rc = 0.8$ mm/year.

Again, if a reliability index that is not smaller than 3.7 is considered acceptable, the fatigue life of the chain link should be 15 years for the case S3 and 13 years for the case S4 instead of 20 years where the corrosion effect is not considered. Therefore, maintenance or line replacement should be done after 13 or 15 years of deployment. In other words, the safety coefficient should not be smaller than 4 for the case S3 and 5 for the case S4 in order to ensure a design fatigue life of 20 years. It's also worth noting that the recommended design safety factor proposed by DNV-OS-E301 (DNV, 2010) for the present S-N curve is 5. Similar conclusions can be made for Figure 3-11 where an annual reduction in diameter of the chain links of 8 mm/year is considered.

5. Simulation of non-Gaussian processes based on Artificial Neural Network

Probabilistic modeling of mooring response is of vital importance for reliability assessment of structural elements. For offshore platforms, mooring responses are often non-Gaussian due to the combination of non-normal input loadings and non-linear system behaviors. A common practice relies on the Gaussian assumption to model uncertainties due to irregular environmental loads and the corresponding structural dynamic responses. Non-linear effects, however, can considerably affect both the extreme and fatigue design of structures (Winterstein, 1988).

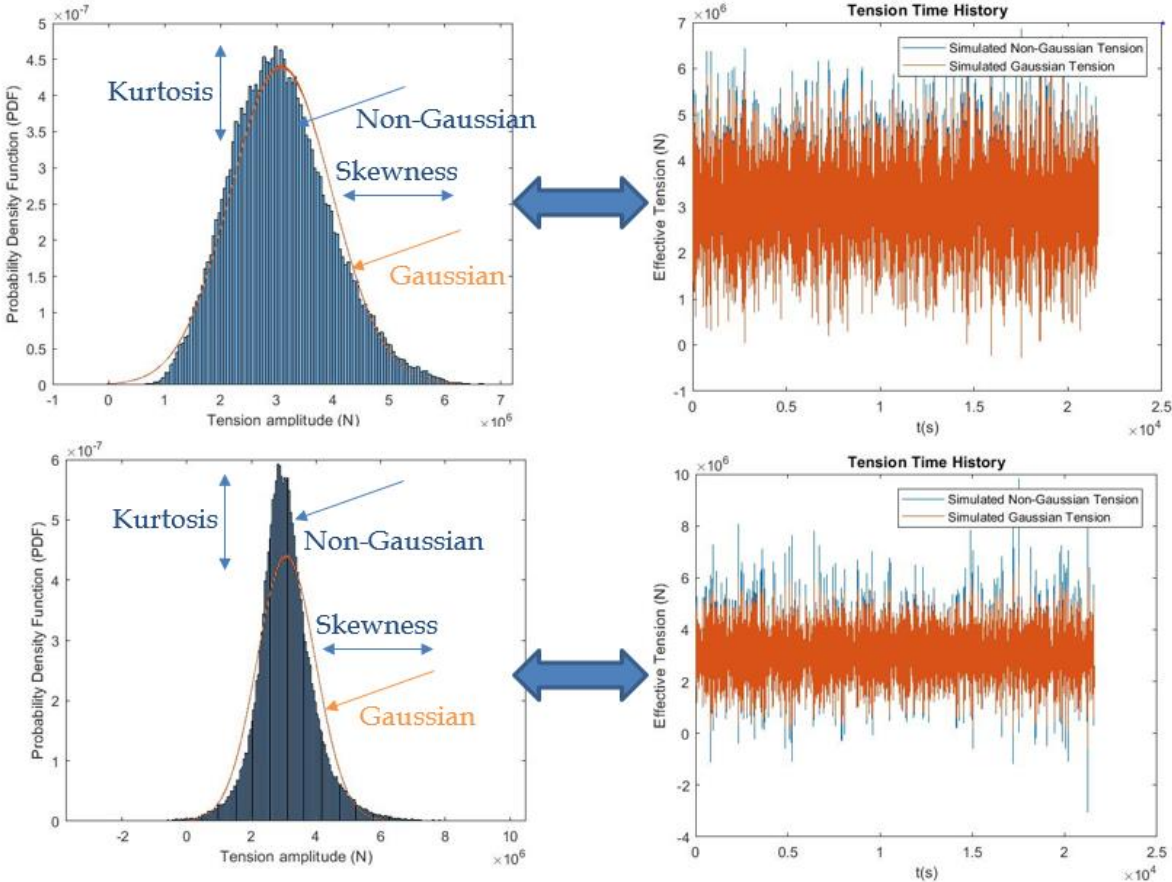


Figure 3-12: Example of a mild (top) and a strong (bottom) non-Gaussian processes and its underlying Gaussian ones.

A mild and a strong non-Gaussian processes are illustrated in Figure 3-12. It can be seen that, a strong non-Gaussian response may have significantly higher peaks and lower troughs comparing with the corresponding Gaussian one. Therefore, it is not correct to estimate such response statistics based on the Gaussian model. Time domain simulation is a common solution to deal with such issue since all nonlinearities can be included in the equations of motion. However, it is also computationally expensive especially when it comes to reliability analysis where an important number of simulations are required for an accurate assessment. Therefore, alternative approaches for simulating non-linear mooring response are of great interest.

Recently, the application of Artificial Neural networks (ANN) attracts more and more attention from the offshore industry. This is mainly due to its ability to model complex non-linear structural behaviors and to deal with large set of data. Several applications have been published such as: Guarize et al. (2007) proposed an efficient hybrid Artificial Neural Network (ANN)–Finite Element Method (FEM) procedure for nonlinear mapping of the current and past system excitations (input) to produce subsequent system response (output) for the random dynamic analysis of mooring lines and risers. Christiansen et al. (2015) proposed a hybrid method combining classical numerical models and artificial neural networks (ANN) to reduce computational time for active truncated experiments. Several other applications of ANN for fatigue estimate, reliability assessment and health monitoring have also been investigated by Sidarta et al. (2017), Li et al. (2017), Kalra et al. (2005), Kim et al. (2016), Yasserli et al. (2010), Pinna et al. (2013), Aqdam et al. (2018), Vazquez-Hernandez et al. (2006), etc.

ANNs are computer models inspired by the biological neural networks that constitute animal brains. An ANN is a collection of connected processing units called artificial neurons. Each connection (so-called edge) between neurons, like the synapses in a biological brain, can transmit a signal from one neuron to another. Artificial neurons and edges typically have a weight which adjusts as learning proceeds. In an ANN model, first, the neurons at its input layer receive input signals. Then, the signals propagate through the hidden layers and reach the output layer, producing the output signals of the ANN model. A neural network with only one intermediate (hidden) layer is illustrated in Figure 3-13. The following description of ANN is based on the recent research work of Sidarta et al. (2017).

An input signal (x_i) is transferred to an output signal (y_i) by each neuron i based on an activation function (which is commonly sigmoidal with a scaling parameter α and a constant ε) written as following

$$y_i = \frac{2\alpha}{1 + \exp(-\varepsilon x_i)} - \alpha \quad (3.35)$$

where α, ε are often assumed equal to 1.

The connection (edge) of a neuron i in a layer to a neuron j in the next layer typically have a weight (w_{ij}), the input signal to neuron j is computed as

$$x_j = \sum_{i=1}^m w_{ij} y_i + b_j \quad (3.36)$$

where m - the number of neurons in the layer containing neuron i .

w_{ij} - the connection weight

b_j - the weight of the connection between a bias neuron and neuron j .

The back-propagation learning algorithm is employed to train the ANN model where the connection weights between neurons are modified by having the computed output errors back-propagated through the neural network.

An output error (e_j) for each neuron j can be calculated as

$$e_j = t_j - y_j \quad (3.37)$$

where t_j - the target value; y_j - the computed output

A total error (E) can be calculated as

$$E = \frac{1}{2} \sum_{j=1}^n e_j^2 \quad (3.38)$$

The computed error is then used to modify the connection weights as (Sidarta et al., 2017)

$$\Delta w_{ij} = \eta \frac{\partial E}{\partial w_{ij}} = \eta \frac{\partial E}{\partial e_j} \frac{\partial e_j}{\partial y_j} \frac{\partial y_j}{\partial x_j} \frac{\partial x_j}{\partial w_{ij}} \quad (3.39)$$

where η - the learning rate

The new connection weight can be calculated as

$$w_{ij}^{\text{new}} = w_{ij}^{\text{old}} + \Delta w_{ij} \quad (3.40)$$

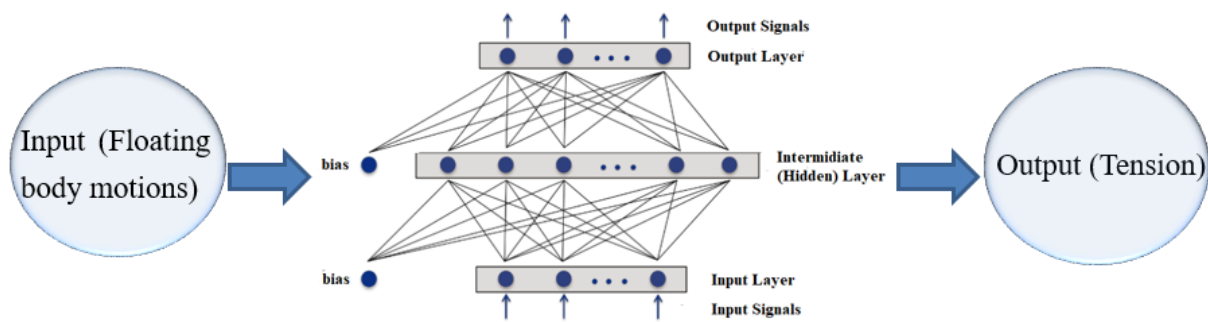


Figure 3-13: A neural network with only one intermediate (hidden) layer (based on Sidarta et al., 2017).

In the following, an Artificial Neural Network (ANN) is used in order to build a system identification model based on a measured input (e.g. floater motions) and a measured output (e.g. tension response in mooring lines).

On the one hand, the ANN model could be an interesting tool for mooring monitoring since based on measured floater motions (which can be obtained via on-board and off-the-shelf 6 degrees of freedom sensors) one can simulate directly tension response in mooring lines (which means being less relied on tension measurements from tension sensors). On the other hand, when a large number of simulation is required, the ANN model can also be used to simulate mooring response based on simulated floater motions as input instead of performing time-consuming time-domain simulation.

In section 5.1, first, the ANN model is used to simulate mooring response for a full 3-hours sea state based on a part of measured data for the same sea state (e.g. calibration for one sea state). Furthermore, it can also be used to simulate mooring response for another sea state that the network has never been trained for (calibration for multiple sea states). The same exercises have been performed by Gurley et al. (1996) and Sidarta et al. (2017).

In section 5.2, the authors attempt to evaluate the statistical properties of the simulated mooring tension response by performing different number of simulations (i.e. 1, 5, 10, 30, 100, 1000, 2000, 5000 and 10000 as it can be seen in section 5.2) in order to eventually study the influence of the number of simulations on reliability estimate based the so-called ANN-based Monte Carlo simulations. Moreover, it is found that mooring reliability analysis can be performed with a very impressive computational time based on the present approach. This is done by using the author's Matlab script incorporated with the Neural Net Fitting app in Matlab (Matlab, 2017).

5.1 Artificial Neural Network (ANN) for simulation of nonlinear mooring response

Calibration for one sea state

In the following, a neural network with a single hidden layer containing 10 neurons is trained in order to simulate the tension response at the fairlead point of a mooring line for an extreme sea state (as discussed in Table 2-4 in **Chapter 2**). Time domain dynamic mooring analysis is performed using OrcaFlex in order to obtain 3-hours time histories of the 6 degree of floater motions and tension response in mooring lines which will be later considered as measured signals. The training is done by using 10 realizations of 3-minutes long of 6-degrees of floater motions as input and 10 realizations of 3-minutes long of the corresponding tension time history at the fairlead connection point in a mooring line as output. The increase in the number of neurons did not improve significantly the results. Once the neural network has been trained, full 3-hours signals of the 6-degrees of floater motions are required as input to the neural network in order to simulate the full 3-hours tension response signal. The input floater motions are chosen randomly between 10 realizations of floater motions time histories calculated by Orcaflex. Indeed, it is recommended by API-RP-2SK (API, 2005) that five to ten 3-hours simulations are required for a good confidence of standard deviation and extreme responses.

It should also be noted that the total 30-minutes training period was not optimized but leads to acceptable computational time (2 to 6 seconds for a standard computer) and is only 17% of the full 3-hours signal.

The neural network training, which includes the training step (70 % of the input data), validation step (15 % of the input data) and test step (15 % of the input data), is performed using the Neural Net Fitting app in Matlab (Matlab, 2017). Figure 3-14 shows the regression results for each step where the relationship between network predictions and targets are plotted. It can be observed that the network is well trained since all data points remain near the $Y=T$ line and the Regression values, R , are nearly unity.

Figures 3-15 and 3-16 show a comparison of the sample tension computed by using time domain simulation in Orcaflex (which is considered here as the measured tension) and the simulated tension based on the neural network. It can be seen that a very good match between the measured tension and the ANN-simulated one is observed (Figure 3-15). Moreover, the corresponding PDFs are also found in a very good match (Figure

3-16) which show the advantage of the ANN when it comes to preserving PDF shape and statistical properties (as can also be seen in Table 3-6).

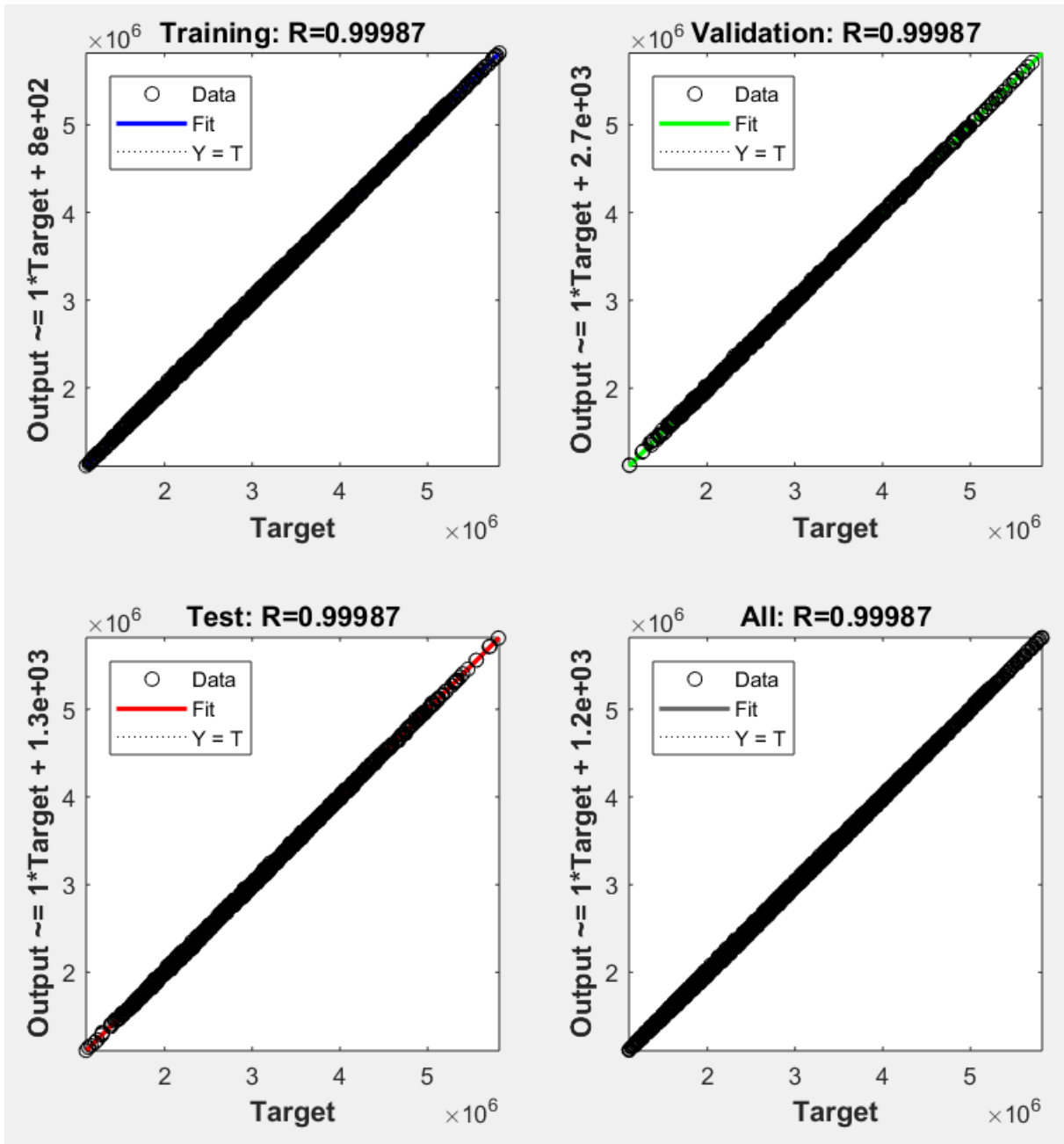


Figure 3-14: Regression results.

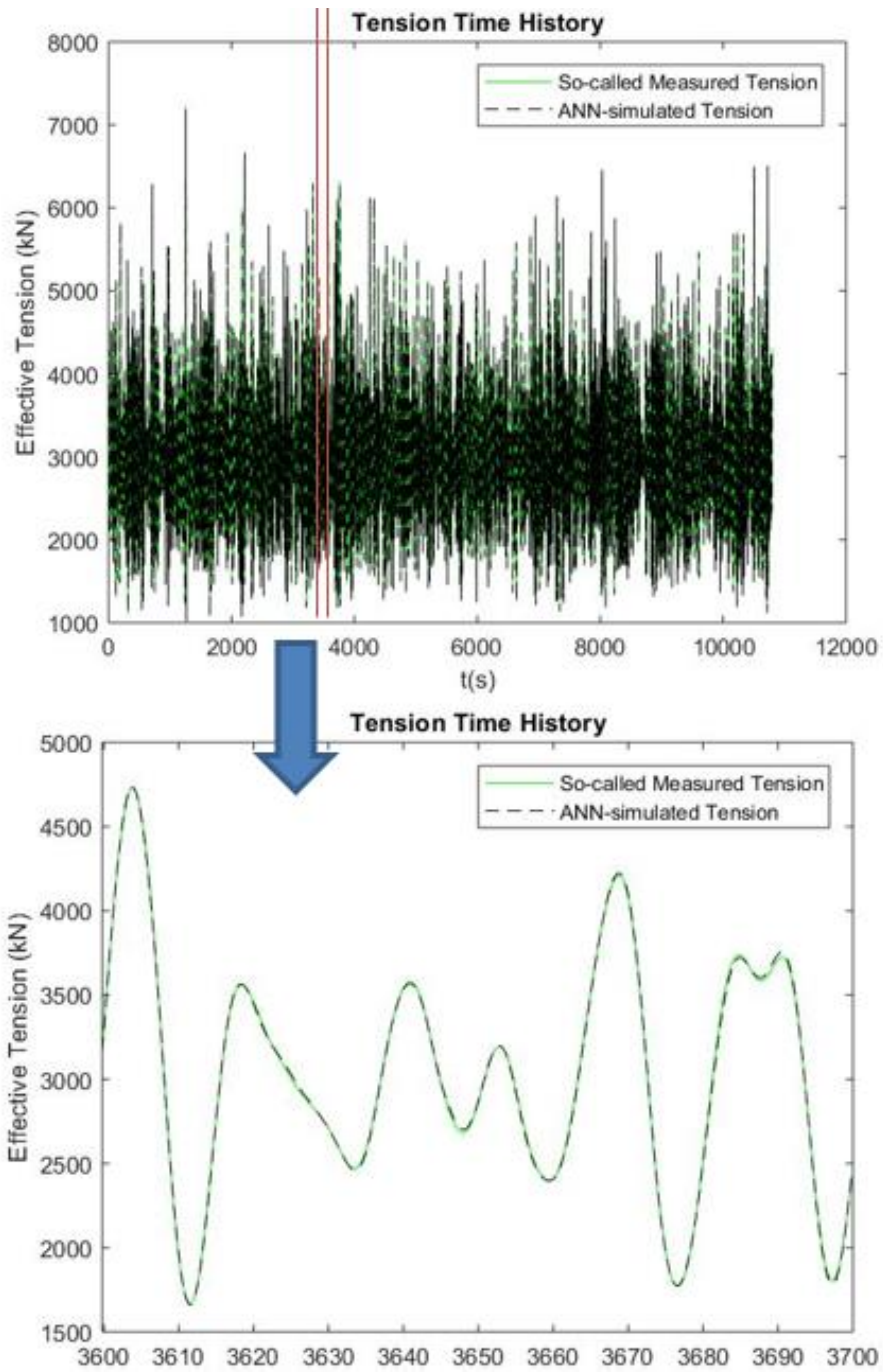


Figure 3-15: Comparison of a tension sample with the simulated tension based on the neural network.

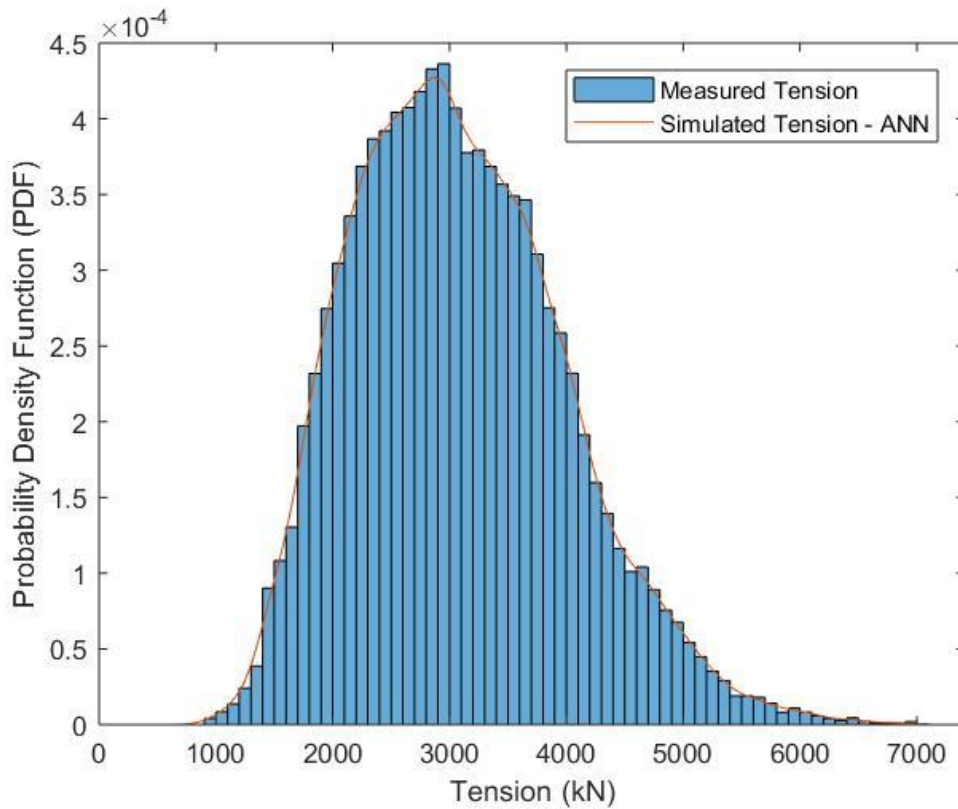


Figure 3-16: Comparison of the PDF of a tension sample with the simulated tension based on the neural network.

Calibration for multiple sea states

Table 3-5: Different sea states taken as input to train the neural network.

Sea states / Spectral type		Jonswap
Hs (m)	Tp (s)	Gamma
1.25	4.5	3.3
4.75	10.5	3.3
2.61	13.8	3.3
4.25	9.5	3.3
4.75	12.5	3.3
3.75	16.5	3.3
2.25	16.5	3.3
3.75	13.5	3.3
3.75	18.5	3.3
2.25	18.5	3.3
3.75	11.25	3.3
1.25	3.5	3.3
2.25	6.5	3.3
3.75	17.35	3.3
3.25	7.5	3.3

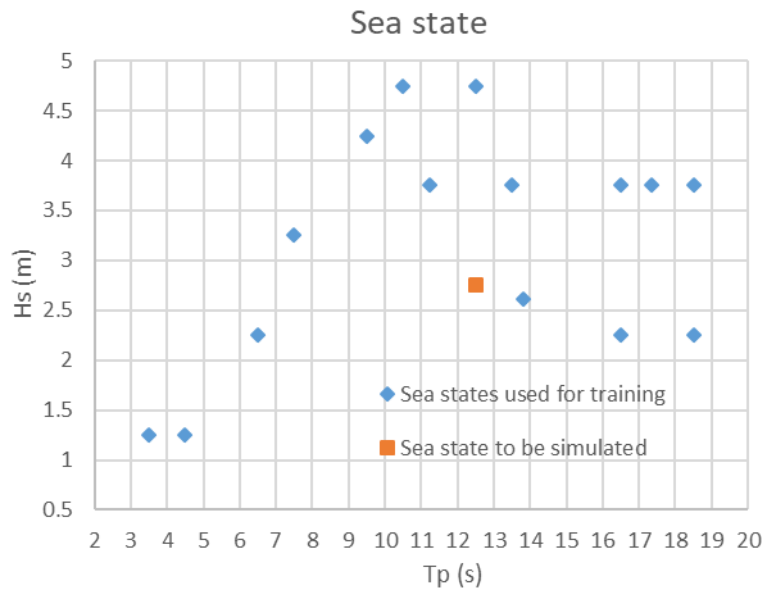


Figure 3-17: Sea states used for training the neural network and sea state to be simulated.

In the following example, measured signals for different sea states are used as input to train the neural network and then simulate the full response signal for another sea state that the network has never been trained for. In the following, input data (which is 2-minutes long for each signal) for 15 sea states as presented in Table 3-5 and Figure 3-17 have been used as input to train the neural network. For the sake of simplification, only one wave direction is considered as in Figure 2-1, **chapter 2**. Current and wind is not considered for the same reason. The trained neural network is then used for simulating the tension response at the fairlead point of the front line 1 for another sea state (i.e. $H_s = 2.75$ m, $T_p = 12.5$ s).

It can be observed in Figure 3-18 that the network is well trained since all data points remain near the $Y=T$ line and the Regression values, R , are nearly unity. It worth to note that the training is done by using the input data for only 15 sea states (blue points in Figure 3-17) but not the sea state that needs to be simulated (orange point in Figure 3-17).

Figures 3-19 and 3-20 show a comparison of the sample tension computed by the numerical time domain simulation (so-called here the measured tension) and the simulated tension based on the neural network. It can be seen that a very good match is observed between the measured tension and the ANN-simulated one (Figure 3-19) and also between corresponding PDFs (Figure 3-20).

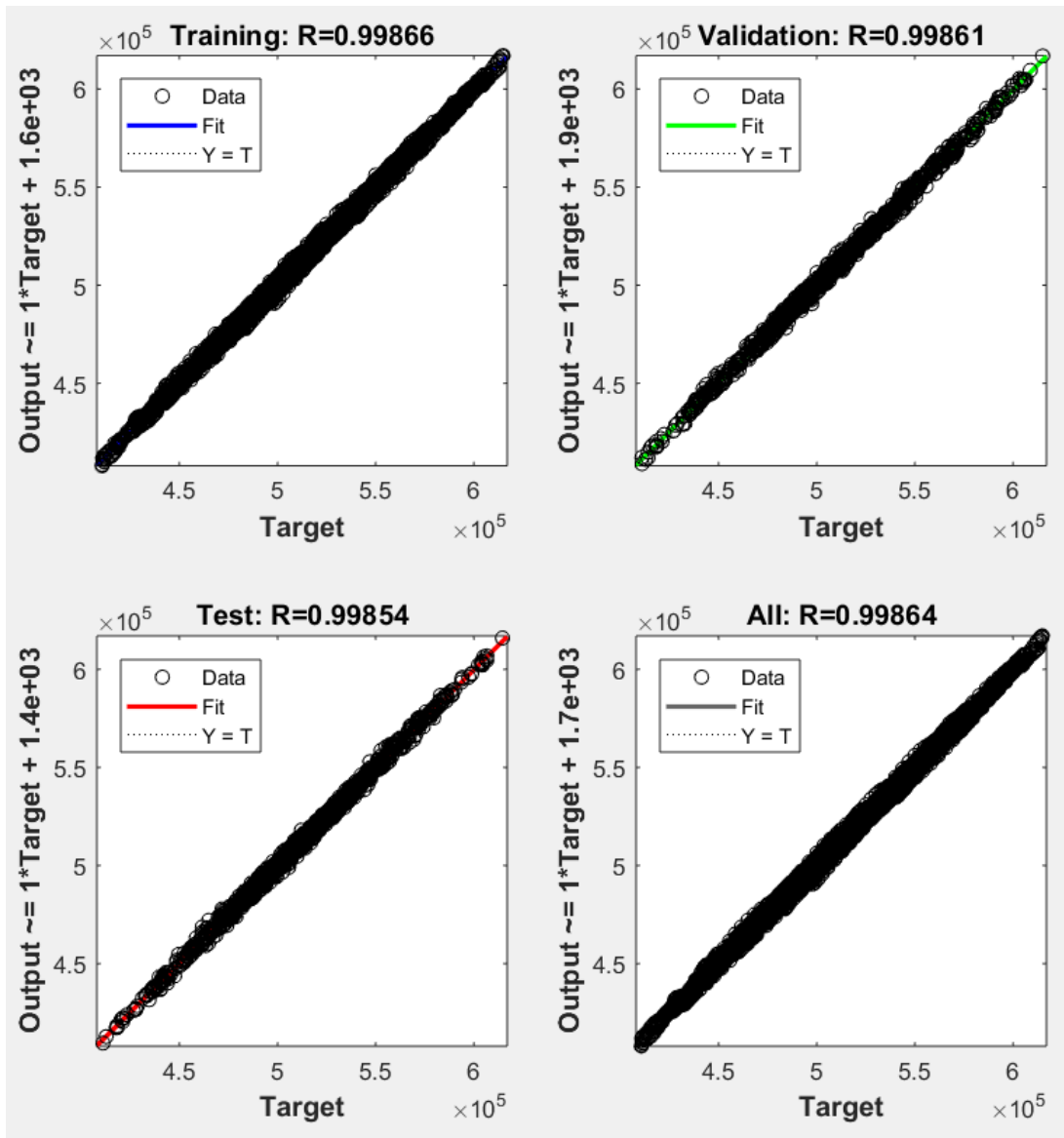


Figure 3-18: Regression results.

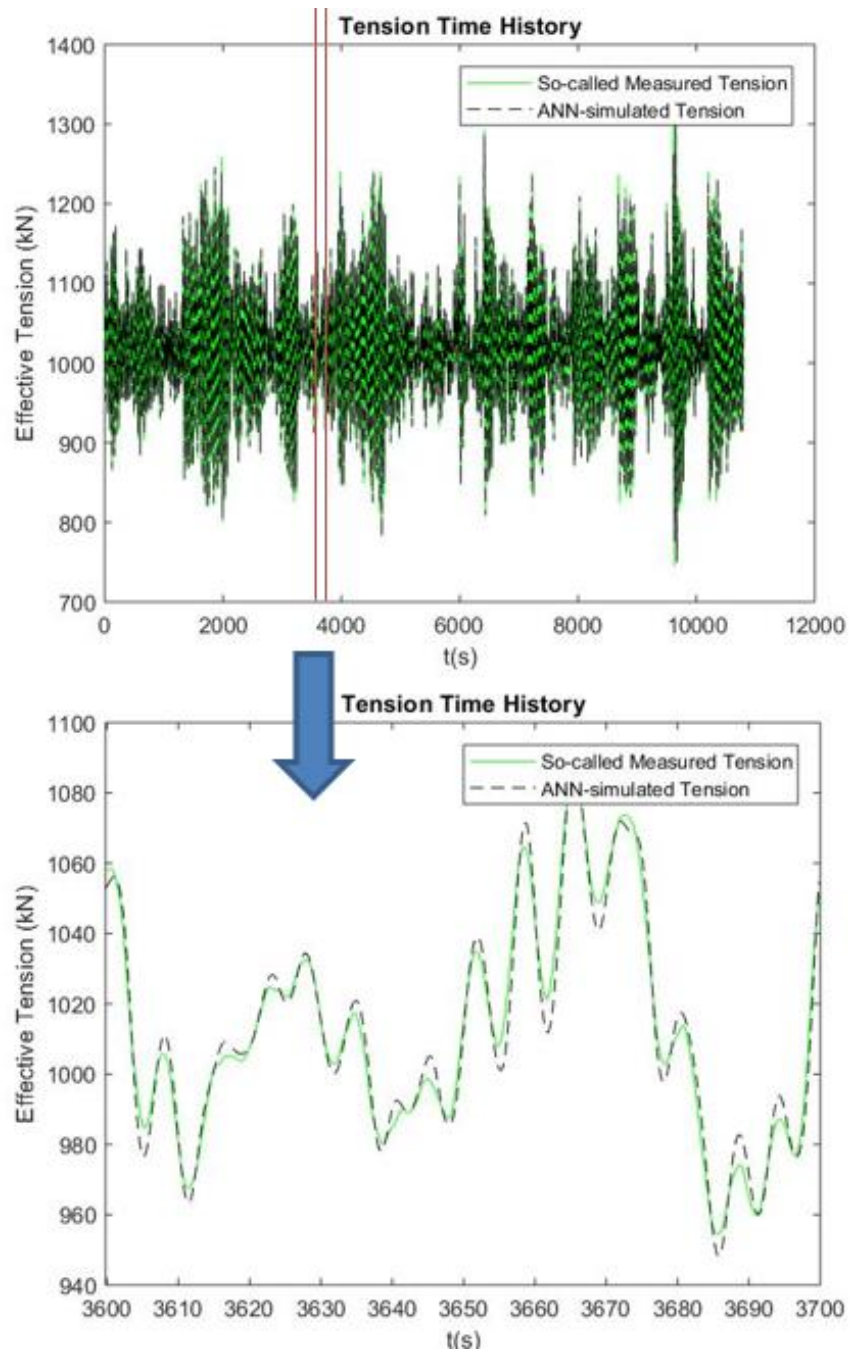


Figure 3-19: Comparison of a tension sample with the simulated tension based on the neural network (fatigue sea state $H_s = 2.75$ m, $T_p = 12.5$ s).

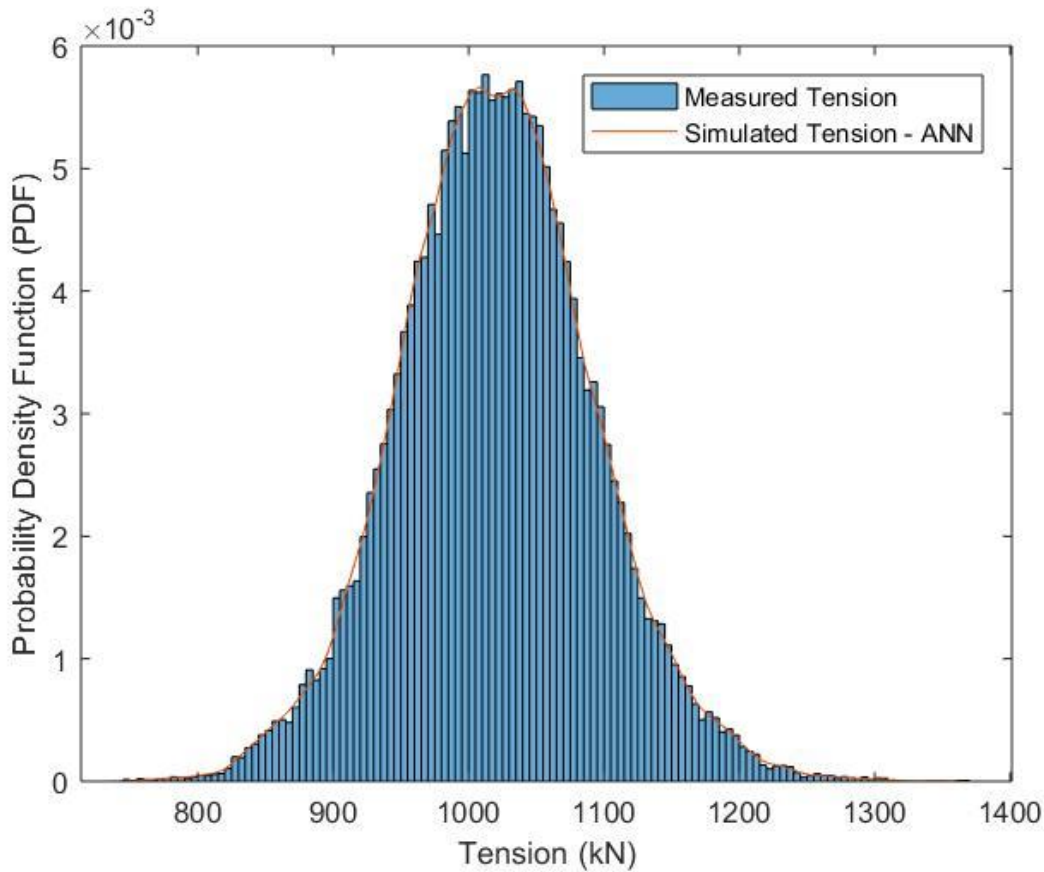


Figure 3-20: Comparison of the PDF of a tension sample with the simulated tension based on the neural network (fatigue sea state $H_s = 2.75$ m, $T_p = 12.5$ s).

5.2 Comparison and application for reliability assessment

Comparison of statistical parameters

The first application of the neural network (calibration for one sea state) mentioned in the previous section is further discussed here in order to assess the reliability in storm condition (ULS). It seems necessary to define here the maximum tension of each 3-hours signal, which is the maximum value observed during that 3-hours simulation. In Table 3-6 maximum tension means the mean value of every maximum tensions

observed for a number of, N_s , simulations (i.e. $\text{MeanTmax} = \sum_{i=1}^{N_s} \frac{T_{\text{max},i}}{N_s}$ where $T_{\text{max},i}$ is

the maximum tension of the i^{th} simulation). The values of statistical moments (i.e. mean, standard deviation, skewness, kurtosis) presented in Table 3-6 are also the mean values of such moments for N_s simulations. It can be seen that, the neural network gives good and stable prediction of maximum tension and statistical moments. Moreover, the computational time is very efficient (i.e. ≈ 4 s in average for one simulation). It is interesting to see quite significant differences between the mean standard deviation of the 10 so-called measured tension signals and what obtained from the ANN simulations (i.e. for 1, 5, 10, 30, 100, 1000, 2000, 5000 and 10000

simulations). However, another run of 10 ANN simulations was performed resulting in a mean standard deviation of 1158.4 kN, which raises the question that 10 3-hours realizations might not be enough to provide stable estimate of standard deviation of the response for the present case study?

.

Table 3-6: Statistical properties considering the number of simulations

Properties/ Methods	10 time domain simulations (so-called measured signals)	ANN_1 simulation	ANN_5 simulations	ANN_10 simulations	ANN_30 simulations	ANN_100 simulations	ANN_1000 simulations	ANN_2000 simulations	ANN_5000 simulations	ANN_10000 simulations
Mean (kN)	3078.7	3080	3078.4	3076.9	3078.3	3077.4	3078.2	3079.1	3078.3	3077.7
Std (kN)	1124.8	905.69	907.35	904.81	908.67	909.28	905.19	909.97	912.1226	918.736
Skewness	0.4605	0.4543	0.4673	0.4404	0.4767	0.4851	0.4748	0.4707	0.4474	0.4774
Kurtosis	3.0113	2.9488	3.0476	2.9052	3.2023	3.4105	3.944	3.0351	6.6202	6.6907
Maximum tension (kN)	7177.43	6740.1	7177.1	6875.9	7536.1	7232.1	7167.3	7176.6	7261.2	7296.3
Average CPU time	≈ 1800 s *10	≈ 4 s	≈ 9 s	≈ 36 s	≈ 98 s	≈ 305 s	≈ 3324 s	≈ 7042 s	≈ 27918 s	≈ 48160 s

ANN-based Monte Carlo simulation for reliability assessment of mooring lines

It is concluded by Rendón-Conde et al., (2015) that the ANN model could be a promising option for reliability assessment considering nonlinear structural response thanks to its accuracy and computational efficiency. This is particularly interesting for mooring reliability assessment in extreme sea states (ULS) where nonlinear mooring response which relates extreme peak mooring loads are largely significant and should be carefully considered. For that, an ANN-based Monte Carlo reliability assessment approach is discussed in the following.

The ULS case study discussed in section 3.3 of **chapter 2** of this manuscript (or Pham et al. (2019-a)) is re-considered in the following for reliability assessment. The extreme sea state observed at the SEMREV sea test site (as presented in Table 2-4 of **chapter 2**) is used in the calculation. It should be noted that in the following, the author focuses only on capturing the nonlinearity of mooring response in term of extreme peak mooring loads. Therefore, only mooring response due to this extreme sea state at a specific point during operation is considered. In other words, for a 3-hours sea state, the mooring response can be considered as a stationary random process, i.e. its statistical parameters are independent of time.

The failure function in the Ultimate Limit State (ULS), G_{ULS} , can be calculated as

$$G_{ULS} = T_{BS} - T_{smax} \quad (3.41)$$

where

T_{BS} - the Breaking Strength of the mooring component, which is considered as a time-independent log-normal distributed random variable (with $Mean_T_{BS} = 1.2 \times MBS$, and the Coefficient of Variation (COV) equals to 0.05 for the chain link connected to fairlead (Gao et al., 2005)).

T_{smax} - the maximum tension estimated by the ANN-based Monte Carlo simulation.

The probability of failure (P_f) is approximated by the number of observations, N_s , where $G_{ULS} \leq 0$, which can be written as

$$P_{f_ULS} = \frac{\sum_{i=1}^N N_f}{N_s} \quad (3.42)$$

where $N_f = 1$ if $G_{ULS} \leq 0$; $N_f = 0$ if $G_{ULS} > 0$.

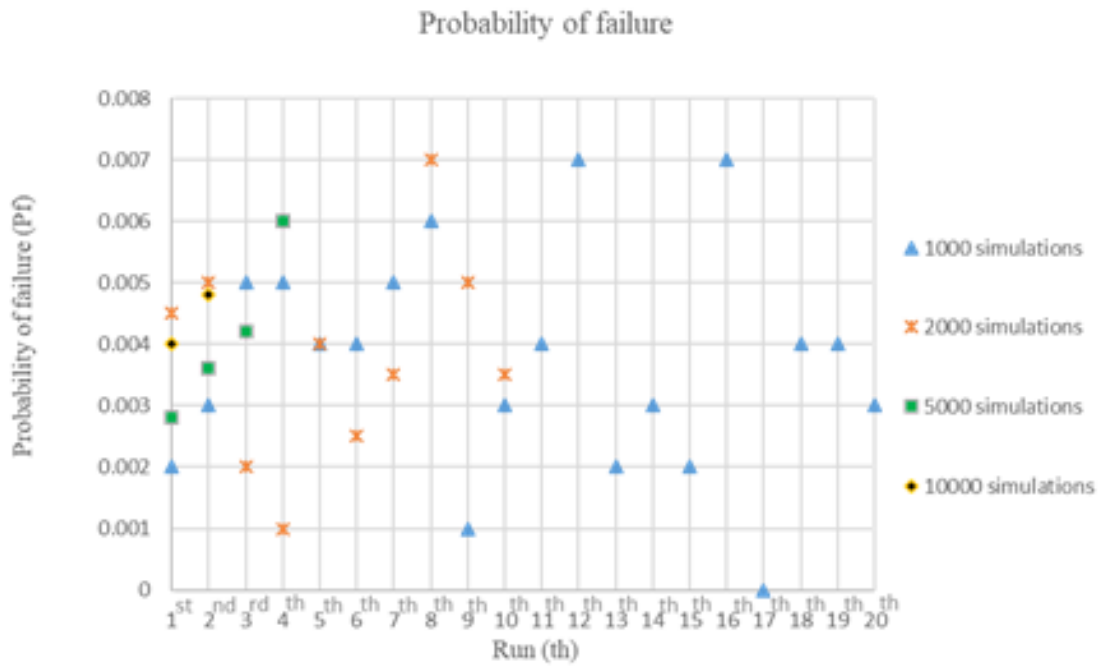
In the following, reliability assessment is implemented using the ANN-based Monte Carlo simulation approach considering different number of simulations, $N_s = 1000, 2000, 5000, 10000$. The probability of failure estimated for different run (th) and the are shown in Table 3-7.

Table 3-7: Reliability assessment by using the ANN-based Monte Carlo simulation

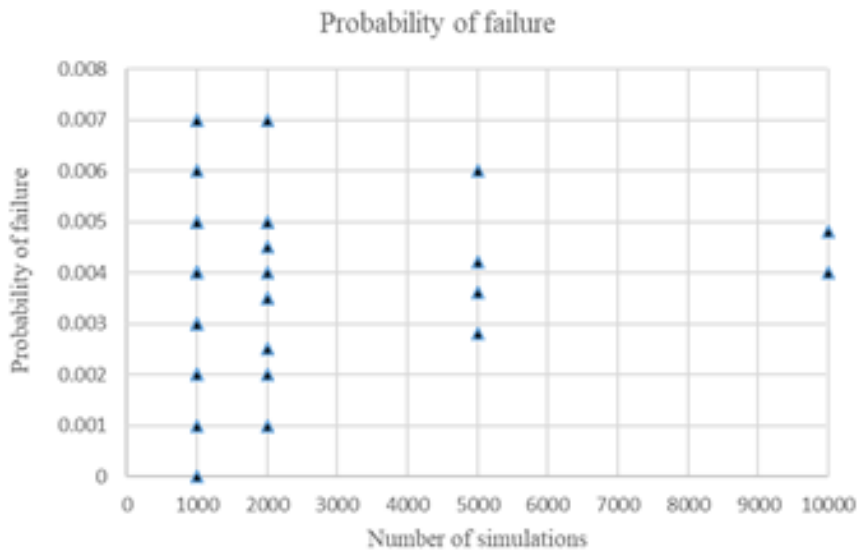
Run (th)	Number of simulations	Probability of failure						
1st	1000	0.002	2000	0.0045	5000	0.0028	10000	0.004
2nd	1000	0.003	2000	0.005	5000	0.0036	10000	0.0048
3rd	1000	0.005	2000	0.002	5000	0.0042		
4th	1000	0.005	2000	0.001	5000	0.006		
5th	1000	0.004	2000	0.004				
6th	1000	0.004	2000	0.0025				
7th	1000	0.005	2000	0.0035				
8th	1000	0.006	2000	0.007				
9th	1000	0.001	2000	0.005				
10th	1000	0.003	2000	0.0035				
11th	1000	0.004						
12th	1000	0.007						
13th	1000	0.002						
14th	1000	0.003						
15th	1000	0.002						
16th	1000	0.007						
17th	1000	0						
18th	1000	0.004						
19th	1000	0.004						
20th	1000	0.003						

Table 3-8: Mean Probability of failure for each number of simulations

Number of simulations	Mean probability of failure
1000 (20)	0.0037
2000 (10)	0.0038
5000 (4)	0.0042
10000 (2)	0.0044



(a)



(b)

Figure 3-21 (a, b): Probability of failure (P_f) for different run (th) considering the number of simulations (N_s).

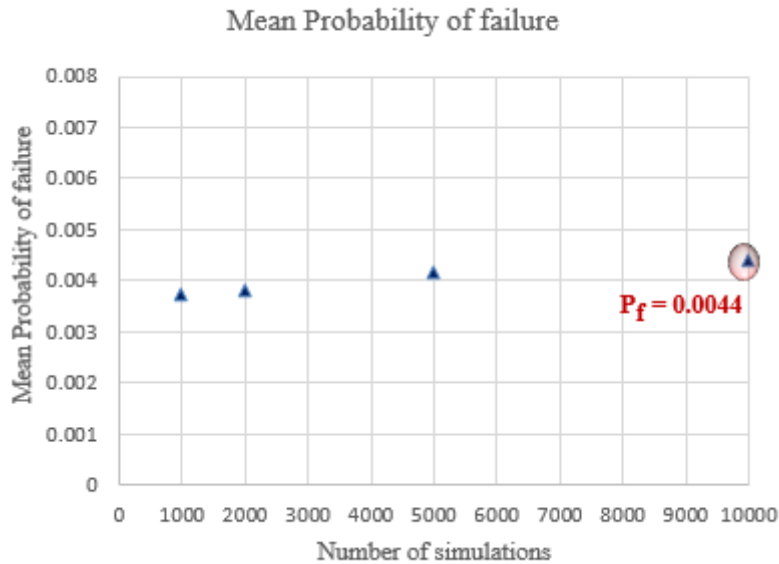


Figure 3-22: Mean probability of failure (P_f) for different number of simulations (N_s).

The results presented in Table 3-7 are plotted in Figure 3-21 (a, b) showing that the larger the number of simulations the less dispersion between the estimates of P_f for different runs is observed. Therefore, increasing the number of simulations seems to be the best option to obtain a more precise estimate of the probability of failure. The mean probability of failure for each number of simulations (i.e. mean P_f for the 20 runs of 1000 simulations, mean P_f for the 10 runs of 2000 simulations, mean P_f for the 4 runs of 5000 simulations, mean P_f for the 2 runs of 10000 simulations) is presented in Table 3-8 and Figure 3-22 showing that closely similar mean probability of failure might be expected for the same total number of simulations.

Finally, it only takes approximately less than 14 hours to run a 10,000 simulations sample, which confirms that the ANN-based Monte Carlo simulation could be a promising solution for reliability assessment of mooring lines in extreme sea conditions (ULS).

The design safety factor approach, API-RP-2SK (API, 2005)

Another common design approach recommended by API-RP-2SK (API, 2005) is to use a total safety factor on mooring component strength to ensure redundancy against mooring breakage.

The maximum design tension of the mooring component is chosen as

$$T_{\max_design} < \frac{MBS}{SF} \tag{3.43}$$

where $\frac{\text{MBS}}{\text{SF}}$ – the design breaking strength of the mooring component

MBS – the Minimum Breaking Strength of the mooring component.

SF – the minimum safety factor of the mooring components taken as 1.67 according to API RP 2SK (API, 2005).

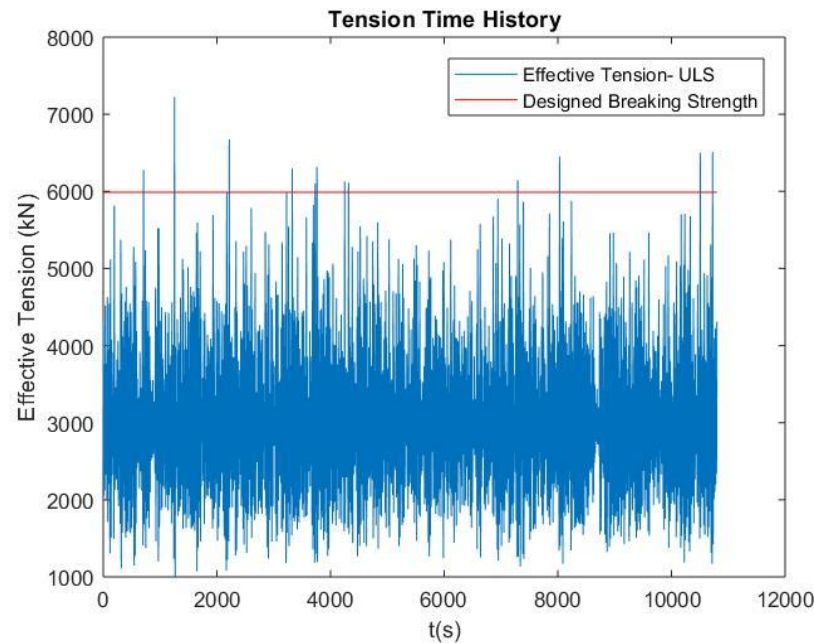


Figure 3-23: A time history of the tension response at fairlead point of the front line 1 in the ULS condition.

A time history of the tension response at the fairlead point of the front line 1 in storm condition (ULS) is plotted together with the designed breaking tension (i.e. considering the strength safety factor) in Figure 3-23 for illustration. It is concluded by Pham et al. (2019-a) that in this case study, the studied line is considered fail according to API-RP-2SK (API, 2005) if a safety factor equals to 1.67 is applied on the Minimum Breaking Strength (MBS) of the chain section. This is coincident with the conclusion made above where the probability of failure estimated by the ANN-based Monte Carlo simulation approach for 10000 simulations is also quite high (i.e. $P_f = 0.0048$ for the second run of 10000 simulations). It is worth to note that DNV-OS-E301 (DNV, 2010) requires a target annual probability of failure equals to 10^{-4} for the ULS for the consequence class 1 (i.e. where mooring system failure is unlikely to lead to unacceptable consequences such as loss of life, collision with an adjacent platform, uncontrolled outflow of oil or gas, capsizing or sinking).

6. Conclusions

A hybrid methodology which combines modeling and monitoring of mooring lines has been proposed. The methodology aims to clarify the mechanics of the mooring lines response, to understand why and how those responses are modified during deployment, and how those modifications can be accounted for in order to update the actual state and predict the remaining allowable service life of the system. The author believes that once the present methodology can be properly implemented, not only the actual state of the mooring lines (i.e. residual breaking strength and stiffness of mooring components, marine growth, corrosion, etc.) will be better controlled but also the cumulative fatigue and reliability will be better estimated. Based on that, decisions regarding maintenance or replacement of lines can be made. Furthermore, a comprehensive methodology for modeling and life monitoring also means a closer look on the design safety factor, and as a consequence, a more cost-effective design. However, the methodology requires a full understanding of the mechanical behaviors of all the mooring components and the marine environmental factors involved which are usually complicated to comprehend such as the modified mechanical behaviors due to the internal abrasion of nylon, the development and influence of marine growth, corrosion and wear on structural dynamic behaviors, etc. These should be the topic of the future work that might include a great amount of laboratory tests and site measurements.

Cutting edge methods for fatigue analysis, reliability assessment and simulation of mooring responses have also been adopted in order to better estimate the fatigue damage and reliability of mooring lines. The improved frequency domain fatigue approach is proven capable of capturing the non-Gaussian and wide-band effect of mooring response. Moreover, the analytical formula of the fatigue damage allows considering directly the uncertainties of the environmental loading and the S-N fatigue curves of mooring components. The ANN-based Monte Carlo simulation appears to be a promising option for reliability assessment of mooring lines in extreme sea conditions (ULS) where an important number of simulations is required. Such analysis can be implemented with a reasonable computational time (i.e. 14 hours for 10000 simulations with a standard computer) based on the so-called ANN-based Monte Carlo reliability assessment. It was found that a large number of simulations are required for a reasonable estimate of probability of failure which is comparable with the reliability

criteria according to DNV-OS-E301 (DNV, 2010) and the safety factor approach according to API RP 2SK (API, 2005).

7. References

- API. American Petroleum Institute. API-RP-2SK. Design and Analysis of Stationkeeping Systems for Floating Structures. 2005.
- Aqdam H. R., Etefagh M.M., Hassannejad R. Health monitoring of mooring lines in floating structures using artificial neural networks, *Ocean Eng.* 164 (2018) 284–297.
- Ayala-Uraga E., Moan T. Time-variant reliability assessment of FPSO hull girder with long cracks. *Journal of Offshore Mechanics and Arctic Engineering*; Vol. 129, pp. 81-89. 2007.
- Benasciutti D., Tovo R. (2005). Comparison of spectral methods for fatigue damage assessment in bimodal random processes. *ICOSSAR 2005*, pp.3181-3188.
- Benasciutti, D. & Tovo, R. 2004. Spectral methods for lifetime prediction under wide-band stationary random processes. In press in *Int. J. Fatigue*.
- Bendat J.S., Piersol A.G. *Random data: analysis and measurement procedures*. 3th edition, A Wiley Interscience publication, 2000.
- Bitner-Gregersen E.M., Cramer E.H., Løseth R. Uncertainties of load characteristics and fatigue damage of ship structures, *Mar. Struct.* 8 (1995) 97–117.
- Braccesi C., Cianetti F., Lori G., Pioli D., 2009. The frequency domain approach in virtual fatigue estimation of non-linear systems: The problem of non-Gaussian states of stress. *International Journal of Fatigue* 31:766-775.
- Breitung K. Asymptotic approximations for multinormal integrals. *J Eng Mech* 1984. 110(3):357–66.
- Brindley W., Comley Andrew P. North Sea Mooring Systems: How Reliable Are They? In: *ASME 2014 33rd International Conference on Ocean, Offshore and Arctic Engineering* 1AT01A025. 2014.
- Bureau Veritas. Guidance Note NI 604 DT R00 E. Fatigue of Top Chain of Mooring Lines due to In-plane and Out-of-plane bending. (2014).
- BV (Bureau Veritas). 2015. NR 493 DT R03 E. Classification of Mooring Systems for Permanent and Mobile Offshore Units.

Christiansen, N. H., Voie, P. E. T., Høgsberg, J. (2015), “Artificial Neural Networks for Reducing Computational Effort in Active Truncated Model Testing of Mooring Lines,” Proceedings of the ASME 2015 34th International Conference on Ocean, Offshore and Arctic Engineering, OMAE2015, St. John’s, Newfoundland, Canada.

Christensen L., Friis-Madsen E. and Kofoed J.P. (2005). The wave energy challenge. The Wave Dragon case. Proceedings of PowerGen 2005 Europe conference, Milan, Italy.

Cianetti F., Palmieri M., Braccesi C., Morettini G. Correction formula approach to evaluate fatigue damage induced by non-Gaussian stress state. AIAS 2017 International Conference on Stress Analysis, AIAS 2017, 6-9 September 2017, Pisa, Italy.

Der Kiureghian A., Lin H., Hwang S. Second-order reliability approximations. J Eng Mech 1987. 113(8):1208–25.

DNV. Offshore Standard - Position Mooring. DNV OS-E301, 2010.

Fiessler B., Rackwitz R., Neumann H. Quadratic limit states in structural reliability. J Eng Mech Div 1979. 105(4):661–76.

Finucane M. Details of Gryphon incident of 4th February 2011 and lessons learned. Aberdeen IOSH Conference 2012.

Gao Z., Moan T., Heggelund S.E. Time Variant Reliability of Mooring System Considering Corrosion Deterioration, 24th Int. Conf. Offshore Mech. Arct. Eng. Vol. 2. (2005) 203–210.

Gao Z. Stochastic Response Analysis of Mooring Systems with Emphasis on Frequency-domain Analysis of Fatigue due to Wide-band Response Processes. PhD thesis. Norwegian University of Science and Technology. 2008.

Gao Z., Moan T. Frequency domain multi-modal formulation for fatigue analysis of Gaussian and non-Gaussian wide-band process. Centre for Ship and Ocean Structure, Norwegian University of Science and Technology, 2010.

Guarize R., Matos N. A. F., Sagrilo L. V. S., Lima E. C. P. (2007). Neural networks in the dynamic response analysis of slender marine structures. Applied Ocean Research, 29, 191-198.

- Gurley K., Kareem A., Tognarelli M.A. Simulation of a Class of Non-Normal Random Processes. *International Journal of Nonlinear Mechanics*. 31(5), 601-617, 1996.
- Hagen O., Tvedt L. Vector process out-crossing as a parallel system sensitivity measure. *American Society of Civil Engineers, Journal of Engineering Mechanics*; Vol. 117, No. 10, pp. 2201-2220. 1991.
- Harnois V., Thies P.R., Johanning L. On Peak Mooring Loads and the Influence of Environmental Conditions for Marine Energy Converters. *J. Mar. Sci. Eng.* **2016**, 4, 29.
- Hasofer A.M., Lind N.C. An exact and invariant first-order reliability format. *J Eng Mech Div (ASCE)* 1974. 100:111–21.
- Hertz J., Krogh A., Palmer A. G. (1991), *Introduction to the Theory of Neural Computation*, Addison-Wesley, Redwood City, CA.
- Haykin S. (1999), *Neural Networks: A Comprehensive Foundation*, 2nd Edition, Prentice Hall, NJ.
- Horn J.T., Krokstad J.R., Leira B.J. Impact of model uncertainties on the fatigue reliability of offshore wind turbines, *Mar. Struct.* 64 (2019) 174–185.
- Hørte T., Lie H., Mathisen J. Calibration of an ultimate limit state for mooring lines 17th Conference of Mechanics and Arctic Engineering. OMAE 98-1457. 1998.
- Jiao G., Moan T. (1990). Probabilistic analysis of fatigue due to Gaussian load processes, *Probabilistic Engineering Mechanics*. Vol.5 No.2 pp.76-83.
- Kalra R, Deo MC, Kumar R, Agarwal VK. 2005. Artificial neural network to translate offshore satellite wave data to coastal locations. *Ocean Eng.* 32:1917–1932.
- Kim Y., Kim H., Ahn I.G. A study on the fatigue damage model for Gaussian wideband process of two peaks by an artificial neural network, *Ocean Eng.* 111 (2016) 310–322.
- Larsen K., Mathisen J. (1996) Reliability-based mooring design for a drilling semisubmersible. *Proceedings of the 6th International Offshore and Polar Engineering Conference*, Los Angeles, California; Vol. IV, pp. 457-466.

Lardier J., Moan T. Fatigue Reliability of Catenary Mooring Lines Under Corrosion Effect. Proceedings of the ASME 27th International Conference on Offshore Mechanics and Arctic Engineering OMAE2008. June 15-20, 2008, Estoril, Portugal (2008).

Li C.B., Choung J. Fatigue damage analysis for a floating offshore wind turbine mooring line using the artificial neural network approach, Ships Offshore Struct. 12 (2017) S288–S295.

Luo W., Ahilan R.V. (1991). Mooring safety assessment using reliability techniques. Proceedings of the Offshore Technology Conference, Houston; Paper No. 6783.

Liu H., Lian Y., Li L., Zhang Y. Experimental Investigation on Dynamic Stiffness of Damaged Synthetic Fiber Ropes for Deepwater Moorings, J. Offshore Mech. Arct. Eng. 137 (2015) 061401.

Liu P-L., Der Kiureghian A. Optimization algorithms for structural reliability. Struct Saf 1991. 9(3):161–77.

Ma K., Energy C., Company T., Duggal A., Smedley P., Exploration B.P. A Historical Review on Integrity Issues of Permanent Mooring Systems. OTC 24025, 2013.

Madsen H.O., Krenk S. & Lind N.C. Methods for Structural Safety. Prentice-Hall, New Jersey. 1986.

Marley, M.J. & Moan, T. Time variant formulation for fatigue reliability. Proceedings of the 11th International Conference on Offshore Mechanics and Arctic Engineering, Alberta, Canada; Paper No. OMAE92-1203. 1992.

Mathisen J., Larsen K., Hørte T., Lie H. Calibration of Progressive Collapse Limit State for Mooring Lines. 17th Conference of Mechanics and Arctic Engineering. OMAE 98-1458. 1998.

Mathisen J., Hørte T. Calibration of a Fatigue Limit State for Mooring Lines. International Conference on Computational Methods in Marine Engineering. MARINE 2005, Barcelone. 2005.

Matlab. Fit Data with a Shallow Neural Network.
<https://www.mathworks.com/help/deeplearning/gs/fit-data-with-a-neural->

- network.html;jsessionid=ab1f941a17915104bb5c4553c070. (Accessed : 10 Avril 2017).
- Melchers R.E., Moan T., Gao Z. Corrosion of working chains continuously immersed in seawater. *Journal of Marine Science and Technology*; Vol. 12, No. 2, pp. 102-110. (2007).
- Melchers R.E. *Structural Reliability: Analysis and Prediction*. Ellis Horwood, UK. 1987.
- Mršnik M., Slavič J., Boltezar M. Frequency-domain methods for a vibration fatigue-life estimation – Application to real data. *International Journal of Fatigue*, 47:8– 17, 2013.
- Pham H.D., Cartraud P., Schoefs F., Soulard T., Berhault C. Dynamic Modeling of Nylon Mooring Lines for a Floating Wind Turbine. *Appl. Ocean Res.*, 87, pp. 1-8. 2019-a.
- Pham H-D., Schoefs F., Soulard T., Cartraud P., Pham H-H., Berhault C. Methodology for modeling and service life monitoring of mooring lines of floating wind turbines. *Ocean Engineering*. *Ocean Eng.* 193, 1 December 2019 (2019-b).
- Pham H-H. FPSO - Fiabilité des lignes d'ancrage avec prise en compte de fatigue: Evaluation de la fiabilité des lignes d'ancrage des FPSO au Vietnam avec prise en compte du dommage accumulé de fatigue. PhD thesis. Université de Liège. 2010.
- Pham H.H. Methodology for total reliability evaluation of the mooring lines of floating offshore structures. *The Vietnam Symposium on Advances in Offshore Engineering (VSOE)*, Hanoi, 2018.
- Pham K.H., Dinh Q.C., Mai H.Q., Nguyen V.N. Estimation of the Total Reliability of Offshore Structures in Vietnam Sea Conditions Combining the Ultimate State and Fatigue Limit States. *Proceeding of OCEANS'04 MTS/IEEE/TECHNO-OCEAN/04*, Kobe, Japan, 176-185 (2004).
- Pina A.C, Pina A.A, Albrecht C.H, Lima B.S.L.P, Jacob B.P. 2013. ANN-based surrogate models for the analysis of mooring lines and risers. *Appl Ocean Res.* 41:76– 86.

- Preumont A. Random vibration and spectral analysis. Kluwer Academic Publishers, 1994.
- Rackwitz R., Flessler B. Structural reliability under combined random load sequences. *Comput Struct* 1978. 9(5):486–94.
- Rendón-Conde C., Heredia-Zavoni E. Reliability assessment of mooring lines for floating structures considering statistical parameter uncertainties, *Appl. Ocean Res.* 52 (2015) 295–308.
- Rychlik I. A new definition of the rainflow cycle counting method. *International Journal of Fatigue*, 9 (2): 119-121, 1987.
- Sarkani S., Kihl D. P., Beach J. E., 1994. Fatigue of welded joints under narrowband non-Gaussian loadings., *Probabilist. Eng. Mech.* 9: 179–190.
- Schoefs F., Clément A., Nouy A. Assessment of ROC curves for inspection of random fields, *Struct. Saf.* 31 (2009) 409–419.
- Sidarta D.E., Sullivan J.O., Kyoung J., Lambrakos K. F. Prediction of Offshore Platform Mooring Line Tensions Using Artificial Neural Network. *Proceedings of the ASME 2017 36th International Conference on Ocean, Offshore and Arctic Engineering. OMAE2017.* June 25-30, 2017, Trondheim, Norway.
- Snell R., Ahilan R.V, Versavel T. (1999) Reliability of mooring systems: Applications to polyester moorings. *Proceedings of the Offshore Technology Conference, Houston; Paper No. 10777.*
- Spraul C., Pham H.D, Arnal V., Reynaud M. Effect of Marine Growth on Floating Wind Turbines Mooring Lines Responses. In *AFM 2017 23ème Congrès Français de Mécanique*, 28 Aug – 1 Sept, 2017.
- Thies P.R., Johanning L., Harnois V., Smith H.C.M., Parish D.N. Mooring line fatigue damage evaluation for floating marine energy converters: Field measurements and prediction, *Renew. Energy.* 63: 133–144, 2014.
- Thoft-Christensen P., Baker M.J. *Structural Reliability Theory and its Applications.* Springer Verlag, Berlin, Germany. 1982.
- Tovo R. 2002. Cycle distribution and fatigue damage under broad-band random loading. *Int. J. Fatigue* Vol. 24 (No. 11): 1137-1147.

Tvedt L. Distribution of quadratic forms in normal space—application to structural reliability. *J Eng Mech* 1990. 116(6):1183–97.

Vazquez-Hernandez A.O., Ellwanger G.B., Sagrilo L.V.S. Reliability-based comparative study for mooring lines design criteria, *Appl. Ocean Res.* 28 (2006) 398–406.

Weller S.D., Johanning L., Davies P. MERiFIC deliverable D3.5.3 Best practice report - mooring of floating marine renewable energy devices. 2013.

Winterstein S.R. Nonlinear vibration models for extremes and fatigue. *J Eng Mech* 1988; 114:1772–89.

Wright C., Pakrashi V., Murphy J. The dynamic effects of marine growth on a tension moored floating wind turbine. *Proceedings of Renew 2016, 2nd International Conference on Renewable Energies Offshore*, Lisbon, Portugal, 2016.

Wu Y., Wang T., Eide Ø., Haverty K. Governing factors and locations of fatigue damage on mooring lines of floating structures, *Ocean Eng.* 96 (2015) 109–124.

Xue X., Chen N.Z., Wu Y., Xiong Y., Guo Y. Mooring system fatigue analysis for a semi-submersible, *Ocean Eng.* 156 (2018) 550–563.

Yang S-H., Ringsberga J W., Johnsona E., Huc Z. Biofouling on mooring lines and power cables used in wave energy converter systems—Analysis of fatigue life and energy performance. *Applied Ocean Research* 65 (2017) 166–177.

Yasseri SF, Bahai H, Bazargan H, Aminzadeh A. 2010. Prediction of safe sea-state using finite element method and artificial neural network. *Ocean Eng.* 37:200–207.

Yu L., Das P.K., Barltrop D.P. A new look at the effect of bandwidth and non-normality on fatigue damage. *Fatigue Fract Eng Mater Struct* 2003; 27:51–8.

CHAPTER 4 – CONCLUSIONS AND FUTURE WORK

CHAPTER 4 – CONCLUSIONS AND FUTURE WORK 153
1. CONCLUSIONS..... 154
2. FUTURE WORK 156

1. Conclusions

In this chapter conclusions are drawn according to the research question posed in section 2 of chapter 1 and relating finding.

For convenience, the research questions posed in section 3 of **chapter 1** are repeated:

- 1, Is mooring monitoring necessary? Which methodology should be employed?

As mentioned above, mooring monitoring is currently of great interest for not only MRE developers but also O&G stakeholders since many line failures were observed although they have been designed according to standards. In the **chapter 3** of this manuscript, a comprehensive methodology for modeling and service life monitoring of mooring lines is discussed by the author based on the reliability approach. In our opinion, in order to understand why and how mooring responses are modified during deployment, it is crucial to identify and account for not only the likely modified mechanical behaviors of mooring components but also the marine environmental factors influencing such behaviors. Therefore, we believe that in addition to the current monitoring approach (Thies et al., 2014) that uses directly field measurement to calculate fatigue damage, the numerical modeling should also be implemented in parallel, in a so-called digital twin. Indeed, once the present methodology is properly implemented, not only the actual state of the mooring lines will be better controlled but also the cumulative fatigue will be better estimated. As a consequence, the reliability of the system can be better predicted by fully understanding the actual state of mooring lines such as, residual breaking strength and stiffness of mooring components, better estimating the cumulative fatigue damage and better forecasting disadvantage events (e.g. added damage due to extreme sea states). Then, decisions regarding maintenance or replacement of lines can be made once the estimated reliability level reaches the critical value. Furthermore, a comprehensive methodology for modeling and life monitoring also means a closer look on the design safety factor, and as a consequence, a more cost-effective design. Moreover, since maintenance or replacement of lines for MRE devices in shallow water seems simpler and less costly than for deep-water O&G platforms, the present methodology suggests that those could be the other potential options rather than an over-engineered mooring system which would not be commercially viable for large scale deployments. Finally, the author believes that different safety factors should be considered for MRE devices since those are unmanned structures which are significantly different from Oil & Gas

platforms where the consequences for environment, economy and human losses are not in the same order of magnitude. These factors of safety could be selected based the corresponding allowable levels of reliability of mooring lines and the experience earned during exploitation.

2, How to improve the modeling and fatigue damage estimate of nylon mooring ropes?

In **chapter 2** of this manuscript, an effort has been made for studying the mechanical behaviors of nylon mooring ropes (i.e. load-elongation behaviors, critical modes of fatigue damage and influencing factors) since there is still limit of work on such issues. A practical mooring analysis procedure is suggested by the authors in order to account for the dynamic stiffness of nylon ropes on the mooring line modeling of a semi-submersible type FWT. The procedure is based the original methodology recommended by DNVGL-RP-E305 where the author aims to improve the DNV's procedure in order to capture the tension amplitude effect on dynamic mooring analysis of nylon mooring ropes. However, the present procedure still need to be validated with field measurements in order to check the appropriateness of the proposed modeling assumption. The fatigue characteristics of nylon ropes have also been comprehensively discussed in **chapter 2**. Due to the lack of available data in the literature, a non-destructive testing campaign has been proposed in order to characterize the internal abrasion fatigue of nylon ropes. The procedure might be considered for substituting current internal abrasion fatigue tests approach for nylon ropes which are not fully representative of the ropes real behavior or time-consuming and costly.

3, How to estimate fatigue damage based on numerical modeling and in-situ measurements? Which approaches?

Cutting edge frequency-domain approaches for calculating fatigue damage in mooring lines have also been investigated. More interestingly, the analytical fatigue damage formulation obtained in frequency domain analysis can be applied directly to reliability analysis in fatigue condition (FLS) using the First Order Reliability Method (FORM). This work is presented in **chapter 3**.

4, How reliability analysis can be performed to support making decisions regarding maintenance or replacement of lines?

For mooring lines of floating wind turbines where experience is limited or non-existent, it seems preferable to use directly a reliability approach where partial factors

of safety and characteristic values are replaced by the definition of an acceptable probability of failure. The reliability in both strength criterion (Ultimate Limit State – ULS) and fatigue criterion (Fatigue Limit State – FLS) are checked. Decisions regarding maintenance or replacement of lines can, then, be made based on the reliability estimated during the expected service life. This work is presented in **chapter 3**.

The ANN seems to be an interesting approach for simulation of nonlinear mooring response based on field measurements or numerical samples. For health monitoring of mooring lines, ANN is also an interesting tool for mooring response simulation based on measurements since it allows less required measurements and being less relied on tension sensor. This work is discussed in **Chapter 3**.

2. Future work

The following task will be included in the author's future scope of work:

- 1, Validate the practical procedure for dynamic modeling of nylon mooring ropes with model tests.
- 2, Perform the NDT procedure to characterize the internal abrasion fatigue for nylon ropes.
- 3, Applying the present methodology in order for Accidental Limit State (ALS) and address another common mooring failure mode which is from poor Quality Analysis/Quality Control (QA/QC) in manufacturing or damage from handling and installation.
- 4, Focus on the economic aspects in order to compare different design approaches in order to answer the following question: Which design approach is more economically favorable? An over-engineered design or design with lower reliability but considering maintenance and replacement of lines?
- 5, Further work will be needed in order to optimize the utilization of neural network and to aim for a more complicated application, e.g., a neural network that allows following the likely modified mooring response during the operation due to the modified mechanical behaviors of the system and environmental factors.
- 6, Focus on the ANN for simulation of nonlinear mooring response based on field measurements and the ANN-based Monte Carlo simulation for reliability assessment to draw partial safety factors in order to compare with standards.

7, Adopt more complex models for corrosion and marine growth in order to better estimate the fatigue and reliability of mooring lines.

APPENDIX

LIST OF PUBLICATIONS & COMMUNICATIONS

- Article 1 Pham H.D., Cartraud P., Schoefs F., Soulard T., Berhault C.
Dynamic Modeling of Nylon Mooring Lines for a Floating Wind
Turbine. *Appl. Ocean Res.*, 87 (2019), pp. 1-8.
- Article 2 Pham H.D., Schoefs F., Soulard T., Cartraud P., Pham H.H.,
Berhault C. Methodology for modeling and service life monitoring
of mooring lines of floating wind turbines. *Ocean Eng.* 193, 1
December 2019 (2019-b).
- Conference
paper 1 Spraul C., Pham H.D, Arnal V., Reynaud M. Effect of Marine
Growth on Floating Wind Turbines Mooring Lines Responses. In
AFM 2017 23ème Congrès Français de Mécanique, 28 Aug – 1
Sept, 2017. (Presenting author). pp. 1-17
- Presentation 1 Pham H.D., Cartraud P., Schoefs F., Soulard T. Mooring lines for
Floating Wind Turbines, modeling and monitoring issues. Blue
day – Les Ancrages pour les EMR: Du Chaumard à L’Ancre. 13
March 2019, IFSTTAR – Nantes, France. (Presenting author).
- Presentation 2 Pham H.D., Cartraud P., Schoefs F., Soulard T. Methodology for
modeling and service life monitoring of mooring lines of floating
wind turbines. 2nd International Conference on Health Monitoring
of Civil & Maritime Structures – HeaMES 2019, 23rd - 24th,
Glasgow, UK. (Presenting author).
- Poster 1 Pham H.D., Cartraud P., Schoefs F., Soulard T. Modeling and
service life monitoring of mooring lines for floating wind turbines.
French American Innovation Day – FAID 2019, 18-19 March
2019, Boston, US. (Presenting author).

Titre : Modélisation et Suivi en Service des Lignes d’Ancrages des Éoliennes Flottantes

Mots clés : Eolienne flottantes, Ligne d’ancrage, Nylon, Fatigue, Fiabilité, Simulation non-linéaire

Résumé : On propose dans ce travail une méthodologie pour le suivi en service des lignes d’ancrage des éoliennes flottantes. Tout d’abord, une expression empirique de la raideur dynamique d’un câble en nylon est obtenue à partir des données d’essais dans la littérature. Une procédure pratique de modélisation est proposée en tenant compte de la raideur axiale dynamique non-linéaire des câbles en nylon.

La deuxième partie est consacrée à la prédiction de la durée de vie des lignes d’ancrages. Des méthodes avancées pour l’analyse de fatigue dans le domaine fréquentiel et la simulation des réponses non-linéaires sont donc également étudiées afin de réaliser une estimation rapide de la fatigue et de la résistance dans un cadre fiable. La présente méthodologie vise à faciliter la prise de décisions concernant la maintenance ou le remplacement des lignes en fonction du niveau de fiabilité estimé à différents instants.

Title : Modeling and Service Life Monitoring of Mooring Lines of Floating Wind Turbines

Keywords : Floating Wind Turbine, Mooring line, Nylon, Fatigue, Reliability, Nonlinear simulation

Abstract: In this work a methodology for service life monitoring of mooring lines of floating wind turbines is proposed. First, an empirical expression of dynamic stiffness of a nylon rope is obtained from the testing data in the literature. A practical modeling procedure is proposed which allows accounting for the non-linear dynamic axial stiffness of nylon mooring ropes.

The second part is devoted to the prediction of fatigue life of mooring lines. Cutting-edge methods for fatigue analysis in frequency domain and for simulation of nonlinear mooring response are investigated in order to perform a quick fatigue estimate and strength check in a reliability framework. The present methodology aims to support making decisions regarding maintenance or replacement of lines based on the level of reliability estimated during the expected service life.